Influence of Spatial Rainfall Gradients on River Longitudinal Profiles and the Topographic Expression of Spatio-temporally Variable Climate in Mountain Landscapes

Joel S Leonard[1,1] and Kelin X Whipple[1,1]

[1]Arizona State University

December 1, 2022

Abstract

Mountain landscapes have dynamic climates that, together with tectonic processes, importantly influence their topographic evolution. While spatio-temporal changes in rainfall are ubiquitous in these settings, their influence on river incision has been little studied. Here, we investigate how changes in rainfall pattern should affect both the steady state form and transient evolution of river profiles at the catchment scale using the stream power model. We find that non-uniform rainfall patterns complicate steady state relationships among conventional catchment-wide metrics like mean rainfall, channel steepness, and fluvial relief, which can influence the apparent sensitivity of landscapes and erosion rates to rainfall variations. We also find that transient responses to changes in rainfall pattern have an inherently multi-stage nature that importantly differs from expected responses to uniform changes in rainfall. This has several important implications, specifically for detecting transient responses to changes in rainfall pattern (and more broadly climate) in natural settings, and for interpretations of landscape morphometrics above and below transient knickpoints. We find that disparate responses by rivers and river segments that experience different rainfall conditions, particularly trunk and tributary rivers, are an important factor in understanding catchment-wide responses, and accounting for such disparities may be important for detecting and quantifying landscape sensitivity to rainfall variations. Lastly, we show how explicitly accounting for rainfall patterns in channel steepness calculations, and thus variations in erosional efficiency, may be a necessary step toward overcoming challenges related to rainfall variations, and thus ultimately for advancing understanding of landscape sensitivity to climate in mountain settings.

Joel S. Leonard[1] and Kelin X. Whipple[1] [1]School of Earth and Space Exploration, Arizona State University, Tempe, Arizona, USA

Corresponding Author: Joel S. Leonard (joel.leonard@asu.edu)

Key Points

- Spatially variable rainfall complicates steady state relationships between mean rainfall and conventional topographic and erosion metrics.
- Transient responses to changes in rainfall pattern differ from uniform changes in rainfall, which affects how they may be detected.
- Rainfall gradients can obscure the sensitivity of fluvial erosion to rainfall variations and impede quantification of climate sensitivity.

Abstract

Mountain landscapes have dynamic climates that, together with tectonic processes, influence their topographic evolution. While spatio-temporal changes in rainfall are ubiquitous in these settings, their influence on river incision is understudied. Here, we investigate how changes in rainfall pattern should affect both the steady state form and transient evolution of river profiles at the catchment scale using the stream power model. We find that spatially varied rainfall can complicate steady state relationships between mean rainfall, channel steepness and fluvial relief, depending on where rainfall is concentrated in catchments. As a result, transient profile adjustments to climate changes may proceed contrary to typical expectations, which can ultimately affect the apparent sensitivity of landscapes and erosion rates to climate. Additionally, changes in rainfall pattern cause inherently multi-stage transient responses that differ from responses to uniform changes in rainfall. These results have important implications for detecting transient responses to changes in rainfall pattern (and more broadly climate), and for interpreting of landscape morphometrics above and below knickpoints. Further, we find that disparate responses by rivers that experience different rainfall conditions, particularly trunk and tributary rivers, are an important factor in understanding catchment-wide responses, and accounting for such disparities may be important for detecting and quantifying landscape sensitivity to variations in climate. Lastly, we show how explicitly accounting for rainfall patterns in channel steepness indices, and thus variations in erosional efficiency, has potential to help address challenges related to spatially variable rainfall patterns and advance understanding of landscape sensitivity to climate in mountain settings.

Plain Language Summary

Rainfall in mountain landscapes often varies with elevation; a pattern known as orographic rainfall. Rivers that sculpt these landscapes rely on rainfall for their erosive power, where more rainfall typically means greater erosive power. Rainfall also affects how steep these rivers are, which in turn affects the steepness of the topography around them. Here, we investigate how concentrating rainfall at higher and lower elevations – representing two common orographic rainfall patterns that may be enhanced or relaxed by climate change – influences the steepness mountain rivers, erosion patterns, and thus the evolution of mountain topography. We show that these orographic rainfall patterns complicate simple expected relationships among metrics commonly used to quantify the role of rainfall (and more broadly climate) on the topography of mountain landscapes. Further, we show that rivers respond in unexpected ways to changes in orographic rainfall patterns, as would occur following a change in climate, suggesting that common wisdom about how rivers and mountain landscapes respond to changing climates is incomplete.

1. Introduction 1.1 Motivation

Advances in tectonic geomorphology require quantitative understanding about relationships among climate, tectonics, and erosion. In temperate mountain landscapes, studies of bedrock rivers provide important insights into interactions between these processes (e.g., D'Arcy & Whittaker, 2014; Harel et al., 2016; Kirby & Whipple, 2012; Lague, 2014; Olen et al., 2016; Scherler et al., 2017; Whipple & Tucker, 1999; Whittaker, 2012). However, despite longstanding theoretical support for the notion that climate, like tectonics, has a fundamental role in influencing erosion (e.g., Bonnet & Crave, 2003; Howard & Kerby, 1983; Lague, 2014; Molnar, 2001; Perron, 2017; Rinaldo et al., 1995; Tucker & Slingerland, 1997), a general relationship between climate and erosion has proven elusive (Perron, 2017; Whittaker, 2012). Here, we explore the extent to which this conundrum may reflect limitations in the current framework describing how climate-related signals should be expressed in landscapes that, in turn, may impede recognition of diagnostic characteristics of landscape response to climate change.

Orographic precipitation patterns are ubiquitous in mountain landscapes. In general, they develop from the interaction of humid air masses with topographic relief and can create dramatic spatial and elevation dependent gradients in precipitation (see Roe, 2005 for an overview). For instance, the Olympic, Sierra Nevada, and Wasatch ranges in western North America all experience orographically enhanced precipitation with increasing elevation (e.g., Barros & Lettenmaier, 1994; Barstad & Smith, 2005; Roe, 2005). Alterna-

tively, large tracts along eastern and southern flanks of the Andes and Himalaya, respectively, become more arid as elevation increases (Anders et al., 2006; Bookhagen & Burbank, 2010; Bookhagen & Strecker, 2008; Burbank et al., 2003). While numerous factors affect orographic precipitation patterns in detail, broadly speaking, atmospheric moisture content, topographic characteristics (e.g., relief), and general circulation patterns are primary physical controls on their development (e.g., Held & Soden, 2006; Roe, 2005; Roe et al., 2008; Trenberth et al., 2003). Because atmospheric moisture content depends strongly on temperature (i.e., Clausius-Clapeyron relationship; Held & Soden, 2006; Roe, 2005; Trenberth et al., 2003), shifts in temperature that accompany changes in climate must influence these precipitation patterns (e.g., Mutz et al., 2018; Roe & Baker, 2006; Siler & Roe, 2014). Therefore, if erosional processes in these landscapes are generally sensitive to spatial and/or temporal variations in precipitation, then changing characteristics of orographic precipitation patterns with changes in climate should importantly influence mountain landscape evolution.

In mountainous settings, transverse rivers tend to cross orographic precipitation gradients, which are generally oriented orthogonally to the topographic trend of the range. Their tributaries, on the other hand, typically experience a relatively muted range in precipitation due to their orientation and/or smaller areal extent. Consequently, rivers of different size, orientation, and position often experience dramatically different precipitation conditions. Within large river basins, these differences may be substantial. Exposure to orographic precipitation patterns is expected to systematically affect river profile concavity; increases in precipitation with distance upstream lowers profile concavity, while the opposite trend increases profile concavity (Han et al., 2014, 2015; Roe et al., 2002, 2003; Ward & Galewsky, 2014). Changes in concavity driven by temporal changes in orographic precipitation patterns require longitudinally variable amounts of incision. Furthermore, because transverse rivers set erosional base level for their tributaries, any along-stream variation in incision exhibited by transverse rivers during this adjustment will necessarily drive spatially and temporally variable base level histories for tributaries. Developing a framework that accommodates such variability and its influence on river profile evolution is a fundamental need.

1.2 Approach and Scope

Here, we investigate how spatio-temporal changes in precipitation may influence erosion and topography of mountain landscapes using the stream power model (SPM). First, we show how simple spatial gradients in rainfall, resembling typical orographic precipitation patterns (i.e., increasing or decreasing downstream; herein referred to as bottom-heavy, and top-heavy, respectively), influence river profile form at steady state in one dimension. Next, we use a quasi-two-dimensional numerical model to simulate the response of a transverse river network to a change in rainfall pattern, which we compare to better-understood spatially uniform changes in rainfall. Finally, we discuss some implications for studies set in mountain landscapes. A comprehensive analysis of the co-evolution of orographic rainfall patterns and topography is beyond the scope of this paper. Instead, we focus on characterizing the controls on landscape response to imposed changes in rainfall patterns, highlighting where expectations differ from uniform changes in rainfall, and implications of those differences.

2. Methods 2.1 Model Description

We explore the influence of longitudinal rainfall gradients on large transverse rivers first using a simple 1-dimensional river incision model. We model erosion as detachment-limited (Howard, 1994; Roe et al., 2002; Whipple & Tucker, 1999) following a general form of the SPM:

$$E = KA^mS^n, \text{ (1a)} \quad K = K_p\overline{P}^m, \text{ (1b)} \quad E = K_pQ^mS^n, \text{ (1c)}$$

where E is the erosion rate; K and K_p are erosional efficiency coefficients; A is upstream drainage area; S is the channel slope; $\overline{P}$ is the upstream average rainfall rate; Q is water discharge and is calculated as $\overline{P}A$, which assumes that all rainfall is converted to runoff; and m and n are positive constant exponents (Table 1). We use $n = 2$ and $m = 1$ for all model runs as values of $n > 1$ appear more appropriate in many settings (e.g., Adams et al., 2020; Harel et al., 2016; Lague, 2014). First-order results do not rely on choices of m or n providing the ratio between the two is approximately maintained, but the nonlinear dependence

of erosion rate on slope (i.e., $n = 2$) affects details of the transient behavior. Also, because $m = 1$, K is directly proportional to both $\overline{P}$ and Q. We explicitly treat the influence of climate on erosional efficiency (e.g., Adams et al., 2020; Roe et al., 2002) such that K_p is independent of rainfall, but still encapsulates a number of factors including rock properties and details of erosional processes (Royden & Perron, 2013; Whipple & Tucker, 1999). Rock uplift rate (U) and K_p are spatially and temporally uniform and invariant across model runs.

We define drainage area (A) following Hack, (1957):

$A = k_a x^h + A_c$, (2)

where x is distance along the channel downstream from the drainage divide, k_a and h are constants, and A_c is the upstream drainage area at the channel head – equal to 1 km^2. Channel length (L) and drainage area are fixed and do not evolve over the course of a model run.

For simplicity, we model orographic precipitation as constant gradients in rainfall (i.e., linear changes with distance). Although a constant gradient is a simplification, it is a reasonable approximation to commonly observed orographic rainfall patterns, which can be both top- and bottom-heavy (e.g., Anders et al., 2006; Bookhagen & Burbank, 2010; Bookhagen & Strecker, 2008; Roe, 2005). Further, the framework we develop from these simple rainfall patterns is generally applicable to addressing more complex versions of the fundamental problem we address here – the effects of spatially concentrated rainfall.

2.2 Analysis of River Profiles and Erosion Rates

We quantify river profile form and responses to changes in rainfall patterns using channel steepness indices and erosion rates. These metrics are commonly used, and often in tandem, to study influences of climate and/or tectonics in mountain settings (Adams et al., 2020; Bookhagen & Strecker, 2012; Cyr et al., 2014; DiBiase et al., 2010; Duvall, 2004; Godard et al., 2014; Insel et al., 2010; Kober et al., 2015; Morell et al., 2015; Olen et al., 2016; Ouimet et al., 2009; Portenga et al., 2015; Safran et al., 2005; Scherler et al., 2014; Vanacker et al., 2015; Willenbring et al., 2013).

A widely used metric to analyze river profiles, interpret erosion rates, and make comparisons to the SPM is the normalized channel steepness index, k_{sn}:

$k_{\mathrm{sn}} = S A^{\theta_{\mathrm{ref}}}$, (3)

where $\vartheta_{\rho \epsilon \varphi}$ is the reference concavity index (Wobus et al., 2006). We use a value of $\vartheta_{\rho \epsilon \varphi} = 0.5$, which is common and consistent with our choice of m/n, and also with SPM predictions that $\vartheta_{\rho \epsilon \varphi} = m/n$ [?] 0.5 where rock uplift rate (U) and erosional efficiency (K) are uniform (Tucker & Whipple, 2002). As previously noted, the SPM predicts that orographic rainfall gradients should produce longitudinal variations in K that, in turn, affect the concavity index, ϑ (Han et al., 2014, 2015; Roe et al., 2002, 2003). Any such variations are systematically reflected in the spatial pattern of k_{sn} and ϑ [?] $\vartheta_{\rho \epsilon \varphi}$ is expected. Importantly, however, many studies relate upstream-average values of k_{sn} to measured spatially-averaged erosion rates, which relies on quasi-uniform (or linear) upstream k_{sn} to be valid (Wobus et al., 2006). In cases where systematic longitudinal variations in K affect the downstream pattern of k_{sn} (i.e., upstream k_{sn} varies non-linearly), the meaning of such an average is not obvious.

To address this, we use discharge, rather than drainage area alone, to calculate a modified channel steepness index $k_{sn\text{-}q}$ (Adams et al., 2020):

$k_{sn-q} = S Q^{\theta_{\mathrm{ref}}}$. (4)

Like k_{sn}, $k_{sn\text{-}q}$ is an empirically supported metric independent from the SPM. In principle, however, $k_{sn\text{-}q}$ is analogous to Erosion Index (EI) used by Finlayson et al., (2002) provided that m/n [?] $\vartheta_{\rho \epsilon \varphi}$, such that EI $= (k_{sn\text{-}q})^n$. Also, as k_{sn} is the slope of χ-transformed river profiles in χ-elevation space, if χ is redefined to include precipitation to estimate discharge, slopes of χ-transformed profiles would instead represent $k_{sn\text{-}q}$ (Royden & Perron, 2013; Yang et al., 2015). To the extent that the SPM captures the influence of discharge

on erosional efficiency, it predicts that along-stream variations in $k_{sn\text{-}q}$ should scale with local erosion rate, precisely as it does for k_{sn} where K is spatially uniform. Hereafter, we use k_{sn} and $k_{sn\text{-}q}$ to refer to upstream averaged values, consistent with their common usage in catchment-mean erosion rates analyses, unless we specifically state that they represent local values.

Millennial-scale catchment-averaged erosion rates measured, for example, using cosmogenically-derived [10]Be found in quartz in alluvial sediment (e.g. Bierman & Steig, 1996; Brown et al., 1995; Granger et al., 1996), seek to quantify erosion rates at the river basin scale. At steady state, spatially averaged erosion rate, local incision rate, and rock uplift rate are equivalent; however, during periods of transient adjustment these values differ, complicating interpretations (Willenbring et al., 2013; Wobus et al., 2006). To make our results more portable to studies of natural landscapes, we calculate the spatially averaged erosion rate (E_{avg}) in addition to the instantaneous vertical incision rate (E):

$$E_{\text{avg}_j} = \frac{\sum_{x_h}^{j}(E_j \bullet (A_j - A_{j-1}))}{A_j}, (5)$$

where j corresponds to a downstream node of the profile, and x_h is the channel head.

3. Longitudinal Profiles (1-D) 3.1 Influence of Longitudinal Rainfall Gradients on River Profiles at Steady State

Where rainfall is spatially uniform, topographic metrics (e.g., fluvial relief, channel steepness) at steady state are expected to vary inversely and monotonically with mean rainfall (Figure 1a). However, spatially variable rainfall patterns complicate these expectations, as shown in Figure 1b, where comparisons between rivers that experience different rainfall patterns instead result in positive relationships between these topographic metrics and mean rainfall. This reversal reflects limitations of using spatially averaged metrics where climate is spatially variable (e.g., in most mountain landscapes).

Systematic longitudinal variations in rainfall require that upstream average rainfall values change systematically downstream, which similarly affects erosional efficiency (K), and thus equilibrium channel slope (Equation 1). Where such spatial variations exist, mean values of rainfall and k_{sn} therefore depend on where they are measured. In contrast, where equation 1 holds and $m/n = \vartheta_{\rho\epsilon\varphi}$, $k_{sn\text{-}q}$ is independent of changes in mean rainfall (Figure 1). Comparison of SPM equations for k_{sn} and $k_{sn\text{-}q}$ at steady state ($E = U$) further clarifies this difference:

$$k_{\text{sn}} = \left(\frac{U}{K_p P^m}\right)^{1/n}, (6a) \quad k_{sn-q} = \left(\frac{U}{K_p}\right)^{1/n}. (6b)$$

For spatially uniform rock uplift rate (U) and K_p, steady state fluvial relief (R) is proportional to the upstream integrated discharge (Han et al., 2015; Roe et al., 2003; Royden & Perron, 2013). Integrating equation 1c from base level (x_b) upstream to the channel head (x_h), it can be shown that:

$$R = \left(\frac{U}{K_p}\right)^{1/n} \int_{x_b}^{x_h} Q^{-m/n} \, dx. (7)$$

This demonstrates clearly how fluvial relief depends on the cumulative effect of discharge and implies that fluvial relief does not necessarily scale monotonically with discharge or rainfall measured at any single position, or averaged along any segment of a profile, except under the special condition where rainfall is spatially uniform (Gasparini & Whipple, 2014; Han et al., 2015). This is an important result, particularly for understanding the topographic evolution of mountain landscapes because it suggests that considering how rainfall patterns, specifically, have changed with time is critical to predicting responses to changes in climate. For instance, shifts toward 'wetter' climates may support topographic growth, contrary to expectations and even in the absence of any change in tectonics, depending on where rainfall is concentrated, or vice versa.

3.2 Transient River Profile Response to Changes in Rainfall Patterns

According to the SPM, transient responses to climate change are primarily driven by changes in discharge that, in turn, affect erosional efficiency. In response to climate change, in addition to changes in mean

rainfall, increases or decreases in rainfall may occur in different positions within a catchment, for example by strengthening or relaxing existing orographic rainfall distributions (Roe et al., 2003; Roe & Baker, 2006). Any such change in the pattern of rainfall fundamentally changes how discharge accumulates and can be expected to drive adjustments in the form of river profiles.

Changes in discharge at a given location following a temporal change in rainfall pattern reflect changes upstream average rainfall conditions. (Hereafter we use subscripts i and f, respectively, to denote initial and final steady states, before and after a temporal change in rainfall pattern.) While integrating upstream conditions somewhat buffers discharge from localized variations in rainfall upstream, because it accumulates non-linearly downstream relatively modest systematic variations in rainfall can exert a strong influence. Indeed, contrary to spatially uniform changes in rainfall that cause monotonic changes in discharge everywhere, we find that for a wide range of temporal changes in rainfall patterns discharge may increase in upstream locations ($Q_f > Q_i$) but decrease in downstream locations ($Q_f < Q_i$), or vice versa.

We refer to the position of such a reversal (e.g. from increasing to decreasing discharge or vice versa) as x_{sc}. At this position discharge remains constant, and thus equilibrium river slope does not change following a temporal change in rainfall pattern (at $x = x_{sc}$, $Q_f = Q_i$ and $S_f = S_i$). As we will show, transient responses to temporal changes in rainfall pattern that cause such reversals have distinctive qualities. For now, we note an interesting feature where upstream of x_{sc} initial and final steady state profiles begin to converge (see Figure 2). Thus, x_{sc} marks a local maximum elevation difference between initial and final steady state profiles. This convergent behavior contrasts with expectations for spatially uniform changes in rainfall where the difference in channel bed elevation increases monotonically upstream from the outlet (Figure 1a).

Assuming spatially uniform rock uplift rate and K_p, the maximum difference in elevation along the profile between initial and final steady states, Δz_{Sc}, can be expressed:

$$z_{Sc} = \left(\frac{U}{K_p}\right)^{1/n} \int_{x_b}^{x_{sc}} (Q_f - Q_i)^{-m/n} \text{ dx.} \quad (8)$$

In some circumstances, initial and final steady state profiles can intersect at a position x_{zc} (Figure 2), determined by:

$$0 = \left(\frac{U}{K_p}\right)^{1/n} \int_{x_b}^{x_{zc}} (Q_f - Q_i)^{-m/n} \text{ dx.} \quad (9)$$

Notably, x_{zc} marks a location where the net adjustment to reach steady state elevation changes along the profile from enhanced incision to surface uplift, or vice versa. Temporal changes in rainfall patterns that produce x_{zc} are those that lead to positive relationships between spatially averaged mean rainfall and fluvial relief (Figure 1b).

3.3 Sensitivity Analysis of 1-D River Profiles to Changes in Rainfall Patterns

Next, we explore a simple example scenario to evaluate the sensitivity of discharge and fluvial relief to changes in rainfall pattern. We introduce this analysis here using a steady state profile adjusted to spatially uniform rainfall (Figure 3). While idealized, this simple case is well suited to developing intuition about more complex scenarios, like strengthening or relaxing existing orographic rainfall patterns, which as we show in section 5.1 produce analogous responses to those we discuss here.

We define different fields bounding rainfall gradients that result in different classes of behavior (Figure 3a). Boundaries demarcating these fields are independent of U, K_p, m, and n provided m/n is unchanged. Channel length has a negligible influence for channels longer than a few kilometers where $A >> A_c$, and only minor influence for different m/n ratios (~0.4-0.6). The h exponent in Hack's Law (Equation 2) can influence field boundaries, as indicated in Figure 3a; however, the effect is minor for typical h values (1.67 [?]h [?] 2; e.g., Rigon et al., 1996). Contours of Q_f/Q_i illustrate the extent to which a given rainfall gradient represents a net wetter ($Q_f/Q_i > 1$) or drier ($Q_f/Q_i < 1$) condition (Figure 3b). Contours of R_f/R_i describe the extent to which fluvial relief increases ($R_f/R_i > 1$) or decreases ($R_f/R_i < 1$). These contours show that

6

steady state fluvial relief is sensibly correlated with discharge, but the relationship is complex when rainfall is not spatially uniform.

White fields (Figure 3, both panels) encompass rainfall gradients – and spatially uniform changes in rainfall – where the profile would experience wetter or drier conditions everywhere. Transient adjustments to such gradients generally mimic adjustments to spatially uniform increases or decreases in rainfall, although spatially variable changes are expected to affect adjustments differently than uniform changes in detail (e.g., see section 5.1.2).

Light grey fields (Figure 3a) encompass rainfall gradients where relative changes in discharge and equilibrium slope would invert along the profile, but initial and final steady state profiles would not intersect (i.e., produce x_{sc} , but not x_{zc}). The mode of transient adjustment is variable in space and time upstream of x_{sc} (variably $E > U$ or $E < U$; Figure 2). Despite this, the net change in fluvial relief is inversely related to the change in mean rainfall at steady state, consistent with expectations for spatially uniform changes in rainfall. x_{sc} marks the position of the absolute maximum elevation difference between initial and final steady states in these cases, not the channel head. Therefore, while each point along the profile experiences net incision or surface uplift to reach steady state, the largest differences in elevation between initial and final steady states are along the central part of the profile.

Dark grey fields (Figure 3a) encompass rainfall gradients that produce both x_{sc} and x_{zc} and are characterized by the most complex transient responses (e.g., Figure 2). Implied spatial patterns of relative changes in discharge and slope follow as for light grey fields, and modes of transient adjustment are similarly spatiotemporally variable upstream from x_{sc} . The distinguishing feature of these gradients is that the resulting steady state fluvial relief is positively related to the change in spatially averaged mean rainfall (e.g., Figures 1b, 2), contrary to expectations for spatially uniform changes in rainfall. This results from the non-linear influence of discharge on channel slope and the cumulative influence of downstream slopes on channel elevation. The absolute maximum difference in elevation between initial and final steady states may either be at x_{sc} or at the channel head in these cases depending on specific characteristics of the change in rainfall gradient.

This analysis reveals several interesting ways that changes in rainfall pattern influence river profiles differently than expected for uniform changes. Note, we define our usage of 'complex' transient responses hereafter to include all responses that result in an along-stream inversion in the change in discharge, unless we specify otherwise (i.e., cases where x_{sc} exists; both grey fields in Figure 3a). First, changes in longitudinal rainfall gradients that result in complex transient responses appear relatively common and do not require large changes in rainfall patterns or total rainfall. That these complex responses arise readily from a range of changes in rainfall patterns suggests that they may be a typical aspect of landscape evolution in mountain settings. For instance, this scenario implies topographic growth of incipient mountain ranges may be supported or suppressed by the orographic rainfall patterns they generate, depending on where rainfall is concentrated, even if they experience more total rainfall as a result (e.g., Roe et al., 2003).

Among changes in rainfall pattern where complex responses result in a positive relationship between the change in mean rainfall and fluvial relief (dark grey fields in Figure 3a), changes to top-heavy and bottom-heavy conditions have an asymmetric influence on fluvial relief. Top-heavy gradients in this category always inhibit growth of fluvial relief (R_f/R_i always < 1) and bottom-heavy gradients promote topographic growth, but incremental changes in bottom-heavy gradients result in greater increases (Figure 3). Incremental increases in rainfall upstream (top-heavy) suppress the rate at which slope increases upstream, limiting potential elevation change. In contrast, incremental decreases in rainfall upstream (bottom-heavy) enhance increases in slope upstream and support greater elevations.

To get a sense for potential magnitudes of topographic changes that changes in climate might produce, we tested a wide range of parameters that may be applicable to major mountain ranges (e.g., K_p , U, h , L). We find that a temporal change in rainfall pattern alone may support as much as ˜10^2–10^3 m of change in fluvial relief in the opposite direction expected from the spatially averaged change in mean rainfall (e.g., an

increase in relief associated with an increase in mean rainfall). The same climate change may also drive up to ~10^1–10^2 m of enhanced incision or surface uplift along downstream and central portions of river profiles in the manner consistent with conventional expectations for the change in mean rainfall. This spatially segregated behavior may be particularly important for understanding how adjustments to climate changes are expressed, sediment transport out of mountain catchments, and fluvial terraces to name a few examples. While we do not treat the latter two points further here, they nevertheless warrant more research.

Taken together, this analysis supports the notion that spatially variable changes in rainfall pattern can readily and importantly influence landscape form and processes in ways that fundamentally differ from expectations for spatially uniform changes in rainfall.

4. Transient Catchment Response to Changes in Rainfall Patterns

Many of the ideas laid out above for 1-dimensional profiles intuitively transfer to understanding how signals related to changing rainfall patterns propagate through a drainage network, albeit with some additional considerations. It is important to remember that trunk (transverse) rivers control base level for tributaries. Complex responses, like those described above where both the magnitude and mode of transient adjustment vary along the trunk profile in space and time, necessarily result in varying boundary conditions for tributaries. In addition, tributary responses to these variable base level signals are modulated by the rainfall history experienced by a given tributary, which is always different from the trunk. Finally, adjustments migrate upstream at a finite rate, so there is a time lag between a change in rainfall pattern and arrival of the associated base level signals from the trunk adjustment to a given tributary. The duration of this lag, as well as local rainfall conditions within a tributary catchment, are a function of its position.

Following Riihimaki et al. (2007), we use a quasi-two-dimensional model to explore catchment response. We abstract river basin topology to comprise a single one-dimensional trunk profile and 51 regularly spaced (1 km spacing) one-dimensional tributary profiles. Tributary outlets are fixed to the elevation of the trunk profile at their confluence. Discharge does not pass from tributaries to the trunk river as drainage area along the trunk and each tributary follows Hack's Law (equation 2) independently. This means that there is not two-dimensional hydrological coupling between trunk and tributary rivers through discharge, but transient signals are communicated through variations in tributary base level. This approach allows closely spaced tributaries with identical characteristics to isolate the influence of spatial variations in rainfall within the larger catchment that would not be possible to the same degree with 2-dimensional modelling approaches.

Although our model setup is abstract, it allows us to compare expected patterns of erosion and channel response along the trunk and within small trunk-stream tributaries in a way that is portable to natural river networks. Because drainage area increases along the modeled trunk river following Hack's Law, independent of the distribution of modeled tributaries, at each point along the trunk river discharge accumulation approximates that of a typical drainage basin aligned along the orographic rainfall gradient. In this light, the trellis configuration of tributaries we model is representative of a subset of small, approximately trellised trunk-stream tributaries that typically exist within more complex river network structures and are often targeted for sampling of detrital sediment (e.g., Ouimet et al., 2009). These small tributaries also do not contribute significantly to downstream increases in drainage area (or discharge) of larger rivers into which they drain, meaning discharge accumulation along large rivers is largely decoupled from the hydrology of small tributaries. Therefore, the simplifications we make to the hydrology are also generally consistent with conditions created by targeting small tributaries situated along large rivers in a trellis-like fashion.

In the following, we explore the transient response of modelled river basins to four representative climate change scenarios: (1) a spatially uniform decrease in rainfall, (2) a spatially uniform increase in rainfall, (3) a shift from spatially uniform rainfall to a bottom-heavy rainfall gradient, and (4) a shift from spatially uniform rainfall to a top-heavy rainfall gradient. The initial condition for all models is steady state with spatially uniform rainfall. Imposed changes in rainfall evolve at a linear rate over the first 10 kyr of model time at all points along each channel. Tributaries are modelled with spatially uniform rainfall set by their position along the trunk profile, and individual tributaries experience spatially uniform changes in rainfall

as rainfall gradients evolve. This simplification is consistent with the notion that, due to their smaller areal extent and orientation, tributaries set within mountain-belt scale orographic rainfall patterns generally experience relatively uniform rainfall. As we show in section 5.1, more realistic scenarios, such as the intensification or relaxation of an existing orographic rainfall gradient, produce analogous behavior to these simple scenarios. The simplicity of the idealized scenarios described here makes them especially effective for developing intuition about response characteristics in general.

4.1 Case 1: Spatially Uniform Decrease in Rainfall

The modelled catchment response to a spatially uniform decrease in rainfall is characterized by adjustment to uniformly higher k_{sn} and an increase in steady state fluvial relief. For this model run, rainfall is decreased from 2 to 1 m/yr, causing discharge to decrease similarly by 50% (Movie S1).

Erosion rate decreases across the entire channel network following the change in rainfall, driven by a decrease in erosional efficiency directly proportional in magnitude (i.e., 50%; recall $m = 1$). The resulting disequilibrium, with $E < U$, drives surface uplift and upstream migration of a convex-up slope-break knickpoint, and eventually a ~40% increase in fluvial relief.

In k_{sn}–E_{avg} space (Figure 4a), the decrease in erosional efficiency driven by the change rainfall causes the trunk river and tributary network to shift uniformly onto a different erosional efficiency curve that describes the expected relationship between k_{sn} and erosion rate for a given erosional efficiency at steady state. Specifically, both shift from $K=2 \cdot K_p$ to $K=K_p (K_f = 0.5 \cdot K_i)$. Following this initial shift, the trunk river and individual tributaries approximately follow this new curve ($K=K_p$) during adjustment toward higher erosion rates and k_{sn} to return to steady state, although in detail they deviate slightly. This deviation is a result of averaging segments above and below the migrating knickpoint into mean (upstream-averaged) k_{sn} and erosion rate values. Insofar as the relationship between channel steepness and erosion rate implies a given erosional efficiency, these deviations imply an apparent erosional efficiency different, albeit minor in this case, from the modelled value.

In k_{sn-q}–E_{avg} space (Figure 4b), both the initial and final steady state conditions plot in the same location on the $K=K_p$ curve. Here, the initial decrease in erosional efficiency causes the trunk and tributaries to shift uniformly along this curve to lower k_{sn-q} and erosion rate rather than shifting onto a different curve. During adjustment both generally follow this curve to return to steady state, minor transient deviations as seen for k_{sn} notwithstanding.

4.2 Case 2: Spatially Uniform Increase in Rainfall

The modelled catchment response to a spatially uniform increase in rainfall is characterized by adjustment to uniformly lower k_{sn} and a decrease in steady state fluvial relief. To compare responses, we invert the change in rainfall from the previous example, and rainfall is increased from 1 to 2 m/yr, resulting in a 100% increase in discharge (Movie S2).

We observe a broadly symmetrical response to Case 1, where the twofold increase in rainfall leads to an initial twofold increase in erosion rate ($E > U$) and a ~30% decrease in steady state fluvial relief. The transient knickpoint is concave-up in this case and it broadens as it migrates upstream, as is expected for a concave-up knickpoints where $n > 1$ (Royden & Perron, 2013). The signal of transient adjustment communicated to tributaries is consequently protracted, making adjustments more diffuse.

Responses reflected in k_{sn}–E_{avg} and k_{sn-q}–E_{avg} relationships also mirror Case 1. As is characteristic for k_{sn}, the initial change in erosional efficiency causes the trunk and tributary network to shift onto a different steady state erosional efficiency curve; in this case, from $K =K_p$ to $K = 2 \cdot K_p$, and they generally follow this curve during adjustment (Figure 4a). Minor deviations from this curve exhibit a convex-up pattern (inverted from Case 1) due to the opposite knickpoint shape. Meanwhile in k_{sn-q}–E_{avg} space (Figure 4b), the initial and final equilibrium conditions for both the trunk and tributary network plot in the same location, as in Case 1. The change in rainfall again causes a shift only along the $K=K_p$ curve, but to uniformly higher k_{sn-q} and erosion rate in this case, and they generally follow this curve during adjustment back to steady state.

4.3 Case 3: Spatially Uniform to Bottom-heavy

In this scenario, we model the catchment response to a change in rainfall pattern from spatially uniform 1.5 m/yr to a gradient that decreases upstream from 4 to 0.5 m/yr, resulting in a complex transient response. Mean rainfall increases by ~80%, which remarkably also drives a 30% increase in fluvial relief that contrasts with the 25% decrease expected for a spatially uniform increase in rainfall of the same magnitude (Figure 3b; Movie S3).

4.3.1 Case 3: Trunk Response

In this case, because the change in rainfall is spatially variable along the trunk river, the initial change in erosion rate is also variable. The trunk river experiences an approximately 80% increase in erosion rate at the outlet ($E > U$), and a decrease of 67% in the headwaters ($E < U$), corresponding to the change in upstream average rainfall along its length. At x_{sc} (located ~27 km upstream from the outlet), $Q_f = Q_i$, $S_f = S_i$, and so immediately following the change in rainfall $E = U$. Enhanced incision at the outlet produces a concave-up knickpoint; however, as this knickpoint migrates upstream it progressively sharpens and eventually evolves into an oversteepened convex-up knickpoint, contrasting with expectations for the increase in rainfall (e.g. , Case 2). Oversteepening is a consequence of the upstream decrease in erosional efficiency driven by the rainfall gradient that is exacerbated by, but does not depend on, differing modes of adjustment upstream and downstream of x_{sc} related to the complex response. This is analogous to knickpoint behavior described by Forte et al. (2016) and Darling et al. (2020) where modelled lithologic contacts demarcate similar relative variations in erosional efficiency (i.e. hard rocks over soft rocks). Lastly, we note that everywhere upstream of x_{sc} over-adjusts during the transient response, which is a characteristic of complex responses in general, leading to variable modes of adjustment in time and space. The overadjustment we observe is essentially the whiplash response described by Gasparini et al. (2006, 2007), but notably results here without sediment flux. This continuous evolution of the trunk knickpoint has important consequences for signals passed to tributaries.

4.3.2 Case 3: Tributary Response

Tributary responses to the change in rainfall pattern depend largely on their position. Individual tributaries experience changes in erosional efficiency proportional to their change in rainfall. Changes to both quantities are always different from those of the trunk river at their confluence (Figure 2a inset). Additionally, tributaries also respond to changing boundary conditions related to adjustment of the trunk river. These signals are often conflicting. For example , enhanced incision along the trunk river downstream from x_{sc} causes tributaries there to experience a relative increase in the rate of base-level fall. Alone, this should promote steepening, but higher erosional efficiency (higher rainfall) counteracts steepening. The net effect of this competition plays out differently as a function of tributary position as 1) the discrepancy between the local rainfall conditions experienced by tributaries and the upstream averaged rainfall experienced by the trunk profile narrows upstream (Figure 2a inset), 2) the transient base level signal (i.e., trunk knickpoint) changes shape as it sweeps upstream, and 3) the duration of transient adjustment increases upstream.

4.3.3 Case 3: k_{sn}–E_{avg} and $k_{sn\text{-}q}$–E_{avg}

Plots of k_{sn}–E_{avg} and $k_{sn\text{-}q}$–E_{avg} clarify some additional features of the transient response (Figure 5). The trunk profile exhibits higher k_{sn} and $k_{sn\text{-}q}$ values and spans a relatively narrower range in erosion rates than tributaries during transient adjustment, reflecting the fundamentally different ways they experience the modelled rainfall gradient. This behavior illustrates that the network of tributaries (isolated catchments that individually experience relatively uniform rainfall but collectively span a range of conditions) inherently incorporates a more direct signal of the change in rainfall patterns compared to the trunk, which averages upstream rainfall variations. This is consistent with findings by Han et al. (2015) for steady state landscapes exposed to orographic rainfall and is important for designing an effective sampling strategy in the field – discussed further in section 5.3.

In k_{sn}–E_{avg} space (Figures 5a, 5b), shifts onto different erosional efficiency curves occur as in Cases 1 & 2,

10

but here the spatial rainfall variability causes different positions along the trunk and individual tributaries shift by different amounts. The trunk profile response spans from $K = 0.5 \cdot K_p$ to ~$1.8 \cdot K_p$, while the network of tributaries spans from $K = 0.5 \cdot K_p$ to $4 \cdot K_p$. To first order, points representing a given location along the trunk or a given tributary move along these curves reflecting local erosional efficiency during adjustment toward steady state as in Cases 1 & 2, but again deviate in detail. Trajectories are more complex in this case because of the interplay between changes in erosional efficiency and baselevel variations in modulating tributary channel steepness and the over-adjustments mentioned previously (*c.f.*, Figures 4 & 5). Finally, we note an interesting feature where the range of erosional efficiency values that correspond to upstream mean k_{sn} at steady state for the trunk profile ($K = 0.5 \cdot K_p$ to ~$1.8 \cdot K_p$) are lower than that implied by mean rainfall (i.e., $K =$ ~$2.7 \cdot K_p$; Figures 1b, 5a) – discussed further in section 5.2.

In $k_{sn\text{-}q}$ –E_{avg} space (Figures 5c, 5d), differences between trunk and tributary responses and k_{sn} vs. $k_{sn\text{-}q}$ are readily apparent. Initial and final steady state conditions plot in the same position, as is characteristic of $k_{sn\text{-}q}$ where uplift rate is constant. Following the change in rainfall, the trunk profile expands slightly obliquely to the $K=K_p$ curve, where downstream locations are systematically shifted toward higher erosional efficiency. This shift reflects systematic slope adjustments that must occur along the trunk to bring it into equilibrium with the non-uniform rainfall pattern and decreases with time as these adjustments take place. Apart from this minor shift, different positions along the trunk profile generally follow the $K=K_p$ curve during adjustment back to steady state. In tributaries, on the other hand, the change in rainfall causes expansion precisely along the $K=K_p$ curve because they experience no along-stream variations in rainfall. Tributaries again generally evolve along the $K=K_p$ curve toward steady state (as with cases 1 and 2). Transient morphological adjustments affect this trajectory in detail and deviations, which affect apparent erosional efficiency, are more significant in drier tributaries near the headwaters. Overadjustment is also evident for both the trunk and tributaries in this space, but because transient evolution is generally along the steady state curve, it does not significantly affect the apparent erosional efficiency. As a final note, dispersion around the steady state erosional efficiency curve in $k_{sn\text{-}q}$ –E_{avg} space is minor over the duration of the transient adjustment compared to dispersion in k_{sn} –E_{avg} space – we expand on implications from this point in section 5.3.

4.4 Case 4: Spatially Uniform to Top-heavy

In this final case, we the model the catchment response to a change in rainfall pattern from spatially uniform 1.5 m/yr to a gradient that increases upstream from 0.25 to 2.25 m/yr, which also results in a complex transient response. Mean rainfall decreases by 33% and fluvial relief also decreases by 10% (Figure 3; Movie S4), which contrasts with the 22% increase in fluvial relief expected for a spatially uniform decrease in rainfall of the same magnitude.

4.4.1 Case 4: Trunk Response

In this case, the trunk river experiences a 33% initial decrease in erosional efficiency and erosion rate at the outlet, and a 50% increase in the headwaters following the change in rainfall pattern (Figure 6). This range is significantly narrower than the range of variations in rainfall because of the buffering effect that concentrating rainfall in the headwaters has on downstream changes in discharge (e.g., Figure 2b inset). Like Case 3, because this scenario also exhibits a complex transient response, the transition between decreases in erosion rate downstream and increases upstream is initially at position x_{sc}. Unlike Case 3, knickpoint shape does not invert during transient adjustment and is always convex-up. Interestingly, combined with observations from Case 3, this suggests that complex responses generally are more likely to exhibit convex-up knickpoints. Retention of the knickpoint shape is accommodated by over-adjustment upstream of x_{sc}, specifically by progressively more rapid upstream adjustment (higher erosional efficiency) toward gentler slopes that outpaces downstream adjustment. By the time that the migrating trunk knickpoint reaches positions upstream of x_{sc}, the profile has incised below its equilibrium elevation and is shallower than its equilibrium slope. Thus, the profile is forced to uplift and steepen to reach steady state, preserving the convex-up knickpoint shape (Movie S4).

11

4.4.2 Case 4 Tributary Response

Complexities in the trunk response again dramatically affect the tributary responses, and generally mirror complexities discussed in Case 3. Tributaries again respond to variable and commonly conflicting signals. In this case, tributaries downstream from x_{sc} initially respond to a decrease in rainfall (lower erosional efficiency) by steepening. However, decreases in erosional efficiency along the trunk profile drives steepening and surface uplift, forcing tributaries to respond to a conflicting signal of base-level rise (Movie S4). Additionally, tributaries in downstream locations are relatively much drier and adjust relatively slowly compared to upstream locations. Interestingly, the trunk profile adjusts and communicates transient base-level signals upstream to wetter tributaries relatively quickly compared to the adjustment timescale of these dry tributaries, which follows as the trunk river has much higher erosional efficiency from rainfall concentrated in its headwaters. The initially counterintuitive result of this is that central portions of the catchment are the first to achieve steady state (i.e., both the trunk profile and tributaries achieve the new steady state), followed by the headwaters, and lastly tributaries near the outlet where the transient signal originated, which contrasts with the common expectation of adjustment proceeding in an upstream fashion.

4.3.3 Case 4: k_{sn}–E_{avg} and $k_{sn\text{-}q}$–E_{avg}

Evolution of k_{sn} –E_{avg} and $k_{sn\text{-}q}$ –E_{avg} relationships during the transient response are generally similar to Case 3, but with a few exceptions. First, the disparity between final steady state conditions for the trunk profile and network of tributaries is significantly greater than Case 3 (Figures 6a, 6b), which reflects the extent to which the rainfall pattern buffers variations in erosional efficiency along the trunk. Also, in $k_{sn\text{-}q}$ –E_{avg} space, apparent erosional efficiency is more strongly affected during transient adjustment in the tributary network compared to the trunk profile (transient deviations from the $K=K_p$ curve), but also compared to Case 3. Large deviations are again restricted to drier tributary catchments, and comparison to Case 3 expresses that changes in rainfall have a non-linear effect (Equations 1). That said, even these stronger effects on apparent erosional efficiency in $k_{sn\text{-}q}$ –E_{avg} space are still minor compared to representing any equivalent time in the k_{sn} –E_{avg} relationship with a spatially and temporally uniform erosional efficiency value. Finally, also like Case 3, the range of erosional efficiency values for the trunk profile ($K = $ ˜$1.8 \cdot K_p$ to $2.25 \cdot K_p$) are different, but in this case higher than is implied by mean rainfall (i.e., $K = $ ˜K_p ; Figures 1b, 6a) – discussed further in section 5.2.

5. Discussion

The central themes we have explored so far are how the spatial rainfall pattern influences the channel profile morphology, and how temporal changes in rainfall pattern affect erosion rates and profile morphology during periods of transient adjustment. We have detailed the expected response to along-stream variations in erosional efficiency caused by spatial rainfall gradients according to the SPM and have shown how the transient response to a change in rainfall pattern is fundamentally different from a spatially uniform change in rainfall. A change in rainfall pattern will always result in spatially variable changes of erosion rates that also change with time during the transient response. In some circumstances a given location may, over time, experience both elevated and reduced erosion rates (and channel steepness values) relative to equilibrium in response to a single change in rainfall. It is important to keep in mind, however, that the nature of transient response depends strongly on the initial conditions at the time of the change in rainfall pattern. Therefore, there is a complex relationship between the transient response at any given location or time and both the change in mean rainfall and the final rainfall pattern. In the following discussion, we focus on highlighting some implications for the different expectations that follow from changes in rainfall pattern and discussing examples where conventional expectations based on spatially uniform changes in rainfall can potentially lead researchers astray. Where possible, we attempt to identify additional information or strategies that may be leveraged by future studies.

5.1 Revising Expectations for Erosional and Morphological Responses to Changing Climate
5.1.1 Relative Nature of Erosional Response

To this point, our choice of a steady state initial condition with spatially uniform rainfall has been convenient,

as have been the terms top-heavy and bottom-heavy to describe typical orographic rainfall patterns. While idealized, this provides an intuitive starting point for understanding how more complicated – but almost certainly more realistic – climate change scenarios might play out. Recall, according to the SPM, transient climate-driven changes in erosion rate are dictated by a *relative* change in discharge. Where discharge is increased, erosion rates increase in response and river gradient declines toward a new equilibrium steepness; thus, a river subjected to an increase in discharge can be considered locally, if transiently, oversteepened relative to equilibrium, and vice versa. As we have shown, because discharge generally accumulates non-linearly downstream within a river basin, a change in rainfall pattern can create circumstances where the relative change in discharge inverts along the river length – at position x_{sc} – producing a complex transient response (Figures 2 & 3). This implies that the river is simultaneously oversteepened and understeepened on either side of position x_{sc} . These transient states dictate whether erosion rates initially increase or decrease following the change in rainfall, respectively, not whether the new rainfall pattern is itself top-heavy or bottom-heavy, and the positions of these transient states shift throughout adjustment.

The nature of landscape response to relative changes in discharge implies, for instance, that relaxation of a bottom-heavy rainfall gradient can cause a complex transient response resembling a change from uniform to top-heavy rainfall patterns. That is, a weaker bottom-heavy gradient is relatively top-heavy compared to an extreme bottom-heavy gradient; similarly, a gentler top-heavy gradient is relatively bottom-heavy compared to an extreme top-heavy gradient, and vice versa (Figure 7). Thus, for example, in the case of a change in climate that causes an extreme bottom-heavy rainfall gradient to become less bottom-heavy *and* results in a complex transient response (e.g., Figure 7a), rainfall and erosion rate are expected to increase in the headwaters of the catchment and decrease near the outlet as seen for Case 4 (uniform to top-heavy). This response is not consistent with expectations for any uniform increase or decrease in rainfall, even if such a shift accurately reflects the change in mean rainfall. Therefore, neither the final rainfall pattern alone (i.e., modern observed pattern) nor accurate inference about the relative change in mean rainfall (wetter or drier) necessarily allow a robust prediction of changes in erosion rate within a catchment following a change in climate where rainfall patterns have changed significantly.

Interestingly, changes in climate do not need to involve extreme changes in rainfall patterns (e.g., reversal from top-heavy to bottom-heavy), or to occur over short timescales to drive complex transient responses. Indeed, even subtle changes in rainfall pattern potentially driven by minor, commonly occurring variations temperature and atmospheric conditions (e.g., Mutz et al., 2018; Roe et al., 2003; Siler & Roe, 2014), may induce complex responses and significantly, if temporarily, alter the spatial pattern of erosion in a catchment (Figures 3 & 7). Indeed, such climate changes may have occurred in the Peruvian Andes and eastern-central Himalaya in the transition from Pliocene to Pleistocene climates, the latter represented by Last Glacial Maximum conditions (LGM; Figure 7c & 7d). Even if rivers in each of these ranges were in a transient state during Pliocene time, any adjustment toward equilibrium with the Pliocene rainfall pattern that occurred would then be in disequilibrium with the Pleistocene (LGM) rainfall pattern, and would have driven a complex response.

As transient adjustments proceed relatively more rapidly where rainfall is more concentrated (i.e., erosional efficiency is higher), changes in rainfall pattern have the potential to produce spatially distinct effects different from what would be expected from considering uniform changes in mean climate. Transient adjustments may therefore be relatively enhanced or underdeveloped in different locations within the same catchment, or adjustment to quasi-equilibrium may be essentially complete in some locations while others reflect only an incipient response to the climate change. We noted an example of this behavior in Case 4, where low-elevation dry tributary catchments preserve transient conditions the longest, contrasting with the notion that headwater catchments should be the last to equilibrate. Similarly segregated conditions occur in Case 3, where adjustment to quasi-equilibrium is essentially complete in wet low-elevation catchments long before the migrating trunk knickpoint even reaches drier high-elevation catchments. Because such complex, climate change-driven landscape adjustments are not reasonably captured by a conceptual framework based on spatially uniform changes in rainfall (e.g., compare Cases 3 & 4 to Cases 1 & 2), apparent inconsistencies between expectations and observations have the potential to give a false impression about the primary

forcing(s) controlling erosion rates.

Additionally, if large-scale changes in rainfall patterns like we model develop incrementally over long times-cales (e.g., millions of years), they could still result in complex transient responses. Greenhouse-icehouse transitions and orogenic growth are among many geologically significant events that may cause temporally distinct, sustained, and dramatic changes to climate and/or circulation patterns where complex responses could arise (Mutz et al., 2018; Poulsen et al., 2010; Roe et al., 2003; Zachos et al., 2001), If, for example, the bottom-heavy gradient in Case 3 instead develops over several million years, regardless any added complexity to the general trajectory of this change in rainfall pattern, the result is that it supports a 30% increase fluvial relief despite also increasing total rainfall by ~80%, and channel steepness patterns fundamentally change as the catchment adjusts. Gradual changes in rainfall patterns cause morphological adjustments to become more diffuse, and induce relatively smaller transient changes in erosion rate than abrupt changes. However, the spatial pattern of erosion is still significantly affected (i.e., in excess of a factor or two from steady state) so long as the timescale over which the rainfall pattern evolves does not far exceed that of the catchment adjustment timescale, which may be several million years for large river basins (Roe et al., 2003; Whipple, 2001). As such, the general characteristics of the classes of transient behavior following changes in rainfall pattern toward *relatively* bottom-heavy or top-heavy conditions remain intact, even for long-term transient responses.

5.1.2 Multi-stage Adjustment

It has long been recognized that spatially uniform changes in rainfall should promote transient changes in erosion rate everywhere across a landscape, which cause morphological adjustments to sweep upstream to restore erosional equilibrium (e.g., Tucker & Slingerland, 1997; Whipple & Tucker, 1999). Our model is fully consistent with this expectation under such conditions (e.g., Cases 1 & 2). In addition, we have shown that responses to changes in the rainfall pattern are variable in both space and time (e.g., Cases 3 & 4). As a consequence, following any non-uniform change in rainfall pattern, distinct initial morphological and erosional changes always precede the upstream sweeping adjustments that ultimately restore equilibrium. Contrary to expectations for a uniform change in rainfall, we find that catchments characteristically exhibit a relatively protracted, multi-stage, and spatio-temporally variable response to a single temporal change in rainfall pattern (Figure 8; Movie S5). We emphasize that this behavior is a general characteristic of any spatially variable change in rainfall pattern and is not exclusive to those that induce the complex transient responses. This leads to novel expectations for how transient responses to changes in climate should be expressed across a landscape and has potentially important implications for detecting transient landscape responses to climate changes.

The initial stage of morphological adjustment begins synchronously across the entire river basin following a change in rainfall pattern. At the onset, local erosion rate is everywhere a function of the local relative change in discharge. As this initial stage proceeds, spatial variations in erosion rate along the trunk river produce morphological changes along its length that progress at different rates (variable erosional efficiency). Importantly, this means that initial, or "relict", conditions are often not preserved upstream of slope-break knickpoints on the trunk profile; the profile is progressively modified as adjustment proceeds even upstream of the main knickpoint. Indeed, the resemblance of "unadjusted" profile segments upstream from the main knickpoint to their initial state diminishes with time during the transient response, and thus with relative position upstream. This contrasts with spatially uniform changes in rainfall (and erosional efficiency; e.g., Cases 1&2), or uplift rate that does not affect erosional efficiency, that allow preservation of relict morphological characteristics (e.g., k_{sn}) upstream of migrating transient knickpoints, as is often assumed in analysis and inversions of river profiles (e.g., Clark et al., 2006; Fox et al., 2014; Gallen et al., 2013; Goren et al., 2014; Kirby & Whipple, 2012; Miller et al., 2013; Schoenbohm et al., 2004; Whittaker et al., 2007). More broadly, this contrasts with the notion that adjustments to climate change should simply propagate upstream from base level as is expected for other external changes (e.g., uplift rate). While there is a signal of transient adjustment that indeed migrates upstream, significant amounts of surface uplift, as observed in Case 3 (Movie S3), or incision, as observed in Case 4 (Movie S4), along with changes in channel steepness

14

can occur prior to arrival of this signal. Nevertheless, these changes are in response to the change in climate. Additionally, spatio-temporally variable adjustments along the trunk profile dictate that individual tributaries experience temporally variable rates of base-level fall until the trunk profile reaches a new equilibrium at their confluence (Movie S3 & S4).

The continuous, yet variable nature of base-level fall imposed by the trunk river on tributaries during the initial stage of adjustment generally results in a broad adjustment zone characterized by smooth variations in channel steepness in tributary catchments. Indeed, tributaries in our model located in upstream positions, where this initial adjustment stage is relatively long-lived (compared to tributaries located near the trunk outlet), experience significant changes in slope and relief without formation of any knickpoints (e.g., Figure 8b; Movies S3 & S4). Importantly, this shows that tributaries are not insulated from effects of spatially variable changes in rainfall (variable erosional efficiency) along their trunk river, even if they experience essentially uniform rainfall throughout their history. Furthermore, they may appear relatively well-adjusted (graded) during periods of transient adjustment despite significant deviation from both initial and final steady state conditions (Figure 8b; also see Tributary 2, Movies S3 & S4).

Adjustment to quasi-steady-state conditions along the trunk river, which may or may not be associated with the upstream migration of a significant or obvious slope-break knickpoint, defines the beginning of the second – and final – stage of adjustment in our model landscapes (Figure 8). The rate of base-level fall experienced by a given tributary stabilizes upon local adjustment of the trunk profile, representing a distinct change from the initial stage where the rate of base-level fall is temporally variable. Depending on circumstances, this change may be abrupt and produce a discrete knickpoint that sweeps upstream through the tributary catchment. The change in base-level fall rate is the dominant signal exhibited during this second adjustment stage, although it acts upon the profile state reached during the initial adjustment stage, and it is largely a function of the shape and migration rate of the trunk knickpoint. Both factors are controlled by the integrated response of the trunk profile to this point, and therefore do not relate to the change in rainfall pattern in a direct manner. Therefore, the dominant signal passed to tributaries during this second stage, and any knickpoints that form as a result, generally do not reflect the change in rainfall locally within the tributary catchment, and their relationship to the regional rainfall pattern experienced by the trunk stream is complex. This is directly contrary to expectations for spatially uniform changes in rainfall where changes in slope above and below knickpoints should scale with the magnitude of the change in rainfall (e.g., Whipple, 2001).

Extrapolating these observations to natural, inherently more complex river networks, suggests that broad adjustment zones comprising multiple knickpoints might be associated with a given change in rainfall pattern – in contrast to the single knickpoint or knickzone expected to accompany a spatially uniform change in rainfall magnitude (e.g., Case 1 & 2). For instance, if second-order rivers (*sensu* Hack, 1957) experience spatially variable rainfall patterns in addition to the trunk, then we expect third-order rivers should experience an additional pair of adjustment stages. This implies that the full transient response to changes in rainfall pattern may be expressed in a complex fashion, and potentially across a large areal extent, in large river basins (e.g., Figure 8; Movie S5). If true, this multi-stage adjustment behavior may ultimately pose a significant, still unresolved, challenge to recognizing and quantifying transient responses to changes in climate in many settings.

5.2 Recognizing the Influence of Climate on Topography and Erosion Rates *5.2.1 Steady State Relationships among Channel Steepness, Erosion Rate, and Erosional Efficiency*

The SPM makes specific predictions about the relationships among channel steepness, erosion rate, and erosional efficiency (K) at steady state (Equation 6), and as shown by curves in Figures 4-6. Because the role of climate is encapsulated in K, it is important to remember that a uniform K value implies that the influence of climate is uniform over the spatial and temporal scales of interest. Further, the expectation that basin-average topographic metrics like k_{sn} should relate to rainfall in a simple way generally relies on an assumption of a spatially uniform K value. Rainfall gradients systematically affect this expectation, where bottom-heavy gradients result in higher k_{sn} (lower apparent erosional efficiency), while top-heavy

gradients result in lower k_{sn} (higher apparent erosional efficiency) (Figure 9). The magnitude of this effect (as a percentage of actual erosional efficiency) varies with strength of the rainfall gradient. However, k_{sn} values also vary with erosion rate (uplift rate at steady state; Equation 6a). Therefore, while subtle rainfall gradients affect apparent erosional efficiency to a proportionally lesser degree, they can still substantially influence observed k_{sn} values, even at steady state, where uplift rates are higher. This can be important in natural settings where uplift rates, erosional efficiency, and the form of their relationship to topography are generally unknown.

This analysis has two related and important implications. First, interpretation of the controls on topography (e.g., mean k_{sn}, mean gradient, relief, etc.) in terms of climate sensitivity, uplift, and/or rock properties using measurements from catchments that experience the same mean rainfall, but different rainfall patterns, is not necessarily valid even at steady state. Second, it predicts weaker correlations (more dispersed) between topographic metrics and erosion rate than would be expected if rainfall were always uniformly distributed, as is implied by use of basin-average rainfall (Figure 9), simply from neglecting the rainfall pattern. This prediction applies even before considering any geologic uncertainties (e.g., at quasi-steady-state or potentially transient?), analytical uncertainty, and even if no other variations in K exist. Because rainfall gradients create systematic, rather than random, dispersion around relationships expected for uniformly distributed rainfall, there is not necessarily any expectation that larger datasets will more accurately resolve variations in erosional efficiency unless catchments where rainfall is uniform are isolated, or a correction is made for the influence of spatially variable rainfall (e.g., using k_{sn-q}). Rather, compilation of topographic measurements from basins that do and do not experience rainfall gradients can, in and of itself, obscure or, depending on circumstances, distort the actual influence of rainfall on erosional efficiency (Figure 9). This result is of particular importance for designing future efforts to empirically test the SPM in natural settings.

5.2.2 Misleading Transient Signals

Spatial patterns in erosion rate are commonly used to inform tectonic models and to infer rock uplift rates in mountain landscapes (e.g., Adams et al., 2020; Godard et al., 2014; Kober et al., 2015; Morell et al., 2015; Safran et al., 2005; Scherler et al., 2014). However, we have shown that changes in rainfall patterns can drive long-lived and complex spatial patterns of erosion that differ from expectations for uniform changes in rainfall and thus may not be readily recognized and interpreted. We have also shown that that ongoing transient adjustment may not be obviously expressed in landscape morphology (especially for catchment-mean metrics) under some circumstances. If these caveats are not considered, subtly expressed transient spatial variations in erosion rate may be mistaken as representing quasi-steady state spatial variations in uplift rate (i.e., $E = U$). At once this would give a false impression both about the spatial pattern of uplift and the importance of past climate changes on a landscape's evolution, with direct implications for understanding connections among climate, surface processes, and tectonics. Determining whether there are circumstances in which spatial patterns of erosion and topography produced by changes in rainfall patterns that can be misleading enough to confound interpretations about factors controlling landscape evolution is critically important.

During the early transient adjustment in Case 3 (transition to a bottom-heavy rainfall pattern) there is a clear example of how such confusion may occur (Figure 10). Recall, in this case, early transient adjustment produces a concave-up knickpoint along the trunk profile but as it migrates upstream the shape evolves. This creates a broad adjustment zone. Over the first ˜500 kyr, quasi-steady state adjustment proceeds ˜60% upstream along the trunk, but the broad adjustment zone means most tributaries along this length experience a protracted signal of base-level changes related to trunk adjustment. Because these tributaries all also experience a net increase in rainfall, knickpoints associated with local adjustment of the trunk river (Stage 2) tend to relax as they work upstream making them more diffuse. This protracted competition between local rainfall and spatio-temporally variable rates of base-level fall, generally results in diffuse concave to broad convexo-concave adjustment zones in tributaries (e.g., Figure 8a; Movie S5). Broad adjustment zones, particularly concave-up adjustment zones, are inherently subtle and this can inhibit their recognition. This problem may be further compounded by the influence of sediment flux in natural settings (Brocard & van

der Beek, 2006; Whipple & Tucker, 2002). Indeed, even in our idealized model (i.e., no sediment influence), along-stream variations in trunk and tributary local k_{sn} variation is diffuse (Figure 10c). Based on a lack of significant knickpoints that might indicate transient adjustment and the several-fold spatial variation in erosion rate, one might reasonably interpret relationships depicted in Figure 10a reflect a quasi-steady-state landscape adjusted to a spatial gradient in uplift rate. In the absence of known surface breaking structures that might accommodate this gradient in uplift, blind structures may be inferred, with potential implications for tectonic models. The apparent viability of this interpretation is supported by the SPM if rock uplift rate is assumed to match the observed pattern of catchment averaged erosion rates in tributaries (steady-state conditions) as illustrated in Figure 10b. Figure 10b shows that the predicted steady-state upstream-averaged k_{sn} pattern along the trunk river and mean k_{sn} values exhibited by the tributary network is essentially identical to the transient pattern in Figure 10a. Moreover, even in detail, there are only subtle differences in the along-stream pattern of local k_{sn} between the two scenarios (Figure 10c). Thus, in this instance, k_{sn} patterns and erosion rates that actually record a complex transient response to a change in rainfall pattern could reasonably be mistaken for a steady state landscape adjusted to a spatial gradient in uplift.

Although subtle variations in k_{sn} values might give a misleading impression that a landscape is in quasi-steady-state, the spatial pattern of $k_{sn\text{-}q}$ unambiguously suggests along-stream variations in erosion rate exist along both the trunk river and tributaries. $k_{sn\text{-}q}$ also exhibits a coherent pattern of downstream adjustment that could readily be interpreted as a transient signal sweeping upstream through the catchment that, significantly, is inconsistent with a steady state landscape adjusted to the spatial gradient in uplift shown in Figure 10b (Figure 10c). This example shows the potential usefulness of $k_{sn\text{-}q}$, both as a diagnostic tool for detecting ongoing transient adjustment to changes in rainfall patterns where k_{sn} may be misleading and for resolving the relative influences of tectonics and climate.

Finally, we emphasize that our intention is not to suggest all, or any specific examples, where spatial patterns of rock uplift are inferred from erosion rates and channel steepness patterns are incorrect. Rather, our intention here is to highlight the extent to which confusion may be possible under the right circumstances, and how explicitly accounting for rainfall patterns can be a step toward addressing these challenges.

5.3 Toward Detecting the Influence of Climate on Topography and Erosion Rates

Remote analysis of channel steepness patterns can provide a preliminary means to detect whether the climate may be influencing river profiles in a landscape, and whether transient adjustment to a change in climate may be ongoing. For landscapes well-described by the SPM, discrepancies between rainfall conditions experienced by trunk and tributary basins should cause systematic differences in trunk and tributary k_{sn} (Figures 5&6; Gasparini & Whipple, 2014), but not in $k_{sn\text{-}q}$. As illustrated in Figure 10c, the expected contrast in trunk and tributary k_{sn} is most developed at steady state, but it begins manifesting immediately during transient adjustment as differences in local k_{sn} at confluences that migrate upstream (Figure 10c, Movie S5). In contrast, precise agreement between trunk and tributary $k_{sn\text{-}q}$ is expected at steady state, and it is approximately maintained even during periods of adjustment to a change in rainfall pattern. Agreement between trunk and tributary $k_{sn\text{-}q}$ that weakens upstream from confluences may also be an important indication of ongoing transient adjustment that may be difficult detect from the k_{sn} pattern alone (Figure 10c, e.g., as discussed in section 5.2.2). Therefore, comparison of k_{sn} and $k_{sn\text{-}q}$ patterns may be a useful way to diagnose and further assess the potential extent of influence by rainfall gradients, provided the pattern of discharge accumulation can be reasonably estimated (e.g., using high spatial resolution satellite rainfall or nested stream gauge data).

Following topographic analysis, our results have additional implications for designing effective catchment-averaged erosion rate sampling strategies. Broadly, sampling strategies can be grouped into two classes: nested and distributed, described below. Nested, or hierarchical, sampling strategies comprise multiple samples from the same river basin where some or all samples are collected along the trunk river, and where averages typically integrate over very large (10^2–10^5 km^2) drainage areas (e.g., Abbühl et al., 2010; Henck et al., 2011; Portenga et al., 2015; Reinhardt et al., 2007; Safran et al., 2005; Whittaker et al., 2007; Willenbring et al., 2013; Wittmann et al., 2016). In principle, such strategies can allow researchers to assess reproducibility of individual measurements, test sediment mixing models, and sub-divide basins into different sectors to identify

along-stream variations in erosion rates. Given the complex along-stream patterns of erosion rate we observe in response to changing rainfall patterns and widely disparate responses between trunk and tributary profiles, however, our results suggest that caution is warranted in interpreting patterns of erosion rates collected in a nested fashion. In particular, this includes datasets that compile measurements from along trunk rivers and tributary catchments, but also those that compare samples from different large catchments that experience different mean climates and rainfall patterns, even at quasi-steady-state, because how each reflects and experiences variations in rainfall may be fundamentally different. Furthermore, because we find that along-stream variations in erosion rate due to changes in rainfall pattern are characteristically muted along the trunk profile (e.g., Figure 10a), nested strategies may not be appropriate in many settings, especially if the goal is to measure the influence of climate on fluvial incision.

The other widely used strategy, which we refer to as a distributed sampling strategy, targets single samples from catchments that are distributed across a landscape or mountain front, and typically – though certainly not always – comprises relatively smaller (10^0-10^2 km^2) catchments (e.g., Adams et al., 2020; Binnie et al., 2008; Carretier et al., 2013; DiBiase et al., 2010; Godard et al., 2014; Morell et al., 2015; Ouimet et al., 2009; Scherler et al., 2014). This type of strategy generally allows more freedom to carefully select preferable catchments (relatively uniform channel steepness, rainfall, lithology), with the limitation that spatial variations in erosion at the sub-catchment scale are not resolvable with single measurements. In contrast to muted spatial variations in erosion noted for nested strategies, our model results suggest distributed strategies inherently record a more direct signal of climatic influences than nested approaches, consistent with previous findings by Han et al. (2015). However, if inter-catchment variations in rainfall and therefore erosional efficiency are not accounted for, or transient conditions are not recognized, this sensitivity may cause significant dispersion or distortion in measured relationships among landscape metrics, as shown for $k_{sn} - E_{avg}$ relationships (Figures 5b & 6b), and/or lead to misleading spatial patterns in erosion rate and k_{sn} (Figure 10).

Lastly, we note that transient adjustments in response to changes in rainfall pattern do not significantly affect apparent erosional efficiency in $k_{sn-q} - E_{avg}$ relationships where no variations in rock properties exist, even in response to the dramatic shifts in rainfall patterns that we model, regardless of sampling strategy. Indeed, transient deviations from expected steady state relationships modelled in any location are generally well within the analytical uncertainty of measured catchment-average erosion rates from natural landscapes (Figures 5 and 6). Exceptions to this appear to be limited to scenarios where landscapes experience a shift toward arid climates. Nevertheless, transient, spatially variable patterns of erosion caused by changes in rainfall pattern are reflected in k_{sn-q} patterns with good accuracy in our model (Figure 10c, Movie S3-S5). As such, k_{sn-q} may be used to recognize ongoing adjustment to changes in climate where k_{sn} can be ambiguous. We suggest that k_{sn-q}, or a different metric that encompasses the spatial distribution of rainfall (runoff), may be vital component for future efforts to detect climate's influence on and from topography and erosion rates in mountain landscapes where rainfall is inherently spatially variable.

5.4 Caveats and Limitations

Several important caveats should be kept in mind when evaluating the results and subsequent discussion presented here. First, and foremost, our modelling efforts explicitly assume that landscapes are inherently sensitive to climate (through rainfall) in a manner described by the SPM. While the intuitive support for such sensitivity is strong, and evidence from natural landscapes is mounting that broadly support predictions of the SPM (e.g., Adams, et al., 2020; Harel et al., 2016; Lague, 2014), there remains a large amount of uncertainty about the strength of the sensitivity to climate.

Following the core assumption that the SPM is broadly applicable, we note that our model setup is very simple. We assume that all precipitation is rainfall, all rainfall is converted directly to runoff, and we impose constant rainfall gradients that act precisely along the trunk stream and basin axis and that span the entire length of our modelled river basin. While some river basins set within mountain-belt scale orographic precipitation patterns may indeed experience rainfall patterns consistent with this simple geometry, we note that non-linear, and even non-monotonic, rainfall gradients are common for large river basins or those

characterized by high local relief (Roe, 2005). As noted previously, however, the framework we have developed translates well to these more complex scenarios. In addition, we model tributary catchments that are uniform in size that experience uniform rainfall. Preliminary model investigations suggest that although allowing tributary sizes and rainfall to vary causes some dispersion in the relationships illustrated here, the overall behavior we describe remains the dominant signal. Nevertheless, both aspects warrant further investigation.

Lastly, we emphasize that we use a simple version of the SPM where, among other simplifications, we treat erosion exclusively as detachment limited and do not explicitly model erosional thresholds. While assuming continuum detachment-limited conditions is common, particularly for describing erosion in mountain settings, it may not always be appropriate even in these settings to describe transient behavior (Lague, 2014; Whipple & Tucker, 2002). Related to this, our treatment of K_p , while incrementally more complex than spatially uniform erosional efficiency, remains highly simplified. We do not explore the myriad of other factors that control erosional efficiency (K), and the likelihood that rainfall, or more broadly climate, will influence rock erodibility ($\tilde{K}_p$) and size distribution of sediment delivered to rivers (Ferrier et al., 2013; Murphy et al., 2016; Neely & DiBiase, 2020; Riebe et al., 2015; Sklar et al., 2017).

6. Summary and Conclusions

In this study, we use a simple form of the SPM to explore how spatial rainfall gradients influence both river profiles and expectations about how fluvial landscapes should respond to changes in climate. Notably, because changes in climate in mountain settings involve changes in orographic precipitation patterns, advancing understanding about how changes in climate influence the rivers and topography of mountain landscapes requires a more nuanced, spatially variable, treatment of climate at the catchment scale beyond broadly characterized changes in mean climate. We show that spatially varying rainfall conditions experienced by rivers occupying different landscape positions, specifically trunk and tributary rivers, result in fundamentally different expressions of a given rainfall pattern, and that they respond to changes in rainfall pattern in fundamentally different ways. Further, we show how complex transient responses may arise, and that even modest variations in rainfall patterns can significantly affect spatial patterns of erosion and topographic adjustments that directly contrast with expectations for uniform changes in rainfall. In particular, changes in rainfall pattern characteristically result in multi-stage responses with adjustment zones that can be both spatially extensive and subtly expressed, thus difficult to recognize. Interestingly, these finding suggest more broadly that catchments of different sizes, shapes, and locations set within regional orographic precipitation patterns may have unique, and substantially variable, rainfall histories and responses to changes in climate. These complications raise important questions about how best to interpret spatial variations in erosion rates and their relationship with topography. Finally, we discuss how catchment-scale variations in rainfall generally complicate relationships between conventional topographic metrics (e.g., mean k_{sn}) and erosion rates, even at steady state, and implications for empirical tests of the SPM in natural landscapes. More precise metrics like $k_{sn\text{-}q}$ that leverage ever-increasing resolution of rainfall datasets to better account for the spatial distribution of rainfall – specifically its effect on discharge and runoff – may be a significant step toward overcoming these challenges and may prove vital for future studies seeking to quantify interactions between climate, tectonics, and erosion in mountain landscapes.

Acknowledgments

References

Abbühl, L. M., Norton, K. P., Schlunegger, F., Kracht, O., Aldahan, A., & Possnert, G. (2010). El Niño

forcing on 10Be-based surface denudation rates in the northwestern Peruvian Andes? *Geomorphology* ,*123* (3–4), 257–268. https://doi.org/10.1016/j.geomorph.2010.07.017

Adams, B. A., Whipple, K. X., Forte, A. M., Heimsath, A. M., & Hodges, K. V. (2020). Climate controls on erosion in tectonically active landscapes. *Science Advances* , *6* (42), eaaz3166. https://doi.org/10.1126/sciadv.aaz3166

Anders, A. M., Roe, G. H., Hallet, B., Montgomery, D. R., Finnegan, N. J., & Putkonen, J. (2006). Spatial patterns of precipitation and topography in the Himalaya. *Special Paper of the Geological Society of America* , *398* (03), 39–53. https://doi.org/10.1130/2006.2398(03)

Barros, A. P., & Lettenmaier, D. P. (1994). Dynamic modeling of orographically induced precipitation. *Reviews of Geophysics* ,*32* (3), 265–284. https://doi.org/10.1029/94RG00625

Barstad, I., & Smith, R. B. (2005). Evaluation of an orographic precipitation model. *Journal of Hydrometeorology* , *6* (1), 85–99. https://doi.org/10.1175/JHM-404.1

Bierman, P., & Steig, E. J. (1996). Estimating Rates of Denudation Using Cosmogenic Isotope Abundances in Sediment. *Earth Surface Processes and Landforms* , *21* (2), 125–139. https://doi.org/10.1002/(sici)1096-9837(199602)21:2<125::aid-esp511>3.0.co;2-8

Binnie, S. A., Phillips, W. M., Summerfield, M. A., Fifield, L. K., & Spotila, J. A. (2008). Patterns of denudation through time in the San Bernardino Mountains, California: Implications for early-stage orogenesis. *Earth and Planetary Science Letters* ,*276* (1–2), 62–72. https://doi.org/10.1016/j.epsl.2008.09.008

Bonnet, S., & Crave, A. (2003). Landscape response to climate change: Insights from experimental modeling and implications for tectonic versus climatic uplift of topography. *Geology* , *31* (2), 123–126. https://doi.org/10.1130/0091-7613(2003)031<0123:LRTCCI>2.0.CO;2

Bookhagen, B., & Burbank, D. W. (2010). Toward a complete Himalayan hydrological budget: Spatiotemporal distribution of snowmelt and rainfall and their impact on river discharge. *Journal of Geophysical Research: Earth Surface* , *115* (3), 1–25. https://doi.org/10.1029/2009JF001426

Bookhagen, B., & Strecker, M. R. (2008). Orographic barriers, high-resolution TRMM rainfall, and relief variations along the eastern Andes. *Geophysical Research Letters* , *35* (6), 1–6. https://doi.org/10.1029/2007GL032011

Bookhagen, B., & Strecker, M. R. (2012). Spatiotemporal trends in erosion rates across a pronounced rainfall gradient: Examples from the southern Central Andes. *Earth and Planetary Science Letters* ,*327 –328* , 97–110. https://doi.org/10.1016/j.epsl.2012.02.005

Brocard, G. Y., & van der Beek, P. A. (2006). Influence of incision rate, rock strength, and bedload supply on bedrock river gradients and valley-flat widths: Field-based evidence and calibrations from western Alpine rivers (southeast France). In *Tectonics, Climate, and Landscape Evolution* (Vol. 398, pp. 101–126). Geological Society of America. https://doi.org/10.1130/2006.2398(07)

Brown, E. T., Stallard, R. F., Larsen, M. C., Raisbeck, G. M., & Yiou, F. (1995). Denudation rates determined from the accumulation of in situ-produced 10Be in the luquillo experimental forest, Puerto Rico.*Earth and Planetary Science Letters* , *129* (1–4), 193–202. https://doi.org/10.1016/0012-821X(94)00249-X

Burbank, D. W., Blythe, A. E., Putkonen, J., Pratt-Sitaula, B., Gabet, E., Oskin, M., et al. (2003). Decoupling of erosion and precipitation in the Himalayas. *Nature* , *426* (6967), 652–655. https://doi.org/10.1038/nature02187

Carretier, S., Regard, V., Vassallo, R., Aguilar, G., Martinod, J., Riquelme, R., et al. (2013). Slope and climate variability control of erosion in the Andes of central Chile. *Geology* , *41* (2), 195–198. https://doi.org/10.1130/G33735.1

Clark, M. K., Royden, L. H., Whipple, K. X., Burchfiel, B. C., Zhang, X., & Tang, W. (2006). Use of a regional, relict landscape to measure vertical deformation of the eastern Tibetan Plateau. *Journal of Geophysical Research: Earth Surface*, *111* (3), 1–23. https://doi.org/10.1029/2005JF000294

Cyr, A. J., Granger, D. E., Olivetti, V., & Molin, P. (2014). Distinguishing between tectonic and lithologic controls on bedrock channel longitudinal profiles using cosmogenic 10Be erosion rates and channel steepness index. *Geomorphology*, *209*, 27–38. https://doi.org/10.1016/j.geomorph.2013.12.010

D'Arcy, M., & Whittaker, A. C. (2014). Geomorphic constraints on landscape sensitivity to climate in tectonically active areas. *Geomorphology*, *204*, 366–381. https://doi.org/10.1016/j.geomorph.2013.08.019

Darling, A., Whipple, K., Bierman, P., Clarke, B., & Heimsath, A. (2020). Resistant rock layers amplify cosmogenically-determined erosion rates. *Earth Surface Processes and Landforms*, *45* (2), 312–330. https://doi.org/10.1002/esp.4730

DiBiase, R. A., Whipple, K. X., Heimsath, A. M., & Ouimet, W. B. (2010). Landscape form and millennial erosion rates in the San Gabriel Mountains, CA. *Earth and Planetary Science Letters*, *289* (1–2), 134–144. https://doi.org/10.1016/j.epsl.2009.10.036

Duvall, A. (2004). Tectonic and lithologic controls on bedrock channel profiles and processes in coastal California. *Journal of Geophysical Research*, *109* (F3), 1–18. https://doi.org/10.1029/2003jf000086

Ferrier, K. L., Huppert, K. L., & Perron, J. T. (2013). Climatic control of bedrock river incision. *Nature*, *496* (7444), 206–209. https://doi.org/10.1038/nature11982

Finlayson, D. P., Montgomery, D. R., & Hallet, B. (2002). Spatial coincidence of rapid inferred erosion with young metamorphic massifs in the Himalayas. *Geology*, *30* (3), 219–222. https://doi.org/10.1130/0091-7613(2002)030<0219:SCORIE>2.0.CO;2

Forte, A. M., Yanites, B. J., & Whipple, K. X. (2016). Complexities of landscape evolution during incision through layered stratigraphy with contrasts in rock strength. *Earth Surface Processes and Landforms*, *41* (12), 1736–1757. https://doi.org/10.1002/esp.3947

Fox, M., Goren, L., May, D. A., & Willett, S. D. (2014). Inversion of fluvial channels for paleo-rock uplift rates in Taiwan. *Journal of Geophysical Research: Earth Surface*, *119* (9), 1853–1875. https://doi.org/10.1002/2014jf003196

Gallen, S. F., Wegmann, K. W., & Bohnenstiehl, D. W. R. (2013). Miocene rejuvenation of topographic relief in the southern Appalachians. *GSA Today*, *23* (2), 4–10. https://doi.org/10.1130/GSATG163A.1

Gasparini, N. M., & Whipple, K. X. (2014). Diagnosing climatic and tectonic controls on topography: Eastern flank of the northern Bolivian Andes. *Lithosphere*, *6* (4), 230–250. https://doi.org/10.1130/L322.1

Gasparini, N. M., Bras, R. L., & Whipple, K. X. (2006). Numerical modeling of non–steady-state river profile evolution using a sediment-flux-dependent incision model. In S. D. Willett, N. Hovius, M. T. Brandon, & D. M. Fisher (Eds.), *Tectonics, Climate, and Landscape Evolution* (Vol. 398, p. 0). Geological Society of America. https://doi.org/10.1130/2006.2398(08)

Gasparini, N. M., Whipple, K. X., & Bras, R. L. (2007). Predictions of steady state and transient landscape morphology using sediment-flux-dependent river incision models. *Journal of Geophysical Research: Earth Surface*, *112* (3), 1–20. https://doi.org/10.1029/2006JF000567

Godard, V., Bourlès, D. L., Spinabella, F., Burbank, D. W., Bookhagen, B., Fisher, G. B., et al. (2014). Dominance of tectonics over climate in himalayan denudation. *Geology*, *42* (3), 243–246. https://doi.org/10.1130/G35342.1

Goren, L., Fox, M., & Willett, S. D. (2014). Tectonics from fluvial topography using formal linear inversion: Theory and applications to the Inyo Mountains, California. *Journal of Geophysical Research F: Earth Surface*, *119* (8), 1651–1681. https://doi.org/10.1002/2014JF003079

Granger, D. E., Kirchner, J. W., & Finkel, R. (1996). Spatially averaged long-term erosion rates measured from in situ-produced cosmogenic nuclides in alluvial sediment. *Journal of Geology* ,*104* (3), 249–257. https://doi.org/10.1086/629823

Hack, J. T. (1957). *Studies of Longitudinal Stream Profiles in Virginia and Maryland* . Retrieved from https://pubs.usgs.gov/pp/0294b/report.pdf

Han, J., Gasparini, N. M., Johnson, J. P. L., & Murphy, B. P. (2014). Modeling the influence of rainfall gradients on discharge, bedrock erodibility, and river profile evolution, with application to the Big Island, Hawai'i. *Journal of Geophysical Research: Earth Surface* ,*119* (6), 1418–1440. https://doi.org/10.1002/2013JF002961

Han, J., Gasparini, N. M., & Johnson, J. P. L. (2015). Measuring the imprint of orographic rainfall gradients on the morphology of steady-state numerical fluvial landscapes. *Earth Surface Processes and Landforms* , *40* (10), 1334–1350. https://doi.org/10.1002/esp.3723

Harel, M. A., Mudd, S. M., & Attal, M. (2016). Global analysis of the stream power law parameters based on worldwide 10Be denudation rates.*Geomorphology* , *268* , 184–196. https://doi.org/10.1016/j.geomorph.2016.05.035

Henck, A. C., Huntington, K. W., Stone, J. O., Montgomery, D. R., & Hallet, B. (2011). Spatial controls on erosion in the Three Rivers Region, southeastern Tibet and southwestern China. *Earth and Planetary Science Letters* , *303* (1–2), 71–83. https://doi.org/10.1016/j.epsl.2010.12.038

Howard, A. D. (1994). A detachment-limited model of drainage basin evolution. *Water Resources Research* , *30* (7), 2261–2285. https://doi.org/10.1029/94WR00757

Howard, A. D., & Kerby, G. (1983). Channel changes in badlands.*Geological Society of America Bulletin* , *94* , 739–752.

Insel, N., Ehlers, T. A., Schaller, M., Barnes, J. B., Tawackoli, S., & Poulsen, C. J. (2010). Spatial and temporal variability in denudation across the Bolivian Andes from multiple geochronometers.*Geomorphology* , *122* (1–2), 65–77. https://doi.org/10.1016/j.geomorph.2010.05.014

Kirby, E., & Whipple, K. X. (2012). Expression of active tectonics in erosional landscapes. *Journal of Structural Geology* , *44* , 54–75. https://doi.org/10.1016/j.jsg.2012.07.009

Kober, F., Zeilinger, G., Hippe, K., Marc, O., Lendzioch, T., Grischott, R., et al. (2015). Tectonic and lithological controls on denudation rates in the central Bolivian Andes. *Tectonophysics* , *657* , 230–244. https://doi.org/10.1016/j.tecto.2015.06.037

Lague, D. (2014). The stream power river incision model: Evidence, theory and beyond. *Earth Surface Processes and Landforms* ,*39* (1), 38–61. https://doi.org/10.1002/esp.3462

Miller, S. R., Sak, P. B., Kirby, E., & Bierman, P. R. (2013). Neogene rejuvenation of central Appalachian topography: Evidence for differential rock uplift from stream profiles and erosion rates.*Earth and Planetary Science Letters* , *369 –370* (May), 1–12. https://doi.org/10.1016/j.epsl.2013.04.007

Molnar, P. (2001). Climate change, flooding in arid environments, and erosion rates. *Geology* , *29* (12), 1071–1074. https://doi.org/10.1130/0091-7613(2001)029<1071:CCFIAE>2.0.CO

Morell, K. D., Sandiford, M., Rajendran, C. P., Rajendran, K., Alimanovic, A., Fink, D., & Sanwal, J. (2015). Geomorphology reveals active decollement geometry in the central Himalayan seismic gap.*Lithosphere* , *7* (3), 247–256. https://doi.org/10.1130/L407.1

Murphy, B. P., Johnson, J. P. L., Gasparini, N. M., & Sklar, L. S. (2016). Chemical weathering as a mechanism for the climatic control of bedrock river incision. *Nature* , *532* (7598), 223–227. https://doi.org/10.1038/nature17449

Mutz, S. G., Ehlers, T. A., Werner, M., Lohmann, G., Stepanek, C., & Li, J. (2018). Estimates of late Cenozoic climate change relevant to Earth surface processes in tectonically active orogens. *Earth Surface Dynamics* , *6* (2), 271–301. https://doi.org/10.5194/esurf-6-271-2018

Neely, A. B., & DiBiase, R. A. (2020). Drainage area, bedrock fracture spacing, and weathering controls on landscape-scale patterns in surface sediment grain size. *Earth and Space Science Open Archive* , 1–22. https://doi.org/10.1002/essoar.10502617.1

Olen, S. M., Bookhagen, B., & Strecker, M. R. (2016). Role of climate and vegetation density in modulating denudation rates in the Himalaya. *Earth and Planetary Science Letters* , *445* , 57–67. https://doi.org/10.1016/j.epsl.2016.03.047

Ouimet, W. B., Whipple, K. X., & Granger, D. E. (2009). Beyond threshold hillslopes: Channel adjustment to base-level fall in tectonically active mountain ranges. *Geology* , *37* (7), 579–582. https://doi.org/10.1130/G30013A.1

Perron, J. T. (2017). Climate and the Pace of Erosional Landscape Evolution. *Annual Review of Earth and Planetary Sciences* , *45* (1), 561–591. https://doi.org/10.1146/annurev-earth-060614-105405

Portenga, E. W., Bierman, P. R., Duncan, C., Corbett, L. B., Kehrwald, N. M., & Rood, D. H. (2015). Erosion rates of the Bhutanese Himalaya determined using in situ-produced 10Be. *Geomorphology* , *233* , 112–126. https://doi.org/10.1016/j.geomorph.2014.09.027

Poulsen, C. J., Ehlers, T. A., & Insel, N. (2010). Onset of convective rainfall during gradual late miocene rise of the central andes. *Science* , *328* (5977), 490–493. https://doi.org/10.1126/science.1185078

Reinhardt, L. J., Bishop, P., Hoey, T. B., Dempster, T. J., & Sanderson, D. C. W. (2007). Quantification of the transient response to base-level fall in a small mountain catchment: Sierra Nevada, southern Spain. *Journal of Geophysical Research: Earth Surface* , *112* (3). https://doi.org/10.1029/2006JF000524

Riebe, C. S., Sklar, L. S., Lukens, C. E., & Shuster, D. L. (2015). Climate and topography control the size and flux of sediment produced on steep mountain slopes. *Proceedings of the National Academy of Sciences of the United States of America* , *112* (51), 15574–15579. https://doi.org/10.1073/pnas.1503567112

Rigon, R., Rodriguez-Iturbe, I., Maritan, A., Giacometti, A., Tarboton, D. G., & Rinaldo, A. (1996). On Hack's Law. *Water Resources Research* , *32* (11), 3367–3374. https://doi.org/10.1029/96WR02397

Riihimaki, C. A., Anderson, R. S., & Safran, E. B. (2007). Impact of rock uplift on rates of late Cenozoic Rocky Mountain river incision. *Journal of Geophysical Research: Earth Surface* , *112* (3), 1–15. https://doi.org/10.1029/2006JF000557

Rinaldo, A., Dietrich, W. E., Rigon, R., Vogel, G. K., & Rodrlguezlturbe, I. (1995). Geomorphological signatures of varying climate. *Nature* , *374* (6523), 632–635. https://doi.org/10.1038/374632a0

Roe, G. H. (2005). Orographic Precipitation. *Annual Review of Earth and Planetary Sciences* , *33* (1), 645–671. https://doi.org/10.1146/annurev.earth.33.092203.122541

Roe, G. H., & Baker, M. B. (2006). Microphysical and geometrical controls on the pattern of orographic precipitation. *Journal of the Atmospheric Sciences* , *63* (3), 861–880. https://doi.org/10.1175/JAS3619.1

Roe, G. H., Montgomery, D. R., & Hallet, B. (2002). Effects of orographic precipitation variations on the concavity of steady-state river profiles. *Geology* , *30* (2), 143–146. https://doi.org/10.1130/0091-7613(2002)030<0143:EOOPVO>2.0.CO;2

Roe, G. H., Montgomery, D. R., & Hallet, B. (2003). Orographic precipitation and the relief of mountain ranges. *Journal of Geophysical Research: Solid Earth* , *108* (B6). https://doi.org/10.1029/2001jb001521

Roe, G. H., Whipple, K. X., & Fletcher, J. K. (2008). Feedbacks among climate, erosion, and tectonics in a critical wedge orogen. *American Journal of Science* , *308* (7), 815–842. https://doi.org/10.2475/07.2008.01

Royden, L., & Perron, J. T. (2013). Solutions of the stream power equation and application to the evolution of river longitudinal profiles. *Journal of Geophysical Research: Earth Surface* ,*118* (2), 497–518. https://doi.org/10.1002/jgrf.20031

Safran, E. B., Bierman, P. R., Aalto, R., Dunne, T., Whipple, K. X., & Caffee, M. (2005). Erosion rates driven by channel network incision in the Bolivian Andes. *Earth Surface Processes and Landforms* ,*30* (8), 1007–1024. https://doi.org/10.1002/esp.1259

Scherler, D., Bookhagen, B., & Strecker, M. R. (2014). Tectonic control on 10Be-derived erosion rates in the Garhwal Himalaya, India.*Journal of Geophysical Research: Earth Surface* , *119* (2), 83–105. https://doi.org/10.1002/2013JF002955

Scherler, D., DiBiase, R. A., Fisher, G. B., & Avouac, J. P. (2017). Testing monsoonal controls on bedrock river incision in the Himalaya and Eastern Tibet with a stochastic-threshold stream power model.*Journal of Geophysical Research: Earth Surface* , *122* (7), 1389–1429. https://doi.org/10.1002/2016JF004011

Schoenbohm, L. M., Whipple, K. X., Burchfiel, B. C., & Chen, L. (2004). Geomorphic constraints on surface uplift, exhumation, and plateau growth in the Red River region, Yunnan Province, China. *Bulletin of the Geological Society of America* , *116* (7–8), 895–909. https://doi.org/10.1130/B25364.1

Siler, N., & Roe, G. (2014). How will orographic precipitation respond to surface warming? An idealized thermodynamic perspective.*Geophysical Research Letters* , *41* (7), 2606–2613. https://doi.org/10.1002/2013GL059095

Sklar, L. S., Riebe, C. S., Marshall, J. A., Genetti, J., Leclere, S., Lukens, C. L., & Merces, V. (2017). The problem of predicting the size distribution of sediment supplied by hillslopes to rivers.*Geomorphology* , *277* , 31–49. https://doi.org/10.1016/j.geomorph.2016.05.005

Tucker, G E, & Whipple, K. X. (2002). Topographic outcomes predicted by stream erosion models: Sensitivity analysis and intermodel comparison.*Journal of Geophysical Research: Solid Earth* , *107* (B9), ETG 1-1-ETG 1-16. https://doi.org/10.1029/2001jb000162

Tucker, Gregory E., & Slingerland, R. (1997). Drainage basin responses to climate change. *Water Resources Research* , *33* (8), 2031–2047. https://doi.org/10.1029/97WR00409

Vanacker, V., von Blanckenburg, F., Govers, G., Molina, A., Campforts, B., & Kubik, P. W. (2015). Transient river response, captured by channel steepness and its concavity. *Geomorphology* , *228* , 234–243. https://doi.org/10.1016/j.geomorph.2014.09.013

Ward, D. J., & Galewsky, J. (2014). Exploring landscape sensitivity to the Pacific Trade Wind Inversion on the subsiding island of Hawaii.*Journal of Geophysical Research: Earth Surface* , *119* (9), 2048–2069. https://doi.org/10.1002/2014JF003155

Whipple, K. X. (2001). Fluvial landscape response time: How plausible is steady-state denudation? *American Journal of Science* ,*301* (4–5), 313–325. https://doi.org/10.2475/ajs.301.4-5.313

Whipple, K. X., & Meade, B. J. (2006). Orogen response to changes in climatic and tectonic forcing. *Earth and Planetary Science Letters* , *243* (1–2), 218–228. https://doi.org/10.1016/j.epsl.2005.12.022

Whipple, K. X., & Tucker, G. E. (1999). Dynamics of the stream-power river incision model: Implications for height limits of mountain ranges, landscape response timescales, and research needs. *Journal of Geophysical Research: Solid Earth* , *104* (B8), 17661–17674. https://doi.org/10.1029/1999jb900120

Whipple, K. X., & Tucker, G. E. (2002). Implications of sediment-flux-dependent river incision models for landscape evolution.*Journal of Geophysical Research* , *107* (B2), 2039. https://doi.org/10.1029/2000jb000044

Whittaker, A. C. (2012). How do landscapes record tectonics and climate?*Lithosphere* , *4* (2), 160–164. https://doi.org/10.1130/RF.L003.1

24

Whittaker, A. C., Cowie, P. A., Attal, M., Tucker, G. E., & Roberts, G. P. (2007). Bedrock channel adjustment to tectonic forcing: Implications for predicting river incision rates. *Geology* , *35* (2), 103–106. https://doi.org/10.1130/G23106A.1

Willenbring, J. K., Gasparini, N. M., Crosby, B. T., & Brocard, G. (2013). What does a mean mean? The temporal evolution of detrital cosmogenic denudation rates in a transient landscape. *Geology* ,*41* (12), 1215–1218. https://doi.org/10.1130/G34746.1

Wittmann, H., Malusa, M. G., Resentini, A., Garzanti, E., & Niedermann, S. (2016). The cosmogenic record of mountain erosion transmitted across a foreland basin: Source-to-sink analysis of in situ 10Be, 26Al and 21Ne in sediment of the Po river catchment. *Earth and Planetary Science Letters* , *452* , 258–271. https://doi.org/10.1016/j.epsl.2016.07.017

Wobus, C., Whipple, K. X., Kirby, E., Snyder, N., Johnson, J., Spyropolou, K., et al. (2006). Tectonics from topography: Procedures, promise, and pitfalls. *Special Paper of the Geological Society of America* , *398* (04), 55–74. https://doi.org/10.1130/2006.2398(04)

Yang, R., Willett, S. D., & Goren, L. (2015). In situ low-relief landscape formation as a result of river network disruption.*Nature* , *520* (7548), 526–529. https://doi.org/10.1038/nature14354

Zachos, J., Pagani, H., Sloan, L., Thomas, E., & Billups, K. (2001). Trends, rhythms, and aberrations in global climate 65 Ma to present.*Science* , *292* (5517), 686–693. https://doi.org/10.1126/science.1059412

Figures and Tables

Table 1. Model Parameters	**Table 1.** Model Parameters	
Parameters	Value	Units
U	5.0×10^{-4}	$m \cdot yr^{-1}$
K_p	2.5×10^{-9}	$m^{-1} \cdot yr^{-1}$
m	1	
n	2	
k_a	6.69	
h	1.67	
L		
Trunk	50	km
Tributaries	5	km
A		
Trunk	472	km^2
Tributaries	11	km^2
A_c	1	km^2
Node spacing	25	m
Time step	50	yr
Tributary Spacing	1	km

Figure 1 . Influence of rainfall on channel profile form and topographic metrics at steady state. a) Top row – left panel shows river profiles adjusted to different amounts of spatially uniform rainfall. Corresponding discharge accumulation curves are shown in the middle panel. Right panel shows the relationship between mean rainfall (defined as Q/A) calculated at the outlet, with fluvial relief (R), k_{sn}, and k_{sn-q} for a fixed uniform rock uplift rate. Note, at steady state fluvial relief and k_{sn} are inversely related to mean rainfall, while k_{sn-q} is independent of changes in rainfall. b) Bottom row – all panels as in (a) but for a comparable suite of steady-state profiles adjusted to spatially uniform rainfall, a decreasing upstream rainfall (bottom-heavy) pattern, and an increasing upstream (top-heavy) pattern. Note intersections that occur between profiles in the left panel and middle panels, and that fluvial relief and k_{sn} are positively related to mean rainfall in these cases (right panel), inverted from (a). All other model parameters are equal (see Table 1).

Figure 2 . Schematic illustration of key aspects of complex transient responses – defined in section 3.3 – that can result from changes to a relatively bottom-heavy (a) or a top-heavy rainfall gradient (b) – rainfall shown in inset. Horizontal grey bars highlight resulting net change in fluvial relief (ΔR) and maximum elevation change (Δz_{sc}) along the center of the profile. Colored circles mark positions of x_{sc} (yellow) and x_{zc} (red) that also demarcate segments of net divergent and convergent transient adjustments – see text for definitions and discussion. Net modes of transient adjustment are indicated along top axis. Note reversal at position x_{zc} (net incision downstream, net uplift upstream); however, during transience, adjustment upstream of x_{sc} is variable with time. Inset shows both local rainfall rate (P, blue) and upstream averaged rainfall ($\overline{P}$, black).

26

$P = \overline{P}$ for spatially uniform rainfall; only P is depicted for initial rainfall. Positions of x_{sc} and x_{zc} in inset correspond to those along the profiles in the main figure. Note along-stream offset in position where P and $\overline{P}$ exceed the initial rainfall rate, the latter corresponding to x_{sc}. Also, note that the difference between P and $\overline{P}$ increases systematically downstream.

Figure 3 . Sensitivity analysis of a river profile to different spatial gradients in rainfall. a) Defines general domains of behavior described in the sensitivity analysis shown in (b) – see text for descriptions of different fields. Black star in (a) marks the initial condition; note, initial conditions in panels (a) and (b) are different. Top-heavy and bottom-heavy domains are separated by the 1:1 line. The primary influence of different h values in Hack's Law is on the slope of Q_f / Q_i, as indicated. b) Same as (a) but where the initial profile is adjusted to spatially uniform $P = 1.5$ m/yr, and grey fields in (a) are colored by magnitude of Δz_{sc} (e.g., Figure 2). White stars show rainfall gradient scenarios explored in section 3 – Cases 3 & 4. Contours of Q_f/Q_i are shown in grey dashed lines, and contours of R_f /R_i in black dotted lines.

Figure 4 . Representative time slice of transient evolution for Case 1 (uniform decrease in rainfall) and Case 2 (uniform increase in rainfall) through (a)k_{sn} -E_{avg} and (b)k_{sn-q} -E_{avg} parameter spaces. Case 1 is shown in red shaded domain (transient decrease in erosion rate, $E < U$), and Case 2 is in blue shaded domain (transient increase in erosion rate, $E > U$). Curves expressing the expected steady state relationship between channel steepness and erosion rate with different uniform erosional efficiencies are shown; $K = K_p$, is shown in black solid line, and grey lines show different values of K as multiples of K_p . Vertical dashed lines show percent deviations from steady state erosion rate. Initial and final conditions shown with yellow circles, as labelled. Model data from different positions along the trunk profile and individual tributaries shown with red and blue data points, respectively. Trunk data shown are only profile nodes at tributary junctions – all trunk profile datapoints have a corresponding tributary datapoint at the same position. Trunk profile data show upstream mean values from their respective position, and tributary data show mean values for the tributary profile measured at the junction with the trunk profile.

28

Figure 5 . Transient evolution of the trunk profile (a & c) and network of tributaries (b & d) in Case 3 (spatially uniform to bottom-heavy) through k_{sn} -E_{avg} (a & b) and k_{sn-q} -E_{avg} (b & d) parameter spaces. Layout of individual panels is like Figure 4. Six representative time slices are shown; t_1 shows time at 10 kyr model time (i.e., first timestep following change in rainfall), t_6 is at final steady state. Time intervals are not equal in duration but t_1-t_6 are the same timestep for all panels. Note range in k_{sn} values and erosional efficiency values spanned at final steady state in panels (a) and (b). Also, note the relatively muted responses by the trunk profile relative to the network of tributaries in both k_{sn} and k_{sn-q} . Star in panel (a) shows expected erosional efficiency calculated from equation (1b) based on the final mean rainfall of 2.68 m/yr ($2.68 \cdot K_p$) at steady state, which corresponds to a predicted mean k_{sn} of ~275. Note offset between this value and range of erosional efficiency and k_{sn} values exhibited at t_6.

Figure 6 . Transient evolution of the trunk profile (a & c) and network of tributaries (b & d) in Case 4 (spatially uniform to top-heavy) through k_{sn} -E_{avg} (a & b) and k_{sn-q} -E_{avg} (c & d) parameter spaces; figure layout is same as Figure 5. Like Case 3, the trunk response is muted relative to the network of tributaries, but the disparity is more extreme in this case. Star in panel (a) shows K calculated from equation (1b) based on the final mean rainfall of 1 m/yr ($K = K_p$) at steady state, which corresponds to a predicted mean k_{sn} of ˜450. Again, note offset between this value and range of erosional efficiency and k_{sn} values exhibited at t_6.

Figure 7. Sensitivity analysis where initial conditions use final rainfall patterns from Case 3 (a) and Case 4 (b), and examples from the eastern flank of the Peruvian Andes (c) and eastern-central Himalaya (d). Panel layouts are the same as in Figure 3b. Triangular fields in demarcated in black dashes in (a) and (b) bound rainfall gradients with the same pattern as the initial condition (i.e., bottom-heavy or top-heavy), but cause complex transient responses similar to those expected for reversals in polarity of the rainfall pattern as the rainfall becomes *relatively* bottom- or top-heavy – see section 5.1 for further discussion. Panels (c & d) show examples of climate change scenarios from model simulations reported in supplementary tables by Mutz et al. (2018), for a hypothetical transverse river with parameters in Table 1. Initial condition is set in the Pliocene (PLIO), and representative evolution of the orographic rainfall pattern through to the Last Glacial Maximum (LGM) is plotted, illustrating that climate changes that are predicted to trigger complex responses are likely not uncommon.

Figure 8. Representative examples of multi-stage tributary response in Cases 3 (a) & 4 (b). Note, upstream positions always experience relatively longer initial adjustment stages than downstream positions, regardless of rainfall gradient. Grey shaded and white regions show where initial and final steady states (SS) and different adjustment stages are represented along the profile lengths, as indicated across top axis. a) Shows a tributary located in a relatively downstream position, 15 km from trunk outlet and downstream from x_{sc} after 300 kyr of transient adjustment in Case 3, where the initial adjustment stage is relatively short-lived. Despite this, protracted adjustment creates a several-kilometer-wide adjustment zone with relatively smooth but notable along-stream variations in k_{sn} . This pattern is subtle on the longitudinal profile. b) Shows a tributary located in an upstream position, 45 km from the trunk outlet and upstream from x_{sc} after 1.725 Myr of transient adjustment in Case 4, where the initial adjustment stage is long-lived. The initial adjustment stage reshapes the entire profile prior to adjustment of the trunk profile, but no transient knickpoints or other obvious topographic indicators of such significant modification are present, with smoothly varying local k_{sn} values within 10% of the mean. Also, note overadjustment means that the increase in channel steepness required to reach steady state contrasts with net reduction in channel steepness during transient adjustment.

Figure 9. Plot illustrating how rainfall gradients systematically influence correlation between mean rainfall and k_{sn} at steady state, and consequences for relationship between channel steepness and erosion rate (inset). A common symbology is used in both the main figure and the inset. Expected SPM relationship based on uniform climate (uniform erosional efficiency, K) is shown in solid back line. Grey long-dashed lines represent changes in $K = K_p\, P^m$. Circles colored by mean rainfall reflect scenarios shown in Figure 1 – uniform rainfall of 1, 1.5, and 2 m/yr, and bottom- and top-heavy gradients (also used in Cases 3 & 4). While K_p is equivalent for all scenarios, rainfall gradients cause dispersion (apparent differences in erosional efficiency) from the expected relationship (solid black line) equivalent to differences in K_p of approximately a factor of two (inset). For instance, the bottom-heavy case where mean rainfall is ~2.7 m/yr exhibits an apparent ~50% reduction in erosional efficiency based on mean k_{sn} (plots on K [?] $0.5K_p$ curve in main figure) and thus plots where one would expect a catchment that experiences half as much rainfall to plot in the inset. Dotted line in main figure illustrates, conceptually, how this dispersion could distort inferred relationships between mean rainfall and channel steepness (weaker and quasi-linear in this case), even at steady state and in systems where the SPM is a complete description of the controls on channel profile form. Where

32

uplift rates are unknown, this systematic bias in apparent erosional efficiency due to rainfall gradients is a potential source of dispersion in relationships between k_{sn} and erosion rate (inset).

Figure 10. Illustration of potentially misleading spatial patterns that arise among channel steepness, rainfall, and erosion rates during transient adjustment to a change in rainfall pattern, particularly when erosion rate and morphometrics are averaged at catchment scale – see section 5.1.2 for detailed discussion. a) Shows time slice at 0.5 Myr into transient adjustment of Case 3 (t_2 in Figure 5). For clarity, a subsample of ten data points is shown for each model dataset; connecting dashed line is populated from full model. Thick colored bands (red = trunk, blue = tributaries) show final steady state upstream-averaged k_{sn} pattern toward which the modelled catchment is adjusting. Position of trunk knickpoint, defined as upstream extent of quasi-equilibrium adjustment, is shown by red solid line, and zones describing morphological characteristics of tributary catchments are shown across the top axis (compare both with panel c). b) Modelled steady state k_{sn} and trunk erosion rate pattern of hypothetical catchment experiencing a bottom-heavy rainfall gradient and a spatial gradient in uplift rate that matches the catchment-averaged erosion rate pattern recorded by the tributary network in a). c) Shows planform development of local k_{sn}, k_{sn-q}, and erosion rates at initial and final steady states, a transient time slice from Case 3, and steady state pattern from (b). Downstream is to the left. Transient time slice and tributaries are the same as in panels (a & b). Note that trunk and tributary profiles are not illustrated to scale (Table 1).

33

1 # Influence of Spatial Rainfall Gradients on River Longitudinal

2 # Profiles and the Topographic Expression of Spatio-temporally

3 # Variable Climate in Mountain Landscapes

4 Joel S. Leonard[1] and Kelin X. Whipple[1]

5 [1]School of Earth and Space Exploration, Arizona State University, Tempe, Arizona, USA

6 Corresponding Author: Joel S. Leonard (joel.leonard@asu.edu)

7 **Key Points**

8 - Spatially variable rainfall complicates steady state relationships between mean rainfall and
9   conventional topographic and erosion metrics.
10 - Transient responses to changes in rainfall pattern differ from uniform changes in rainfall, which
11   affects how they may be detected.
12 - Rainfall gradients can obscure the sensitivity of fluvial erosion to rainfall variations and impede
13   quantification of climate sensitivity.

16 **Abstract**

17 Mountain landscapes have dynamic climates that, together with tectonic processes, influence their
18 topographic evolution. While spatio-temporal changes in rainfall are ubiquitous in these settings, their
19 influence on river incision is understudied. Here, we investigate how changes in rainfall pattern should
20 affect both the steady state form and transient evolution of river profiles at the catchment scale using the
21 stream power model. We find that spatially varied rainfall can complicate steady state relationships between
22 mean rainfall, channel steepness and fluvial relief, depending on where rainfall is concentrated in
23 catchments. As a result, transient profile adjustments to climate changes may proceed contrary to typical
24 expectations, which can ultimately affect the apparent sensitivity of landscapes and erosion rates to climate.
25 Additionally, changes in rainfall pattern cause inherently multi-stage transient responses that differ from
26 responses to uniform changes in rainfall. These results have important implications for detecting transient
27 responses to changes in rainfall pattern (and more broadly climate), and for interpreting of landscape

28 morphometrics above and below knickpoints. Further, we find that disparate responses by rivers that

29 experience different rainfall conditions, particularly trunk and tributary rivers, are an important factor in

30 understanding catchment-wide responses, and accounting for such disparities may be important for

31 detecting and quantifying landscape sensitivity to variations in climate. Lastly, we show how explicitly

32 accounting for rainfall patterns in channel steepness indices, and thus variations in erosional efficiency, has

33 potential to help address challenges related to spatially variable rainfall patterns and advance understanding

34 of landscape sensitivity to climate in mountain settings.

35 **Plain Language Summary**

36 Rainfall in mountain landscapes often varies with elevation; a pattern known as orographic rainfall. Rivers

37 that sculpt these landscapes rely on rainfall for their erosive power, where more rainfall typically means

38 greater erosive power. Rainfall also affects how steep these rivers are, which in turn affects the steepness

39 of the topography around them. Here, we investigate how concentrating rainfall at higher and lower

40 elevations – representing two common orographic rainfall patterns that may be enhanced or relaxed by

41 climate change – influences the steepness mountain rivers, erosion patterns, and thus the evolution of

42 mountain topography. We show that these orographic rainfall patterns complicate simple expected

43 relationships among metrics commonly used to quantify the role of rainfall (and more broadly climate) on

44 the topography of mountain landscapes. Further, we show that rivers respond in unexpected ways to

45 changes in orographic rainfall patterns, as would occur following a change in climate, suggesting that

46 common wisdom about how rivers and mountain landscapes respond to changing climates is incomplete.

47 **1. Introduction**

48 **1.1 Motivation**

49 Advances in tectonic geomorphology require quantitative understanding about relationships among

50 climate, tectonics, and erosion. In temperate mountain landscapes, studies of bedrock rivers provide

51 important insights into interactions between these processes (e.g., D'Arcy & Whittaker, 2014; Harel et al.,

52 2016; Kirby & Whipple, 2012; Lague, 2014; Olen et al., 2016; Scherler et al., 2017; Whipple & Tucker,

53 1999; Whittaker, 2012). However, despite longstanding theoretical support for the notion that climate, like

54 tectonics, has a fundamental role in influencing erosion (e.g., Bonnet & Crave, 2003; Howard & Kerby,

55 1983; Lague, 2014; Molnar, 2001; Perron, 2017; Rinaldo et al., 1995; Tucker & Slingerland, 1997), a

56 general relationship between climate and erosion has proven elusive (Perron, 2017; Whittaker, 2012). Here,

57 we explore the extent to which this conundrum may reflect limitations in the current framework describing

58 how climate-related signals should be expressed in landscapes that, in turn, may impede recognition of

59   diagnostic characteristics of landscape response to climate change.

60   Orographic precipitation patterns are ubiquitous in mountain landscapes. In general, they develop from the
61   interaction of humid air masses with topographic relief and can create dramatic spatial and elevation
62   dependent gradients in precipitation (see Roe, 2005 for an overview). For instance, the Olympic, Sierra
63   Nevada, and Wasatch ranges in western North America all experience orographically enhanced
64   precipitation with increasing elevation (e.g., Barros & Lettenmaier, 1994; Barstad & Smith, 2005; Roe,
65   2005). Alternatively, large tracts along eastern and southern flanks of the Andes and Himalaya,
66   respectively, become more arid as elevation increases (Anders et al., 2006; Bookhagen & Burbank, 2010;
67   Bookhagen & Strecker, 2008; Burbank et al., 2003). While numerous factors affect orographic precipitation
68   patterns in detail, broadly speaking, atmospheric moisture content, topographic characteristics (e.g., relief),
69   and general circulation patterns are primary physical controls on their development (e.g., Held & Soden,
70   2006; Roe, 2005; Roe et al., 2008; Trenberth et al., 2003). Because atmospheric moisture content depends
71   strongly on temperature (i.e., Clausius-Clapeyron relationship; Held & Soden, 2006; Roe, 2005; Trenberth
72   et al., 2003), shifts in temperature that accompany changes in climate must influence these precipitation
73   patterns (e.g., Mutz et al., 2018; Roe & Baker, 2006; Siler & Roe, 2014). Therefore, if erosional processes
74   in these landscapes are generally sensitive to spatial and/or temporal variations in precipitation, then
75   changing characteristics of orographic precipitation patterns with changes in climate should importantly
76   influence mountain landscape evolution.

77   In mountainous settings, transverse rivers tend to cross orographic precipitation gradients, which are
78   generally oriented orthogonally to the topographic trend of the range. Their tributaries, on the other hand,
79   typically experience a relatively muted range in precipitation due to their orientation and/or smaller areal
80   extent. Consequently, rivers of different size, orientation, and position often experience dramatically
81   different precipitation conditions. Within large river basins, these differences may be substantial. Exposure
82   to orographic precipitation patterns is expected to systematically affect river profile concavity; increases in
83   precipitation with distance upstream lowers profile concavity, while the opposite trend increases profile
84   concavity (Han et al., 2014, 2015; Roe et al., 2002, 2003; Ward & Galewsky, 2014). Changes in concavity
85   driven by temporal changes in orographic precipitation patterns require longitudinally variable amounts of
86   incision. Furthermore, because transverse rivers set erosional base level for their tributaries, any along-
87   stream variation in incision exhibited by transverse rivers during this adjustment will necessarily drive
88   spatially and temporally variable base level histories for tributaries. Developing a framework that
89   accommodates such variability and its influence on river profile evolution is a fundamental need.

90   **1.2 Approach and Scope**

91   Here, we investigate how spatio-temporal changes in precipitation may influence erosion and topography

92   of mountain landscapes using the stream power model (SPM). First, we show how simple spatial gradients

93   in rainfall, resembling typical orographic precipitation patterns (i.e., increasing or decreasing downstream;

94   herein referred to as bottom-heavy, and top-heavy, respectively), influence river profile form at steady state

95   in one dimension. Next, we use a quasi-two-dimensional numerical model to simulate the response of a

96   transverse river network to a change in rainfall pattern, which we compare to better-understood spatially

97   uniform changes in rainfall. Finally, we discuss some implications for studies set in mountain landscapes.

98   A comprehensive analysis of the co-evolution of orographic rainfall patterns and topography is beyond the

99   scope of this paper. Instead, we focus on characterizing the controls on landscape response to imposed

100   changes in rainfall patterns, highlighting where expectations differ from uniform changes in rainfall, and

101   implications of those differences.

102   **2. Methods**

103   **2.1 Model Description**

104   We explore the influence of longitudinal rainfall gradients on large transverse rivers first using a simple 1-

105   dimensional river incision model. We model erosion as detachment-limited (Howard, 1994; Roe et al.,

106   2002; Whipple & Tucker, 1999) following a general form of the SPM:

107 $E = KA^m S^n,$ (1a)

108 $K = K_p \bar{P}^m,$ (1b)

109 $E = K_p Q^m S^n,$ (1c)

110   where E is the erosion rate; K and K_p are erosional efficiency coefficients; A is upstream drainage area; S is

111   the channel slope; $\bar{P}$ is the upstream average rainfall rate; Q is water discharge and is calculated as $\bar{P}A$,

112   which assumes that all rainfall is converted to runoff; and m and n are positive constant exponents (Table

113   1). We use $n = 2$ and $m = 1$ for all model runs as values of $n > 1$ appear more appropriate in many settings

114   (e.g., Adams et al., 2020; Harel et al., 2016; Lague, 2014). First-order results do not rely on choices of m

115   or n providing the ratio between the two is approximately maintained, but the nonlinear dependence of

116   erosion rate on slope (i.e., $n = 2$) affects details of the transient behavior. Also, because $m = 1$, K is directly

117   proportional to both $\bar{P}$ and Q. We explicitly treat the influence of climate on erosional efficiency (e.g.,

118   Adams et al., 2020; Roe et al., 2002) such that K_p is independent of rainfall, but still encapsulates a number

119   of factors including rock properties and details of erosional processes (Royden & Perron, 2013; Whipple &

120   Tucker, 1999). Rock uplift rate (U) and K_p are spatially and temporally uniform and invariant across model

121   runs.

122   We define drainage area (A) following Hack, (1957):

$$A = k_a x^h + A_c, \tag{2}$$

124   where x is distance along the channel downstream from the drainage divide, k_a and h are constants, and A_c

125   is the upstream drainage area at the channel head – equal to 1 km^2. Channel length (L) and drainage area

126   are fixed and do not evolve over the course of a model run.

127   For simplicity, we model orographic precipitation as constant gradients in rainfall (i.e., linear changes with

128   distance). Although a constant gradient is a simplification, it is a reasonable approximation to commonly

129   observed orographic rainfall patterns, which can be both top- and bottom-heavy (e.g., Anders et al., 2006;

130   Bookhagen & Burbank, 2010; Bookhagen & Strecker, 2008; Roe, 2005). Further, the framework we

131   develop from these simple rainfall patterns is generally applicable to addressing more complex versions of

132   the fundamental problem we address here – the effects of spatially concentrated rainfall.

2.2 Analysis of River Profiles and Erosion Rates

134   We quantify river profile form and responses to changes in rainfall patterns using channel steepness indices

135   and erosion rates. These metrics are commonly used, and often in tandem, to study influences of climate

136   and/or tectonics in mountain settings (Adams et al., 2020; Bookhagen & Strecker, 2012; Cyr et al., 2014;

137   DiBiase et al., 2010; Duvall, 2004; Godard et al., 2014; Insel et al., 2010; Kober et al., 2015; Morell et al.,

138   2015; Olen et al., 2016; Ouimet et al., 2009; Portenga et al., 2015; Safran et al., 2005; Scherler et al., 2014;

139   Vanacker et al., 2015; Willenbring et al., 2013).

140   A widely used metric to analyze river profiles, interpret erosion rates, and make comparisons to the SPM

141   is the normalized channel steepness index, k_{sn}:

$$k_{sn} = SA^{\theta_{ref}}, \tag{3}$$

143   where θ_{ref} is the reference concavity index (Wobus et al., 2006). We use a value of $\theta_{ref} = 0.5$, which is

144   common and consistent with our choice of m/n, and also with SPM predictions that $\theta_{ref} = m/n \approx 0.5$ where

145   rock uplift rate (U) and erosional efficiency (K) are uniform (Tucker & Whipple, 2002). As previously

146   noted, the SPM predicts that orographic rainfall gradients should produce longitudinal variations in K that,

147   in turn, affect the concavity index, θ (Han et al., 2014, 2015; Roe et al., 2002, 2003). Any such variations

148   are systematically reflected in the spatial pattern of k_{sn} and $\theta \neq \theta_{ref}$ is expected. Importantly, however, many

149   studies relate upstream-average values of k_{sn} to measured spatially-averaged erosion rates, which relies on

150   quasi-uniform (or linear) upstream k_{sn} to be valid (Wobus et al., 2006). In cases where systematic

151   longitudinal variations in K affect the downstream pattern of k_{sn} (i.e., upstream k_{sn} varies non-linearly), the

152   meaning of such an average is not obvious.

153   To address this, we use discharge, rather than drainage area alone, to calculate a modified channel steepness

154   index k_{sn-q} (Adams et al., 2020):

155
$$k_{sn-q} = SQ^{\theta_{ref}}. \tag{4}$$

156   Like k_{sn}, k_{sn-q} is an empirically supported metric independent from the SPM. In principle, however, k_{sn-q} is

157   analogous to Erosion Index (EI) used by Finlayson et al., (2002) provided that $m/n \approx \theta_{ref}$, such that EI = $(k_{sn-}$

158    $_q)^n$. Also, as k_{sn} is the slope of χ-transformed river profiles in χ-elevation space, if χ is redefined to include

159   precipitation to estimate discharge, slopes of χ-transformed profiles would instead represent k_{sn-q} (Royden

160   & Perron, 2013; Yang et al., 2015). To the extent that the SPM captures the influence of discharge on

161   erosional efficiency, it predicts that along-stream variations in k_{sn-q} should scale with local erosion rate,

162   precisely as it does for k_{sn} where K is spatially uniform. Hereafter, we use k_{sn} and k_{sn-q} to refer to upstream

163   averaged values, consistent with their common usage in catchment-mean erosion rates analyses, unless we

164   specifically state that they represent local values.

165   Millennial-scale catchment-averaged erosion rates measured, for example, using cosmogenically-derived

166   [10]Be found in quartz in alluvial sediment (e.g. Bierman & Steig, 1996; Brown et al., 1995; Granger et al.,

167   1996), seek to quantify erosion rates at the river basin scale. At steady state, spatially averaged erosion rate,

168   local incision rate, and rock uplift rate are equivalent; however, during periods of transient adjustment these

169   values differ, complicating interpretations (Willenbring et al., 2013; Wobus et al., 2006). To make our

170   results more portable to studies of natural landscapes, we calculate the spatially averaged erosion rate (E_{avg})

171   in addition to the instantaneous vertical incision rate (E):

172
$$E_{avg_j} = \frac{\sum_{x_h}^{j} \left(E_j \cdot (A_j - A_{j-1}) \right)}{A_j}, \tag{5}$$

173   where j corresponds to a downstream node of the profile, and x_h is the channel head.

174   **3. Longitudinal Profiles (1-D)**

175   **3.1 Influence of Longitudinal Rainfall Gradients on River Profiles at Steady State**

176   Where rainfall is spatially uniform, topographic metrics (e.g., fluvial relief, channel steepness) at steady

177   state are expected to vary inversely and monotonically with mean rainfall (Figure 1a). However, spatially

178   variable rainfall patterns complicate these expectations, as shown in Figure 1b, where comparisons between

179   rivers that experience different rainfall patterns instead result in positive relationships between these

180   topographic metrics and mean rainfall. This reversal reflects limitations of using spatially averaged metrics

181   where climate is spatially variable (e.g., in most mountain landscapes).

182   Systematic longitudinal variations in rainfall require that upstream average rainfall values change

183   systematically downstream, which similarly affects erosional efficiency (K), and thus equilibrium channel

184   slope (Equation 1). Where such spatial variations exist, mean values of rainfall and k_{sn} therefore depend on

185   where they are measured. In contrast, where equation 1 holds and $m/n = \theta_{ref}$, $k_{sn\text{-}q}$ is independent of changes

186   in mean rainfall (Figure 1). Comparison of SPM equations for k_{sn} and $k_{sn\text{-}q}$ at steady state ($E = U$) further

187   clarifies this difference:

188
$$k_{sn} = \left(\frac{U}{K_p \bar{P}^m}\right)^{1/n},$$
(6a)

189
$$k_{sn-q} = \left(\frac{U}{K_p}\right)^{1/n}.$$
(6b)

190   For spatially uniform rock uplift rate (U) and K_p, steady state fluvial relief (R) is proportional to the upstream

191   integrated discharge (Han et al., 2015; Roe et al., 2003; Royden & Perron, 2013). Integrating equation 1c

192   from base level (x_b) upstream to the channel head (x_h), it can be shown that:

193
$$R = \left(\frac{U}{K_p}\right)^{1/n} \int_{x_b}^{x_h} Q^{-m/n} \, dx.$$
(7)

194   This demonstrates clearly how fluvial relief depends on the cumulative effect of discharge and implies that

195   fluvial relief does not necessarily scale monotonically with discharge or rainfall measured at any single

196   position, or averaged along any segment of a profile, except under the special condition where rainfall is

197   spatially uniform (Gasparini & Whipple, 2014; Han et al., 2015). This is an important result, particularly

198   for understanding the topographic evolution of mountain landscapes because it suggests that considering

199   how rainfall patterns, specifically, have changed with time is critical to predicting responses to changes in

200   climate. For instance, shifts toward 'wetter' climates may support topographic growth, contrary to

201   expectations and even in the absence of any change in tectonics, depending on where rainfall is

202   concentrated, or vice versa.

203   3.2 Transient River Profile Response to Changes in Rainfall Patterns

204   According to the SPM, transient responses to climate change are primarily driven by changes in discharge
205   that, in turn, affect erosional efficiency. In response to climate change, in addition to changes in mean
206   rainfall, increases or decreases in rainfall may occur in different positions within a catchment, for example
207   by strengthening or relaxing existing orographic rainfall distributions (Roe et al., 2003; Roe & Baker, 2006).
208   Any such change in the pattern of rainfall fundamentally changes how discharge accumulates and can be
209   expected to drive adjustments in the form of river profiles.

210   Changes in discharge at a given location following a temporal change in rainfall pattern reflect changes
211   upstream average rainfall conditions. (Hereafter we use subscripts i and f, respectively, to denote initial and
212   final steady states, before and after a temporal change in rainfall pattern.) While integrating upstream
213   conditions somewhat buffers discharge from localized variations in rainfall upstream, because it
214   accumulates non-linearly downstream relatively modest systematic variations in rainfall can exert a strong
215   influence. Indeed, contrary to spatially uniform changes in rainfall that cause monotonic changes in
216   discharge everywhere, we find that for a wide range of temporal changes in rainfall patterns discharge may
217   increase in upstream locations ($Q_f > Q_i$) but decrease in downstream locations ($Q_f < Q_i$), or vice versa.

218   We refer to the position of such a reversal (e.g. from increasing to decreasing discharge or vice versa) as
219   x_{sc}. At this position discharge remains constant, and thus equilibrium river slope does not change following
220   a temporal change in rainfall pattern (at $x = x_{sc}$, $Q_f = Q_i$ and $S_f = S_i$). As we will show, transient responses
221   to temporal changes in rainfall pattern that cause such reversals have distinctive qualities. For now, we note
222   an interesting feature where upstream of x_{sc} initial and final steady state profiles begin to converge (see
223   Figure 2). Thus, x_{sc} marks a local maximum elevation difference between initial and final steady state
224   profiles. This convergent behavior contrasts with expectations for spatially uniform changes in rainfall
225   where the difference in channel bed elevation increases monotonically upstream from the outlet (Figure
226   1a).

227   Assuming spatially uniform rock uplift rate and K_p, the maximum difference in elevation along the profile
228   between initial and final steady states, Δz_{Sc}, can be expressed:

$$\Delta z_{Sc} = \left(\frac{U}{K_p}\right)^{1/n} \int_{x_b}^{x_{sc}} (Q_f - Q_i)^{-m/n} \, dx. \tag{8}$$

230   In some circumstances, initial and final steady state profiles can intersect at a position x_{zc} (Figure 2),
231   determined by:

232
$$0 = \left(\frac{U}{K_p}\right)^{1/n} \int_{x_b}^{x_{zc}} (Q_f - Q_i)^{-m/n} \, dx. \tag{9}$$

233   Notably, x_{zc} marks a location where the net adjustment to reach steady state elevation changes along the

234   profile from enhanced incision to surface uplift, or vice versa. Temporal changes in rainfall patterns that

235   produce x_{zc} are those that lead to positive relationships between spatially averaged mean rainfall and fluvial

236   relief (Figure 1b).

237   **3.3 Sensitivity Analysis of 1-D River Profiles to Changes in Rainfall Patterns**

238   Next, we explore a simple example scenario to evaluate the sensitivity of discharge and fluvial relief to

239   changes in rainfall pattern. We introduce this analysis here using a steady state profile adjusted to spatially

240   uniform rainfall (Figure 3). While idealized, this simple case is well suited to developing intuition about

241   more complex scenarios, like strengthening or relaxing existing orographic rainfall patterns, which as we

242   show in section 5.1 produce analogous responses to those we discuss here.

243   We define different fields bounding rainfall gradients that result in different classes of behavior (Figure 3a).

244   Boundaries demarcating these fields are independent of U, K_p, m, and n provided m/n is unchanged. Channel

245   length has a negligible influence for channels longer than a few kilometers where $A \gg A_c$, and only minor

246   influence for different m/n ratios ($\sim$0.4-0.6). The h exponent in Hack's Law (Equation 2) can influence field

247   boundaries, as indicated in Figure 3a; however, the effect is minor for typical h values ($1.67 \leq h \leq 2$; e.g.,

248   Rigon et al., 1996). Contours of Q_f/Q_i illustrate the extent to which a given rainfall gradient represents a

249   net wetter ($Q_f/Q_i > 1$) or drier ($Q_f/Q_i < 1$) condition (Figure 3b). Contours of R_f/R_i describe the extent to

250   which fluvial relief increases ($R_f/R_i > 1$) or decreases ($R_f/R_i < 1$). These contours show that steady state

251   fluvial relief is sensibly correlated with discharge, but the relationship is complex when rainfall is not

252   spatially uniform.

253   White fields (Figure 3, both panels) encompass rainfall gradients – and spatially uniform changes in rainfall

254   – where the profile would experience wetter or drier conditions everywhere. Transient adjustments to such

255   gradients generally mimic adjustments to spatially uniform increases or decreases in rainfall, although

256   spatially variable changes are expected to affect adjustments differently than uniform changes in detail

257   (e.g., see section 5.1.2).

258   Light grey fields (Figure 3a) encompass rainfall gradients where relative changes in discharge and

259   equilibrium slope would invert along the profile, but initial and final steady state profiles would not intersect

260   (i.e., produce x_{sc}, but not x_{zc}). The mode of transient adjustment is variable in space and time upstream of

261   x_{sc} (variably $E > U$ or $E < U$; Figure 2). Despite this, the net change in fluvial relief is inversely related to

262   the change in mean rainfall at steady state, consistent with expectations for spatially uniform changes in

263   rainfall. x_{sc} marks the position of the absolute maximum elevation difference between initial and final steady

264   states in these cases, not the channel head. Therefore, while each point along the profile experiences net

265   incision or surface uplift to reach steady state, the largest differences in elevation between initial and final

266   steady states are along the central part of the profile.

267   Dark grey fields (Figure 3a) encompass rainfall gradients that produce both x_{sc} and x_{zc} and are characterized

268   by the most complex transient responses (e.g., Figure 2). Implied spatial patterns of relative changes in

269   discharge and slope follow as for light grey fields, and modes of transient adjustment are similarly spatio-

270   temporally variable upstream from x_{sc}. The distinguishing feature of these gradients is that the resulting

271   steady state fluvial relief is positively related to the change in spatially averaged mean rainfall (e.g., Figures

272   1b, 2), contrary to expectations for spatially uniform changes in rainfall. This results from the non-linear

273   influence of discharge on channel slope and the cumulative influence of downstream slopes on channel

274   elevation. The absolute maximum difference in elevation between initial and final steady states may either

275   be at x_{sc} or at the channel head in these cases depending on specific characteristics of the change in rainfall

276   gradient.

277   This analysis reveals several interesting ways that changes in rainfall pattern influence river profiles

278   differently than expected for uniform changes. Note, we define our usage of 'complex' transient responses

279   hereafter to include all responses that result in an along-stream inversion in the change in discharge, unless

280   we specify otherwise (i.e., cases where x_{sc} exists; both grey fields in Figure 3a). First, changes in

281   longitudinal rainfall gradients that result in complex transient responses appear relatively common and do

282   not require large changes in rainfall patterns or total rainfall. That these complex responses arise readily

283   from a range of changes in rainfall patterns suggests that they may be a typical aspect of landscape evolution

284   in mountain settings. For instance, this scenario implies topographic growth of incipient mountain ranges

285   may be supported or suppressed by the orographic rainfall patterns they generate, depending on where

286   rainfall is concentrated, even if they experience more total rainfall as a result (e.g., Roe et al., 2003).

287   Among changes in rainfall pattern where complex responses result in a positive relationship between the

288   change in mean rainfall and fluvial relief (dark grey fields in Figure 3a), changes to top-heavy and bottom-

289   heavy conditions have an asymmetric influence on fluvial relief. Top-heavy gradients in this category

290   always inhibit growth of fluvial relief (R_f/R_i always < 1) and bottom-heavy gradients promote topographic

291   growth, but incremental changes in bottom-heavy gradients result in greater increases (Figure 3).

292   Incremental increases in rainfall upstream (top-heavy) suppress the rate at which slope increases upstream,

293   limiting potential elevation change. In contrast, incremental decreases in rainfall upstream (bottom-heavy)

294   enhance increases in slope upstream and support greater elevations.

295   To get a sense for potential magnitudes of topographic changes that changes in climate might produce, we

296   tested a wide range of parameters that may be applicable to major mountain ranges (e.g., K_p, U, h, L). We

297   find that a temporal change in rainfall pattern alone may support as much as $\sim 10^2$–10^3 m of change in fluvial

298   relief in the opposite direction expected from the spatially averaged change in mean rainfall (e.g., an

299   increase in relief associated with an increase in mean rainfall). The same climate change may also drive up

300   to $\sim 10^1$–10^2 m of enhanced incision or surface uplift along downstream and central portions of river profiles

301   in the manner consistent with conventional expectations for the change in mean rainfall. This spatially

302   segregated behavior may be particularly important for understanding how adjustments to climate changes

303   are expressed, sediment transport out of mountain catchments, and fluvial terraces to name a few examples.

304   While we do not treat the latter two points further here, they nevertheless warrant more research.

305   Taken together, this analysis supports the notion that spatially variable changes in rainfall pattern can

306   readily and importantly influence landscape form and processes in ways that fundamentally differ from

307   expectations for spatially uniform changes in rainfall.

4. Transient Catchment Response to Changes in Rainfall Patterns

309   Many of the ideas laid out above for 1-dimensional profiles intuitively transfer to understanding how signals

310   related to changing rainfall patterns propagate through a drainage network, albeit with some additional

311   considerations. It is important to remember that trunk (transverse) rivers control base level for tributaries.

312   Complex responses, like those described above where both the magnitude and mode of transient adjustment

313   vary along the trunk profile in space and time, necessarily result in varying boundary conditions for

314   tributaries. In addition, tributary responses to these variable base level signals are modulated by the rainfall

315   history experienced by a given tributary, which is always different from the trunk. Finally, adjustments

316   migrate upstream at a finite rate, so there is a time lag between a change in rainfall pattern and arrival of

317   the associated base level signals from the trunk adjustment to a given tributary. The duration of this lag, as

318   well as local rainfall conditions within a tributary catchment, are a function of its position.

319   Following Riihimaki et al. (2007), we use a quasi-two-dimensional model to explore catchment response.

320   We abstract river basin topology to comprise a single one-dimensional trunk profile and 51 regularly spaced

321   (1 km spacing) one-dimensional tributary profiles. Tributary outlets are fixed to the elevation of the trunk

322   profile at their confluence. Discharge does not pass from tributaries to the trunk river as drainage area along

323   the trunk and each tributary follows Hack's Law (equation 2) independently. This means that there is not

324   two-dimensional hydrological coupling between trunk and tributary rivers through discharge, but transient

325   signals are communicated through variations in tributary base level. This approach allows closely spaced

326   tributaries with identical characteristics to isolate the influence of spatial variations in rainfall within the

327   larger catchment that would not be possible to the same degree with 2-dimensional modelling approaches.

328   Although our model setup is abstract, it allows us to compare expected patterns of erosion and channel

329   response along the trunk and within small trunk-stream tributaries in a way that is portable to natural river

330   networks. Because drainage area increases along the modeled trunk river following Hack's Law,

331   independent of the distribution of modeled tributaries, at each point along the trunk river discharge

332   accumulation approximates that of a typical drainage basin aligned along the orographic rainfall gradient.

333   In this light, the trellis configuration of tributaries we model is representative of a subset of small,

334   approximately trellised trunk-stream tributaries that typically exist within more complex river network

335   structures and are often targeted for sampling of detrital sediment (e.g., Ouimet et al., 2009). These small

336   tributaries also do not contribute significantly to downstream increases in drainage area (or discharge) of

337   larger rivers into which they drain, meaning discharge accumulation along large rivers is largely decoupled

338   from the hydrology of small tributaries. Therefore, the simplifications we make to the hydrology are also

339   generally consistent with conditions created by targeting small tributaries situated along large rivers in a

340   trellis-like fashion.

341   In the following, we explore the transient response of modelled river basins to four representative climate

342   change scenarios: (1) a spatially uniform decrease in rainfall, (2) a spatially uniform increase in rainfall, (3)

343   a shift from spatially uniform rainfall to a bottom-heavy rainfall gradient, and (4) a shift from spatially

344   uniform rainfall to a top-heavy rainfall gradient. The initial condition for all models is steady state with

345   spatially uniform rainfall. Imposed changes in rainfall evolve at a linear rate over the first 10 kyr of model

346   time at all points along each channel. Tributaries are modelled with spatially uniform rainfall set by their

347   position along the trunk profile, and individual tributaries experience spatially uniform changes in rainfall

348   as rainfall gradients evolve. This simplification is consistent with the notion that, due to their smaller areal

349   extent and orientation, tributaries set within mountain-belt scale orographic rainfall patterns generally

350   experience relatively uniform rainfall. As we show in section 5.1, more realistic scenarios, such as the

351   intensification or relaxation of an existing orographic rainfall gradient, produce analogous behavior to these

352   simple scenarios. The simplicity of the idealized scenarios described here makes them especially effective

353   for developing intuition about response characteristics in general.

354   **4.1 Case 1: Spatially Uniform Decrease in Rainfall**

355   The modelled catchment response to a spatially uniform decrease in rainfall is characterized by adjustment

356   to uniformly higher k_{sn} and an increase in steady state fluvial relief. For this model run, rainfall is decreased

357   from 2 to 1 m/yr, causing discharge to decrease similarly by 50% (Movie S1).

358   Erosion rate decreases across the entire channel network following the change in rainfall, driven by a

359   decrease in erosional efficiency directly proportional in magnitude (i.e., 50%; recall $m = 1$). The resulting

360   disequilibrium, with $E < U$, drives surface uplift and upstream migration of a convex-up slope-break

361   knickpoint, and eventually a ~40% increase in fluvial relief.

362   In k_{sn}–E_{avg} space (Figure 4a), the decrease in erosional efficiency driven by the change rainfall causes the

363   trunk river and tributary network to shift uniformly onto a different erosional efficiency curve that describes

364   the expected relationship between k_{sn} and erosion rate for a given erosional efficiency at steady state.

365   Specifically, both shift from $K=2 \cdot K_p$ to $K=K_p$ ($K_f = 0.5 \cdot K_i$). Following this initial shift, the trunk river and

366   individual tributaries approximately follow this new curve ($K=K_p$) during adjustment toward higher erosion

367   rates and k_{sn} to return to steady state, although in detail they deviate slightly. This deviation is a result of

368   averaging segments above and below the migrating knickpoint into mean (upstream-averaged) k_{sn} and

369   erosion rate values. Insofar as the relationship between channel steepness and erosion rate implies a given

370   erosional efficiency, these deviations imply an apparent erosional efficiency different, albeit minor in this

371   case, from the modelled value.

372   In $k_{sn\text{-}q}$–E_{avg} space (Figure 4b), both the initial and final steady state conditions plot in the same location on

373   the $K=K_p$ curve. Here, the initial decrease in erosional efficiency causes the trunk and tributaries to shift

374   uniformly along this curve to lower $k_{sn\text{-}q}$ and erosion rate rather than shifting onto a different curve. During

375   adjustment both generally follow this curve to return to steady state, minor transient deviations as seen for

376   k_{sn} notwithstanding.

4.2 Case 2: Spatially Uniform Increase in Rainfall

378   The modelled catchment response to a spatially uniform increase in rainfall is characterized by adjustment

379   to uniformly lower k_{sn} and a decrease in steady state fluvial relief. To compare responses, we invert the

380   change in rainfall from the previous example, and rainfall is increased from 1 to 2 m/yr, resulting in a 100%

381   increase in discharge (Movie S2).

382   We observe a broadly symmetrical response to Case 1, where the twofold increase in rainfall leads to an

383   initial twofold increase in erosion rate ($E > U$) and a ~30% decrease in steady state fluvial relief. The

384   transient knickpoint is concave-up in this case and it broadens as it migrates upstream, as is expected for a

385   concave-up knickpoints where $n > 1$ (Royden & Perron, 2013). The signal of transient adjustment

386   communicated to tributaries is consequently protracted, making adjustments more diffuse.

387   Responses reflected in k_{sn}–E_{avg} and $k_{sn\text{-}q}$–E_{avg} relationships also mirror Case 1. As is characteristic for k_{sn},

388   the initial change in erosional efficiency causes the trunk and tributary network to shift onto a different

389   steady state erosional efficiency curve; in this case, from $K = K_p$ to $K = 2 \cdot K_p$, and they generally follow this

390   curve during adjustment (Figure 4a). Minor deviations from this curve exhibit a convex-up pattern (inverted

391   from Case 1) due to the opposite knickpoint shape. Meanwhile in $k_{sn\text{-}q}$–E_{avg} space (Figure 4b), the initial

392   and final equilibrium conditions for both the trunk and tributary network plot in the same location, as in

393   Case 1. The change in rainfall again causes a shift only along the $K=K_p$ curve, but to uniformly higher $k_{sn\text{-}}$

394      $_q$ and erosion rate in this case, and they generally follow this curve during adjustment back to steady state.

4.3 Case 3: Spatially Uniform to Bottom-heavy

396   In this scenario, we model the catchment response to a change in rainfall pattern from spatially uniform 1.5

397   m/yr to a gradient that decreases upstream from 4 to 0.5 m/yr, resulting in a complex transient response.

398   Mean rainfall increases by ~80%, which remarkably also drives a 30% increase in fluvial relief that

399   contrasts with the 25% decrease expected for a spatially uniform increase in rainfall of the same magnitude

400   (Figure 3b; Movie S3).

401   *4.3.1 Case 3: Trunk Response*

402   In this case, because the change in rainfall is spatially variable along the trunk river, the initial change in

403   erosion rate is also variable. The trunk river experiences an approximately 80% increase in erosion rate at

404   the outlet ($E > U$), and a decrease of 67% in the headwaters ($E < U$), corresponding to the change in

405   upstream average rainfall along its length. At x_{sc} (located ~27 km upstream from the outlet), $Q_f = Q_i$, $S_f =$

406   S_i, and so immediately following the change in rainfall $E = U$. Enhanced incision at the outlet produces a

407   concave-up knickpoint; however, as this knickpoint migrates upstream it progressively sharpens and

408   eventually evolves into an oversteepened convex-up knickpoint, contrasting with expectations for the

409   increase in rainfall (e.g., Case 2). Oversteepening is a consequence of the upstream decrease in erosional

410   efficiency driven by the rainfall gradient that is exacerbated by, but does not depend on, differing modes of

411   adjustment upstream and downstream of x_{sc} related to the complex response. This is analogous to knickpoint

412   behavior described by Forte et al. (2016) and Darling et al. (2020) where modelled lithologic contacts

413   demarcate similar relative variations in erosional efficiency (i.e. hard rocks over soft rocks). Lastly, we note

414   that everywhere upstream of x_{sc} over-adjusts during the transient response, which is a characteristic of

415   complex responses in general, leading to variable modes of adjustment in time and space. The

416   overadjustment we observe is essentially the whiplash response described by Gasparini et al. (2006, 2007),

417   but notably results here without sediment flux. This continuous evolution of the trunk knickpoint has

418   important consequences for signals passed to tributaries.

419   *4.3.2 Case 3: Tributary Response*

420   Tributary responses to the change in rainfall pattern depend largely on their position. Individual tributaries

421   experience changes in erosional efficiency proportional to their change in rainfall. Changes to both

422   quantities are always different from those of the trunk river at their confluence (Figure 2a inset).

423   Additionally, tributaries also respond to changing boundary conditions related to adjustment of the trunk

424   river. These signals are often conflicting. For example , enhanced incision along the trunk river downstream

425   from x_{sc} causes tributaries there to experience a relative increase in the rate of base-level fall. Alone, this

426   should promote steepening, but higher erosional efficiency (higher rainfall) counteracts steepening. The net

427   effect of this competition plays out differently as a function of tributary position as 1) the discrepancy

428   between the local rainfall conditions experienced by tributaries and the upstream averaged rainfall

429   experienced by the trunk profile narrows upstream (Figure 2a inset), 2) the transient base level signal (i.e.,

430   trunk knickpoint) changes shape as it sweeps upstream, and 3) the duration of transient adjustment increases

431   upstream.

432   *4.3.3 Case 3: k_{sn}–E_{avg} and k_{sn-q}–E_{avg}*

433   Plots of k_{sn}–E_{avg} and k_{sn-q}–E_{avg} clarify some additional features of the transient response (Figure 5). The

434   trunk profile exhibits higher k_{sn} and k_{sn-q} values and spans a relatively narrower range in erosion rates than

435   tributaries during transient adjustment, reflecting the fundamentally different ways they experience the

436   modelled rainfall gradient. This behavior illustrates that the network of tributaries (isolated catchments that

437   individually experience relatively uniform rainfall but collectively span a range of conditions) inherently

438   incorporates a more direct signal of the change in rainfall patterns compared to the trunk, which averages

439   upstream rainfall variations. This is consistent with findings by Han et al. (2015) for steady state landscapes

440   exposed to orographic rainfall and is important for designing an effective sampling strategy in the field –

441   discussed further in section 5.3.

442   In k_{sn}–E_{avg} space (Figures 5a, 5b), shifts onto different erosional efficiency curves occur as in Cases 1 & 2,

443   but here the spatial rainfall variability causes different positions along the trunk and individual tributaries

444   shift by different amounts. The trunk profile response spans from $K = 0.5 \cdot K_p$ to $\sim 1.8 \cdot K_p$, while the network

445   of tributaries spans from $K = 0.5 \cdot K_p$ to $4 \cdot K_p$. To first order, points representing a given location along the

446   trunk or a given tributary move along these curves reflecting local erosional efficiency during adjustment

447   toward steady state as in Cases 1 & 2, but again deviate in detail. Trajectories are more complex in this case

448   because of the interplay between changes in erosional efficiency and baselevel variations in modulating

449   tributary channel steepness and the over-adjustments mentioned previously (*c.f.*, Figures 4 & 5). Finally,

450   we note an interesting feature where the range of erosional efficiency values that correspond to upstream

451   mean k_{sn} at steady state for the trunk profile ($K = 0.5 \cdot K_p$ to $\sim 1.8 \cdot K_p$) are lower than that implied by mean

452   rainfall (i.e., $K = \sim 2.7 \cdot K_p$; Figures 1b, 5a) – discussed further in section 5.2.

453   In $k_{sn\text{-}q}$–E_{avg} space (Figures 5c, 5d), differences between trunk and tributary responses and k_{sn} vs. $k_{sn\text{-}q}$ are

454   readily apparent. Initial and final steady state conditions plot in the same position, as is characteristic of $k_{sn\text{-}}$

455    $_q$ where uplift rate is constant. Following the change in rainfall, the trunk profile expands slightly obliquely

456   to the $K=K_p$ curve, where downstream locations are systematically shifted toward higher erosional

457   efficiency. This shift reflects systematic slope adjustments that must occur along the trunk to bring it into

458   equilibrium with the non-uniform rainfall pattern and decreases with time as these adjustments take place.

459   Apart from this minor shift, different positions along the trunk profile generally follow the $K=K_p$ curve

460   during adjustment back to steady state. In tributaries, on the other hand, the change in rainfall causes

461   expansion precisely along the $K=K_p$ curve because they experience no along-stream variations in rainfall.

462   Tributaries again generally evolve along the $K=K_p$ curve toward steady state (as with cases 1 and 2).

463   Transient morphological adjustments affect this trajectory in detail and deviations, which affect apparent

464   erosional efficiency, are more significant in drier tributaries near the headwaters. Overadjustment is also

465   evident for both the trunk and tributaries in this space, but because transient evolution is generally along

466   the steady state curve, it does not significantly affect the apparent erosional efficiency. As a final note,

467   dispersion around the steady state erosional efficiency curve in $k_{sn\text{-}q}$–E_{avg} space is minor over the duration

468   of the transient adjustment compared to dispersion in k_{sn}–E_{avg} space – we expand on implications from this

469   point in section 5.3.

4.4 Case 4: Spatially Uniform to Top-heavy

471   In this final case, we the model the catchment response to a change in rainfall pattern from spatially uniform

472   1.5 m/yr to a gradient that increases upstream from 0.25 to 2.25 m/yr, which also results in a complex

473   transient response. Mean rainfall decreases by 33% and fluvial relief also decreases by 10% (Figure 3;

474   Movie S4), which contrasts with the 22% increase in fluvial relief expected for a spatially uniform decrease

475   in rainfall of the same magnitude.

476   *4.4.1 Case 4: Trunk Response*

477   In this case, the trunk river experiences a 33% initial decrease in erosional efficiency and erosion rate at the

478   outlet, and a 50% increase in the headwaters following the change in rainfall pattern (Figure 6). This range

479   is significantly narrower than the range of variations in rainfall because of the buffering effect that

480   concentrating rainfall in the headwaters has on downstream changes in discharge (e.g., Figure 2b inset).

481   Like Case 3, because this scenario also exhibits a complex transient response, the transition between

482   decreases in erosion rate downstream and increases upstream is initially at position x_{sc}. Unlike Case 3,

483   knickpoint shape does not invert during transient adjustment and is always convex-up. Interestingly,

484   combined with observations from Case 3, this suggests that complex responses generally are more likely to

485   exhibit convex-up knickpoints. Retention of the knickpoint shape is accommodated by over-adjustment

486   upstream of x_{sc}, specifically by progressively more rapid upstream adjustment (higher erosional efficiency)

487   toward gentler slopes that outpaces downstream adjustment. By the time that the migrating trunk knickpoint

488   reaches positions upstream of x_{sc}, the profile has incised below its equilibrium elevation and is shallower

489   than its equilibrium slope. Thus, the profile is forced to uplift and steepen to reach steady state, preserving

490   the convex-up knickpoint shape (Movie S4).

491   *4.4.2 Case 4 Tributary Response*

492   Complexities in the trunk response again dramatically affect the tributary responses, and generally mirror

493   complexities discussed in Case 3. Tributaries again respond to variable and commonly conflicting signals.

494   In this case, tributaries downstream from x_{sc} initially respond to a decrease in rainfall (lower erosional

495   efficiency) by steepening. However, decreases in erosional efficiency along the trunk profile drives

496   steepening and surface uplift, forcing tributaries to respond to a conflicting signal of base-level rise (Movie

497   S4). Additionally, tributaries in downstream locations are relatively much drier and adjust relatively slowly

498   compared to upstream locations. Interestingly, the trunk profile adjusts and communicates transient base-

499   level signals upstream to wetter tributaries relatively quickly compared to the adjustment timescale of these

500   dry tributaries, which follows as the trunk river has much higher erosional efficiency from rainfall

501   concentrated in its headwaters. The initially counterintuitive result of this is that central portions of the

502   catchment are the first to achieve steady state (i.e., both the trunk profile and tributaries achieve the new

503   steady state), followed by the headwaters, and lastly tributaries near the outlet where the transient signal

504   originated, which contrasts with the common expectation of adjustment proceeding in an upstream fashion.

505   *4.3.3 Case 4: k_{sn}–E_{avg} and $k_{sn\text{-}q}$–E_{avg}*

506   Evolution of k_{sn}–E_{avg} and k_{sn-q}–E_{avg} relationships during the transient response are generally similar to Case

507   3, but with a few exceptions. First, the disparity between final steady state conditions for the trunk profile

508   and network of tributaries is significantly greater than Case 3 (Figures 6a, 6b), which reflects the extent to

509   which the rainfall pattern buffers variations in erosional efficiency along the trunk. Also, in k_{sn-q}–E_{avg} space,

510   apparent erosional efficiency is more strongly affected during transient adjustment in the tributary network

511   compared to the trunk profile (transient deviations from the $K=K_p$ curve), but also compared to Case 3.

512   Large deviations are again restricted to drier tributary catchments, and comparison to Case 3 expresses that

513   changes in rainfall have a non-linear effect (Equations 1). That said, even these stronger effects on apparent

514   erosional efficiency in k_{sn-q}–E_{avg} space are still minor compared to representing any equivalent time in the

515   k_{sn}–E_{avg} relationship with a spatially and temporally uniform erosional efficiency value. Finally, also like

516   Case 3, the range of erosional efficiency values for the trunk profile ($K = \sim1.8 \cdot K_p$ to $2.25 \cdot K_p$) are different,

517   but in this case higher than is implied by mean rainfall (i.e., $K = \sim K_p$; Figures 1b, 6a) – discussed further in

518   section 5.2.

519   **5. Discussion**

520   The central themes we have explored so far are how the spatial rainfall pattern influences the channel profile

521   morphology, and how temporal changes in rainfall pattern affect erosion rates and profile morphology

522   during periods of transient adjustment. We have detailed the expected response to along-stream variations

523   in erosional efficiency caused by spatial rainfall gradients according to the SPM and have shown how the

524   transient response to a change in rainfall pattern is fundamentally different from a spatially uniform change

525   in rainfall. A change in rainfall pattern will always result in spatially variable changes of erosion rates that

526   also change with time during the transient response. In some circumstances a given location may, over time,

527   experience both elevated and reduced erosion rates (and channel steepness values) relative to equilibrium

528   in response to a single change in rainfall. It is important to keep in mind, however, that the nature of transient

529   response depends strongly on the initial conditions at the time of the change in rainfall pattern. Therefore,

530   there is a complex relationship between the transient response at any given location or time and both the

531   change in mean rainfall and the final rainfall pattern. In the following discussion, we focus on highlighting

532   some implications for the different expectations that follow from changes in rainfall pattern and discussing

533   examples where conventional expectations based on spatially uniform changes in rainfall can potentially

534   lead researchers astray. Where possible, we attempt to identify additional information or strategies that may

535   be leveraged by future studies.

536   **5.1 Revising Expectations for Erosional and Morphological Responses to Changing Climate**

537   *5.1.1 Relative Nature of Erosional Response*

538   To this point, our choice of a steady state initial condition with spatially uniform rainfall has been
539   convenient, as have been the terms top-heavy and bottom-heavy to describe typical orographic rainfall
540   patterns. While idealized, this provides an intuitive starting point for understanding how more complicated
541   – but almost certainly more realistic – climate change scenarios might play out. Recall, according to the
542   SPM, transient climate-driven changes in erosion rate are dictated by a *relative* change in discharge. Where
543   discharge is increased, erosion rates increase in response and river gradient declines toward a new
544   equilibrium steepness; thus, a river subjected to an increase in discharge can be considered locally, if
545   transiently, oversteepened relative to equilibrium, and vice versa. As we have shown, because discharge
546   generally accumulates non-linearly downstream within a river basin, a change in rainfall pattern can create
547   circumstances where the relative change in discharge inverts along the river length – at position x_{sc} –
548   producing a complex transient response (Figures 2 & 3). This implies that the river is simultaneously
549   oversteepened and understeepened on either side of position x_{sc}. These transient states dictate whether
550   erosion rates initially increase or decrease following the change in rainfall, respectively, not whether the
551   new rainfall pattern is itself top-heavy or bottom-heavy, and the positions of these transient states shift
552   throughout adjustment.

553   The nature of landscape response to relative changes in discharge implies, for instance, that relaxation of a
554   bottom-heavy rainfall gradient can cause a complex transient response resembling a change from uniform
555   to top-heavy rainfall patterns. That is, a weaker bottom-heavy gradient is relatively top-heavy compared to
556   an extreme bottom-heavy gradient; similarly, a gentler top-heavy gradient is relatively bottom-heavy
557   compared to an extreme top-heavy gradient, and vice versa (Figure 7). Thus, for example, in the case of a
558   change in climate that causes an extreme bottom-heavy rainfall gradient to become less bottom-heavy *and*
559   results in a complex transient response (e.g., Figure 7a), rainfall and erosion rate are expected to increase
560   in the headwaters of the catchment and decrease near the outlet as seen for Case 4 (uniform to top-heavy).
561   This response is not consistent with expectations for any uniform increase or decrease in rainfall, even if
562   such a shift accurately reflects the change in mean rainfall. Therefore, neither the final rainfall pattern alone
563   (i.e., modern observed pattern) nor accurate inference about the relative change in mean rainfall (wetter or
564   drier) necessarily allow a robust prediction of changes in erosion rate within a catchment following a change
565   in climate where rainfall patterns have changed significantly.

566   Interestingly, changes in climate do not need to involve extreme changes in rainfall patterns (e.g., reversal
567   from top-heavy to bottom-heavy), or to occur over short timescales to drive complex transient responses.
568   Indeed, even subtle changes in rainfall pattern potentially driven by minor, commonly occurring variations
569   temperature and atmospheric conditions (e.g., Mutz et al., 2018; Roe et al., 2003; Siler & Roe, 2014), may

570 induce complex responses and significantly, if temporarily, alter the spatial pattern of erosion in a catchment

571 (Figures 3 & 7). Indeed, such climate changes may have occurred in the Peruvian Andes and eastern-central

572 Himalaya in the transition from Pliocene to Pleistocene climates, the latter represented by Last Glacial

573 Maximum conditions (LGM; Figure 7c & 7d). Even if rivers in each of these ranges were in a transient

574 state during Pliocene time, any adjustment toward equilibrium with the Pliocene rainfall pattern that

575 occurred would then be in disequilibrium with the Pleistocene (LGM) rainfall pattern, and would have

576 driven a complex response.

577 As transient adjustments proceed relatively more rapidly where rainfall is more concentrated (i.e., erosional

578 efficiency is higher), changes in rainfall pattern have the potential to produce spatially distinct effects

579 different from what would be expected from considering uniform changes in mean climate. Transient

580 adjustments may therefore be relatively enhanced or underdeveloped in different locations within the same

581 catchment, or adjustment to quasi-equilibrium may be essentially complete in some locations while others

582 reflect only an incipient response to the climate change. We noted an example of this behavior in Case 4,

583 where low-elevation dry tributary catchments preserve transient conditions the longest, contrasting with the

584 notion that headwater catchments should be the last to equilibrate. Similarly segregated conditions occur in

585 Case 3, where adjustment to quasi-equilibrium is essentially complete in wet low-elevation catchments long

586 before the migrating trunk knickpoint even reaches drier high-elevation catchments. Because such complex,

587 climate change-driven landscape adjustments are not reasonably captured by a conceptual framework based

588 on spatially uniform changes in rainfall (e.g., compare Cases 3 & 4 to Cases 1 & 2), apparent inconsistencies

589 between expectations and observations have the potential to give a false impression about the primary

590 forcing(s) controlling erosion rates.

591 Additionally, if large-scale changes in rainfall patterns like we model develop incrementally over long

592 timescales (e.g., millions of years), they could still result in complex transient responses. Greenhouse-

593 icehouse transitions and orogenic growth are among many geologically significant events that may cause

594 temporally distinct, sustained, and dramatic changes to climate and/or circulation patterns where complex

595 responses could arise (Mutz et al., 2018; Poulsen et al., 2010; Roe et al., 2003; Zachos et al., 2001), If, for

596 example, the bottom-heavy gradient in Case 3 instead develops over several million years, regardless any

597 added complexity to the general trajectory of this change in rainfall pattern, the result is that it supports a

598 30% increase fluvial relief despite also increasing total rainfall by ~80%, and channel steepness patterns

599 fundamentally change as the catchment adjusts. Gradual changes in rainfall patterns cause morphological

600 adjustments to become more diffuse, and induce relatively smaller transient changes in erosion rate than

601 abrupt changes. However, the spatial pattern of erosion is still significantly affected (i.e., in excess of a

602   factor or two from steady state) so long as the timescale over which the rainfall pattern evolves does not far

603   exceed that of the catchment adjustment timescale, which may be several million years for large river basins

604   (Roe et al., 2003; Whipple, 2001). As such, the general characteristics of the classes of transient behavior

605   following changes in rainfall pattern toward *relatively* bottom-heavy or top-heavy conditions remain intact,

606   even for long-term transient responses.

607   *5.1.2 Multi-stage Adjustment*

608   It has long been recognized that spatially uniform changes in rainfall should promote transient changes in

609   erosion rate everywhere across a landscape, which cause morphological adjustments to sweep upstream to

610   restore erosional equilibrium (e.g., Tucker & Slingerland, 1997; Whipple & Tucker, 1999). Our model is

611   fully consistent with this expectation under such conditions (e.g., Cases 1 & 2). In addition, we have shown

612   that responses to changes in the rainfall pattern are variable in both space and time (e.g., Cases 3 & 4). As

613   a consequence, following any non-uniform change in rainfall pattern, distinct initial morphological and

614   erosional changes always precede the upstream sweeping adjustments that ultimately restore equilibrium.

615   Contrary to expectations for a uniform change in rainfall, we find that catchments characteristically exhibit

616   a relatively protracted, multi-stage, and spatio-temporally variable response to a single temporal change in

617   rainfall pattern (Figure 8; Movie S5). We emphasize that this behavior is a general characteristic of any

618   spatially variable change in rainfall pattern and is not exclusive to those that induce the complex transient

619   responses. This leads to novel expectations for how transient responses to changes in climate should be

620   expressed across a landscape and has potentially important implications for detecting transient landscape

621   responses to climate changes.

622   The initial stage of morphological adjustment begins synchronously across the entire river basin following

623   a change in rainfall pattern. At the onset, local erosion rate is everywhere a function of the local relative

624   change in discharge. As this initial stage proceeds, spatial variations in erosion rate along the trunk river

625   produce morphological changes along its length that progress at different rates (variable erosional

626   efficiency). Importantly, this means that initial, or "relict", conditions are often not preserved upstream of

627   slope-break knickpoints on the trunk profile; the profile is progressively modified as adjustment proceeds

628   even upstream of the main knickpoint. Indeed, the resemblance of "unadjusted" profile segments upstream

629   from the main knickpoint to their initial state diminishes with time during the transient response, and thus

630   with relative position upstream. This contrasts with spatially uniform changes in rainfall (and erosional

631   efficiency; e.g., Cases 1&2), or uplift rate that does not affect erosional efficiency, that allow preservation

632   of relict morphological characteristics (e.g., k_{sn}) upstream of migrating transient knickpoints, as is often

633   assumed in analysis and inversions of river profiles (e.g., Clark et al., 2006; Fox et al., 2014; Gallen et al.,

634   2013; Goren et al., 2014; Kirby & Whipple, 2012; Miller et al., 2013; Schoenbohm et al., 2004; Whittaker

635   et al., 2007). More broadly, this contrasts with the notion that adjustments to climate change should simply

636   propagate upstream from base level as is expected for other external changes (e.g., uplift rate). While there

637   is a signal of transient adjustment that indeed migrates upstream, significant amounts of surface uplift, as

638   observed in Case 3 (Movie S3), or incision, as observed in Case 4 (Movie S4), along with changes in

639   channel steepness can occur prior to arrival of this signal. Nevertheless, these changes are in response to

640   the change in climate. Additionally, spatio-temporally variable adjustments along the trunk profile dictate

641   that individual tributaries experience temporally variable rates of base-level fall until the trunk profile

642   reaches a new equilibrium at their confluence (Movie S3 & S4).

643   The continuous, yet variable nature of base-level fall imposed by the trunk river on tributaries during the

644   initial stage of adjustment generally results in a broad adjustment zone characterized by smooth variations

645   in channel steepness in tributary catchments. Indeed, tributaries in our model located in upstream positions,

646   where this initial adjustment stage is relatively long-lived (compared to tributaries located near the trunk

647   outlet), experience significant changes in slope and relief without formation of any knickpoints (e.g., Figure

648   8b; Movies S3 & S4). Importantly, this shows that tributaries are not insulated from effects of spatially

649   variable changes in rainfall (variable erosional efficiency) along their trunk river, even if they experience

650   essentially uniform rainfall throughout their history. Furthermore, they may appear relatively well-adjusted

651   (graded) during periods of transient adjustment despite significant deviation from both initial and final

652   steady state conditions (Figure 8b; also see Tributary 2, Movies S3 & S4).

653   Adjustment to quasi-steady-state conditions along the trunk river, which may or may not be associated with

654   the upstream migration of a significant or obvious slope-break knickpoint, defines the beginning of the

655   second – and final – stage of adjustment in our model landscapes (Figure 8). The rate of base-level fall

656   experienced by a given tributary stabilizes upon local adjustment of the trunk profile, representing a distinct

657   change from the initial stage where the rate of base-level fall is temporally variable. Depending on

658   circumstances, this change may be abrupt and produce a discrete knickpoint that sweeps upstream through

659   the tributary catchment. The change in base-level fall rate is the dominant signal exhibited during this

660   second adjustment stage, although it acts upon the profile state reached during the initial adjustment stage,

661   and it is largely a function of the shape and migration rate of the trunk knickpoint. Both factors are

662   controlled by the integrated response of the trunk profile to this point, and therefore do not relate to the

663   change in rainfall pattern in a direct manner. Therefore, the dominant signal passed to tributaries during

664   this second stage, and any knickpoints that form as a result, generally do not reflect the change in rainfall

665   locally within the tributary catchment, and their relationship to the regional rainfall pattern experienced by

666   the trunk stream is complex. This is directly contrary to expectations for spatially uniform changes in

667   rainfall where changes in slope above and below knickpoints should scale with the magnitude of the change

668   in rainfall (e.g., Whipple, 2001).

669   Extrapolating these observations to natural, inherently more complex river networks, suggests that broad

670   adjustment zones comprising multiple knickpoints might be associated with a given change in rainfall

671   pattern – in contrast to the single knickpoint or knickzone expected to accompany a spatially uniform

672   change in rainfall magnitude (e.g., Case 1 & 2). For instance, if second-order rivers (*sensu* Hack, 1957)

673   experience spatially variable rainfall patterns in addition to the trunk, then we expect third-order rivers

674   should experience an additional pair of adjustment stages. This implies that the full transient response to

675   changes in rainfall pattern may be expressed in a complex fashion, and potentially across a large areal

676   extent, in large river basins (e.g., Figure 8; Movie S5). If true, this multi-stage adjustment behavior may

677   ultimately pose a significant, still unresolved, challenge to recognizing and quantifying transient responses

678   to changes in climate in many settings.

679   **5.2 Recognizing the Influence of Climate on Topography and Erosion Rates**

680   *5.2.1 Steady State Relationships among Channel Steepness, Erosion Rate, and Erosional Efficiency*

681   The SPM makes specific predictions about the relationships among channel steepness, erosion rate, and

682   erosional efficiency (K) at steady state (Equation 6), and as shown by curves in Figures 4-6. Because the

683   role of climate is encapsulated in K, it is important to remember that a uniform K value implies that the

684   influence of climate is uniform over the spatial and temporal scales of interest. Further, the expectation that

685   basin-average topographic metrics like k_{sn} should relate to rainfall in a simple way generally relies on an

686   assumption of a spatially uniform K value. Rainfall gradients systematically affect this expectation, where

687   bottom-heavy gradients result in higher k_{sn} (lower apparent erosional efficiency), while top-heavy gradients

688   result in lower k_{sn} (higher apparent erosional efficiency) (Figure 9). The magnitude of this effect (as a

689   percentage of actual erosional efficiency) varies with strength of the rainfall gradient. However, k_{sn} values

690   also vary with erosion rate (uplift rate at steady state; Equation 6a). Therefore, while subtle rainfall gradients

691   affect apparent erosional efficiency to a proportionally lesser degree, they can still substantially influence

692   observed k_{sn} values, even at steady state, where uplift rates are higher. This can be important in natural

693   settings where uplift rates, erosional efficiency, and the form of their relationship to topography are

694   generally unknown.

695   This analysis has two related and important implications. First, interpretation of the controls on topography

696   (e.g., mean k_{sn}, mean gradient, relief, etc.) in terms of climate sensitivity, uplift, and/or rock properties using

697   measurements from catchments that experience the same mean rainfall, but different rainfall patterns, is not

698   necessarily valid even at steady state. Second, it predicts weaker correlations (more dispersed) between

699   topographic metrics and erosion rate than would be expected if rainfall were always uniformly distributed,

700   as is implied by use of basin-average rainfall (Figure 9), simply from neglecting the rainfall pattern. This

701   prediction applies even before considering any geologic uncertainties (e.g., at quasi-steady-state or

702   potentially transient?), analytical uncertainty, and even if no other variations in *K* exist. Because rainfall

703   gradients create systematic, rather than random, dispersion around relationships expected for uniformly

704   distributed rainfall, there is not necessarily any expectation that larger datasets will more accurately resolve

705   variations in erosional efficiency unless catchments where rainfall is uniform are isolated, or a correction

706   is made for the influence of spatially variable rainfall (e.g., using k_{sn-q}). Rather, compilation of topographic

707   measurements from basins that do and do not experience rainfall gradients can, in and of itself, obscure or,

708   depending on circumstances, distort the actual influence of rainfall on erosional efficiency (Figure 9). This

709   result is of particular importance for designing future efforts to empirically test the SPM in natural settings.

710   *5.2.2 Misleading Transient Signals*

711   Spatial patterns in erosion rate are commonly used to inform tectonic models and to infer rock uplift rates

712   in mountain landscapes (e.g., Adams et al., 2020; Godard et al., 2014; Kober et al., 2015; Morell et al.,

713   2015; Safran et al., 2005; Scherler et al., 2014). However, we have shown that changes in rainfall patterns

714   can drive long-lived and complex spatial patterns of erosion that differ from expectations for uniform

715   changes in rainfall and thus may not be readily recognized and interpreted. We have also shown that that

716   ongoing transient adjustment may not be obviously expressed in landscape morphology (especially for

717   catchment-mean metrics) under some circumstances. If these caveats are not considered, subtly expressed

718   transient spatial variations in erosion rate may be mistaken as representing quasi-steady state spatial

719   variations in uplift rate (i.e., $E = U$). At once this would give a false impression both about the spatial pattern

720   of uplift and the importance of past climate changes on a landscape's evolution, with direct implications

721   for understanding connections among climate, surface processes, and tectonics. Determining whether there

722   are circumstances in which spatial patterns of erosion and topography produced by changes in rainfall

723   patterns that can be misleading enough to confound interpretations about factors controlling landscape

724   evolution is critically important.

725   During the early transient adjustment in Case 3 (transition to a bottom-heavy rainfall pattern) there is a clear

726   example of how such confusion may occur (Figure 10). Recall, in this case, early transient adjustment

727   produces a concave-up knickpoint along the trunk profile but as it migrates upstream the shape evolves.

728   This creates a broad adjustment zone. Over the first ~500 kyr, quasi-steady state adjustment proceeds ~60%

729   upstream along the trunk, but the broad adjustment zone means most tributaries along this length experience

730   a protracted signal of base-level changes related to trunk adjustment. Because these tributaries all also

731   experience a net increase in rainfall, knickpoints associated with local adjustment of the trunk river (Stage

732   2) tend to relax as they work upstream making them more diffuse. This protracted competition between

733   local rainfall and spatio-temporally variable rates of base-level fall, generally results in diffuse concave to

734   broad convexo-concave adjustment zones in tributaries (e.g., Figure 8a; Movie S5). Broad adjustment

735   zones, particularly concave-up adjustment zones, are inherently subtle and this can inhibit their recognition.

736   This problem may be further compounded by the influence of sediment flux in natural settings (Brocard &

737   van der Beek, 2006; Whipple & Tucker, 2002). Indeed, even in our idealized model (i.e., no sediment

738   influence), along-stream variations in trunk and tributary local k_{sn} variation is diffuse (Figure 10c). Based

739   on a lack of significant knickpoints that might indicate transient adjustment and the several-fold spatial

740   variation in erosion rate, one might reasonably interpret relationships depicted in Figure 10a reflect a quasi-

741   steady-state landscape adjusted to a spatial gradient in uplift rate. In the absence of known surface breaking

742   structures that might accommodate this gradient in uplift, blind structures may be inferred, with potential

743   implications for tectonic models. The apparent viability of this interpretation is supported by the SPM if

744   rock uplift rate is assumed to match the observed pattern of catchment averaged erosion rates in tributaries

745   (steady-state conditions) as illustrated in Figure 10b. Figure 10b shows that the predicted steady-state

746   upstream-averaged k_{sn} pattern along the trunk river and mean k_{sn} values exhibited by the tributary network

747   is essentially identical to the transient pattern in Figure 10a. Moreover, even in detail, there are only subtle

748   differences in the along-stream pattern of local k_{sn} between the two scenarios (Figure 10c). Thus, in this

749   instance, k_{sn} patterns and erosion rates that actually record a complex transient response to a change in

750   rainfall pattern could reasonably be mistaken for a steady state landscape adjusted to a spatial gradient in

751   uplift.

752   Although subtle variations in k_{sn} values might give a misleading impression that a landscape is in quasi-

753   steady-state, the spatial pattern of k_{sn-q} unambiguously suggests along-stream variations in erosion rate exist

754   along both the trunk river and tributaries. k_{sn-q} also exhibits a coherent pattern of downstream adjustment

755   that could readily be interpreted as a transient signal sweeping upstream through the catchment that,

756   significantly, is inconsistent with a steady state landscape adjusted to the spatial gradient in uplift shown in

757   Figure 10b (Figure 10c). This example shows the potential usefulness of k_{sn-q}, both as a diagnostic tool for

758   detecting ongoing transient adjustment to changes in rainfall patterns where k_{sn} may be misleading and for

759   resolving the relative influences of tectonics and climate.

760   Finally, we emphasize that our intention is not to suggest all, or any specific examples, where spatial

761   patterns of rock uplift are inferred from erosion rates and channel steepness patterns are incorrect. Rather,

762   our intention here is to highlight the extent to which confusion may be possible under the right

763   circumstances, and how explicitly accounting for rainfall patterns can be a step toward addressing these

764   challenges.

765   **5.3 Toward Detecting the Influence of Climate on Topography and Erosion Rates**

766   Remote analysis of channel steepness patterns can provide a preliminary means to detect whether the

767   climate may be influencing river profiles in a landscape, and whether transient adjustment to a change in

768   climate may be ongoing. For landscapes well-described by the SPM, discrepancies between rainfall

769   conditions experienced by trunk and tributary basins should cause systematic differences in trunk and

770   tributary k_{sn} (Figures 5&6; Gasparini & Whipple, 2014), but not in $k_{sn\text{-}q}$. As illustrated in Figure 10c, the

771   expected contrast in trunk and tributary k_{sn} is most developed at steady state, but it begins manifesting

772   immediately during transient adjustment as differences in local k_{sn} at confluences that migrate upstream

773   (Figure 10c, Movie S5). In contrast, precise agreement between trunk and tributary $k_{sn\text{-}q}$ is expected at steady

774   state, and it is approximately maintained even during periods of adjustment to a change in rainfall pattern.

775   Agreement between trunk and tributary $k_{sn\text{-}q}$ that weakens upstream from confluences may also be an

776   important indication of ongoing transient adjustment that may be difficult detect from the k_{sn} pattern alone

777   (Figure 10c, e.g., as discussed in section 5.2.2). Therefore, comparison of k_{sn} and $k_{sn\text{-}q}$ patterns may be a

778   useful way to diagnose and further assess the potential extent of influence by rainfall gradients, provided

779   the pattern of discharge accumulation can be reasonably estimated (e.g., using high spatial resolution

780   satellite rainfall or nested stream gauge data).

781   Following topographic analysis, our results have additional implications for designing effective catchment-

782   averaged erosion rate sampling strategies. Broadly, sampling strategies can be grouped into two classes:

783   nested and distributed, described below. Nested, or hierarchical, sampling strategies comprise multiple

784   samples from the same river basin where some or all samples are collected along the trunk river, and where

785   averages typically integrate over very large (10^2–10^5 km^2) drainage areas (e.g., Abbühl et al., 2010; Henck

786   et al., 2011; Portenga et al., 2015; Reinhardt et al., 2007; Safran et al., 2005; Whittaker et al., 2007;

787   Willenbring et al., 2013; Wittmann et al., 2016). In principle, such strategies can allow researchers to assess

788   reproducibility of individual measurements, test sediment mixing models, and sub-divide basins into

789   different sectors to identify along-stream variations in erosion rates. Given the complex along-stream

790   patterns of erosion rate we observe in response to changing rainfall patterns and widely disparate responses

791   between trunk and tributary profiles, however, our results suggest that caution is warranted in interpreting

792   patterns of erosion rates collected in a nested fashion. In particular, this includes datasets that compile

793 measurements from along trunk rivers and tributary catchments, but also those that compare samples from

794 different large catchments that experience different mean climates and rainfall patterns, even at quasi-

795 steady-state, because how each reflects and experiences variations in rainfall may be fundamentally

796 different. Furthermore, because we find that along-stream variations in erosion rate due to changes in

797 rainfall pattern are characteristically muted along the trunk profile (e.g., Figure 10a), nested strategies may

798 not be appropriate in many settings, especially if the goal is to measure the influence of climate on fluvial

799 incision.

800 The other widely used strategy, which we refer to as a distributed sampling strategy, targets single samples

801 from catchments that are distributed across a landscape or mountain front, and typically – though certainly

802 not always – comprises relatively smaller (10^0-10^2 km^2) catchments (e.g., Adams et al., 2020; Binnie et al.,

803 2008; Carretier et al., 2013; DiBiase et al., 2010; Godard et al., 2014; Morell et al., 2015; Ouimet et al.,

804 2009; Scherler et al., 2014). This type of strategy generally allows more freedom to carefully select

805 preferable catchments (relatively uniform channel steepness, rainfall, lithology), with the limitation that

806 spatial variations in erosion at the sub-catchment scale are not resolvable with single measurements. In

807 contrast to muted spatial variations in erosion noted for nested strategies, our model results suggest

808 distributed strategies inherently record a more direct signal of climatic influences than nested approaches,

809 consistent with previous findings by Han et al. (2015). However, if inter-catchment variations in rainfall

810 and therefore erosional efficiency are not accounted for, or transient conditions are not recognized, this

811 sensitivity may cause significant dispersion or distortion in measured relationships among landscape

812 metrics, as shown for k_{sn}–E_{avg} relationships (Figures 5b & 6b), and/or lead to misleading spatial patterns in

813 erosion rate and k_{sn} (Figure 10).

814 Lastly, we note that transient adjustments in response to changes in rainfall pattern do not significantly

815 affect apparent erosional efficiency in k_{sn-q}–E_{avg} relationships where no variations in rock properties exist,

816 even in response to the dramatic shifts in rainfall patterns that we model, regardless of sampling strategy.

817 Indeed, transient deviations from expected steady state relationships modelled in any location are generally

818 well within the analytical uncertainty of measured catchment-average erosion rates from natural landscapes

819 (Figures 5 and 6). Exceptions to this appear to be limited to scenarios where landscapes experience a shift

820 toward arid climates. Nevertheless, transient, spatially variable patterns of erosion caused by changes in

821 rainfall pattern are reflected in k_{sn-q} patterns with good accuracy in our model (Figure 10c, Movie S3-S5).

822 As such, k_{sn-q} may be used to recognize ongoing adjustment to changes in climate where k_{sn} can be

823 ambiguous. We suggest that k_{sn-q}, or a different metric that encompasses the spatial distribution of rainfall

824 (runoff), may be vital component for future efforts to detect climate's influence on and from topography

825   and erosion rates in mountain landscapes where rainfall is inherently spatially variable.

826   **5.4 Caveats and Limitations**

827   Several important caveats should be kept in mind when evaluating the results and subsequent discussion
828   presented here. First, and foremost, our modelling efforts explicitly assume that landscapes are inherently
829   sensitive to climate (through rainfall) in a manner described by the SPM. While the intuitive support for
830   such sensitivity is strong, and evidence from natural landscapes is mounting that broadly support predictions
831   of the SPM (e.g., Adams, et al., 2020; Harel et al., 2016; Lague, 2014), there remains a large amount of
832   uncertainty about the strength of the sensitivity to climate.

833   Following the core assumption that the SPM is broadly applicable, we note that our model setup is very
834   simple. We assume that all precipitation is rainfall, all rainfall is converted directly to runoff, and we impose
835   constant rainfall gradients that act precisely along the trunk stream and basin axis and that span the entire
836   length of our modelled river basin. While some river basins set within mountain-belt scale orographic
837   precipitation patterns may indeed experience rainfall patterns consistent with this simple geometry, we note
838   that non-linear, and even non-monotonic, rainfall gradients are common for large river basins or those
839   characterized by high local relief (Roe, 2005). As noted previously, however, the framework we have
840   developed translates well to these more complex scenarios. In addition, we model tributary catchments that
841   are uniform in size that experience uniform rainfall. Preliminary model investigations suggest that although
842   allowing tributary sizes and rainfall to vary causes some dispersion in the relationships illustrated here, the
843   overall behavior we describe remains the dominant signal. Nevertheless, both aspects warrant further
844   investigation.

845   Lastly, we emphasize that we use a simple version of the SPM where, among other simplifications, we treat
846   erosion exclusively as detachment limited and do not explicitly model erosional thresholds. While assuming
847   continuum detachment-limited conditions is common, particularly for describing erosion in mountain
848   settings, it may not always be appropriate even in these settings to describe transient behavior (Lague, 2014;
849   Whipple & Tucker, 2002). Related to this, our treatment of K_p, while incrementally more complex than
850   spatially uniform erosional efficiency, remains highly simplified. We do not explore the myriad of other
851   factors that control erosional efficiency (K), and the likelihood that rainfall, or more broadly climate, will
852   influence rock erodibility ($\sim K_p$) and size distribution of sediment delivered to rivers (Ferrier et al., 2013;
853   Murphy et al., 2016; Neely & DiBiase, 2020; Riebe et al., 2015; Sklar et al., 2017).

854   **6. Summary and Conclusions**

855   In this study, we use a simple form of the SPM to explore how spatial rainfall gradients influence both river

856   profiles and expectations about how fluvial landscapes should respond to changes in climate. Notably,

857   because changes in climate in mountain settings involve changes in orographic precipitation patterns,

858   advancing understanding about how changes in climate influence the rivers and topography of mountain

859   landscapes requires a more nuanced, spatially variable, treatment of climate at the catchment scale beyond

860   broadly characterized changes in mean climate. We show that spatially varying rainfall conditions

861   experienced by rivers occupying different landscape positions, specifically trunk and tributary rivers, result

862   in fundamentally different expressions of a given rainfall pattern, and that they respond to changes in

863   rainfall pattern in fundamentally different ways. Further, we show how complex transient responses may

864   arise, and that even modest variations in rainfall patterns can significantly affect spatial patterns of erosion

865   and topographic adjustments that directly contrast with expectations for uniform changes in rainfall. In

866   particular, changes in rainfall pattern characteristically result in multi-stage responses with adjustment

867   zones that can be both spatially extensive and subtly expressed, thus difficult to recognize. Interestingly,

868   these finding suggest more broadly that catchments of different sizes, shapes, and locations set within

869   regional orographic precipitation patterns may have unique, and substantially variable, rainfall histories and

870   responses to changes in climate. These complications raise important questions about how best to interpret

871   spatial variations in erosion rates and their relationship with topography. Finally, we discuss how

872   catchment-scale variations in rainfall generally complicate relationships between conventional topographic

873   metrics (e.g., mean k_{sn}) and erosion rates, even at steady state, and implications for empirical tests of the

874   SPM in natural landscapes. More precise metrics like k_{sn-q} that leverage ever-increasing resolution of rainfall

875   datasets to better account for the spatial distribution of rainfall – specifically its effect on discharge and

876   runoff – may be a significant step toward overcoming these challenges and may prove vital for future studies

877   seeking to quantify interactions between climate, tectonics, and erosion in mountain landscapes.

878   **Acknowledgments**

886   **References**

887 Abbühl, L. M., Norton, K. P., Schlunegger, F., Kracht, O., Aldahan, A., & Possnert, G. (2010). El Niño
888   forcing on 10Be-based surface denudation rates in the northwestern Peruvian Andes?
889   *Geomorphology*, *123*(3–4), 257–268. https://doi.org/10.1016/j.geomorph.2010.07.017

890 Adams, B. A., Whipple, K. X., Forte, A. M., Heimsath, A. M., & Hodges, K. V. (2020). Climate controls
891   on erosion in tectonically active landscapes. *Science Advances*, *6*(42), eaaz3166.
892   https://doi.org/10.1126/sciadv.aaz3166

893 Anders, A. M., Roe, G. H., Hallet, B., Montgomery, D. R., Finnegan, N. J., & Putkonen, J. (2006). Spatial
894   patterns of precipitation and topography in the Himalaya. *Special Paper of the Geological Society of*
895   *America*, *398*(03), 39–53. https://doi.org/10.1130/2006.2398(03)

896 Barros, A. P., & Lettenmaier, D. P. (1994). Dynamic modeling of orographically induced precipitation.
897   *Reviews of Geophysics*, *32*(3), 265–284. https://doi.org/10.1029/94RG00625

898 Barstad, I., & Smith, R. B. (2005). Evaluation of an orographic precipitation model. *Journal of*
899   *Hydrometeorology*, *6*(1), 85–99. https://doi.org/10.1175/JHM-404.1

900 Bierman, P., & Steig, E. J. (1996). Estimating Rates of Denudation Using Cosmogenic Isotope
901   Abundances in Sediment. *Earth Surface Processes and Landforms*, *21*(2), 125–139.
902   https://doi.org/10.1002/(sici)1096-9837(199602)21:2<125::aid-esp511>3.0.co;2-8

903 Binnie, S. A., Phillips, W. M., Summerfield, M. A., Fifield, L. K., & Spotila, J. A. (2008). Patterns of
904   denudation through time in the San Bernardino Mountains, California: Implications for early-stage
905   orogenesis. *Earth and Planetary Science Letters*, *276*(1–2), 62–72.
906   https://doi.org/10.1016/j.epsl.2008.09.008

907 Bonnet, S., & Crave, A. (2003). Landscape response to climate change: Insights from experimental
908   modeling and implications for tectonic versus climatic uplift of topography. *Geology*, *31*(2), 123–
909   126. https://doi.org/10.1130/0091-7613(2003)031<0123:LRTCCI>2.0.CO;2

910 Bookhagen, B., & Burbank, D. W. (2010). Toward a complete Himalayan hydrological budget:
911   Spatiotemporal distribution of snowmelt and rainfall and their impact on river discharge. *Journal of*
912   *Geophysical Research: Earth Surface*, *115*(3), 1–25. https://doi.org/10.1029/2009JF001426

913 Bookhagen, B., & Strecker, M. R. (2008). Orographic barriers, high-resolution TRMM rainfall, and relief
914   variations along the eastern Andes. *Geophysical Research Letters*, *35*(6), 1–6.
915   https://doi.org/10.1029/2007GL032011

916 Bookhagen, B., & Strecker, M. R. (2012). Spatiotemporal trends in erosion rates across a pronounced
917   rainfall gradient: Examples from the southern Central Andes. *Earth and Planetary Science Letters*,

918   *327–328*, 97–110. https://doi.org/10.1016/j.epsl.2012.02.005

919   Brocard, G. Y., & van der Beek, P. A. (2006). Influence of incision rate, rock strength, and bedload

920   supply on bedrock river gradients and valley-flat widths: Field-based evidence and calibrations from

921   western Alpine rivers (southeast France). In *Tectonics, Climate, and Landscape Evolution* (Vol. 398,

922   pp. 101–126). Geological Society of America. https://doi.org/10.1130/2006.2398(07)

923   Brown, E. T., Stallard, R. F., Larsen, M. C., Raisbeck, G. M., & Yiou, F. (1995). Denudation rates

924   determined from the accumulation of in situ-produced 10Be in the luquillo experimental forest,

925   Puerto Rico. *Earth and Planetary Science Letters*, *129*(1–4), 193–202. https://doi.org/10.1016/0012-

926   821X(94)00249-X

927   Burbank, D. W., Blythe, A. E., Putkonen, J., Pratt-Sitaula, B., Gabet, E., Oskin, M., et al. (2003).

928   Decoupling of erosion and precipitation in the Himalayas. *Nature*, *426*(6967), 652–655.

929   https://doi.org/10.1038/nature02187

930   Carretier, S., Regard, V., Vassallo, R., Aguilar, G., Martinod, J., Riquelme, R., et al. (2013). Slope and

931   climate variability control of erosion in the Andes of central Chile. *Geology*, *41*(2), 195–198.

932   https://doi.org/10.1130/G33735.1

933   Clark, M. K., Royden, L. H., Whipple, K. X., Burchfiel, B. C., Zhang, X., & Tang, W. (2006). Use of a

934   regional, relict landscape to measure vertical deformation of the eastern Tibetan Plateau. *Journal of

935   Geophysical Research: Earth Surface*, *111*(3), 1–23. https://doi.org/10.1029/2005JF000294

936   Cyr, A. J., Granger, D. E., Olivetti, V., & Molin, P. (2014). Distinguishing between tectonic and

937   lithologic controls on bedrock channel longitudinal profiles using cosmogenic 10Be erosion rates

938   and channel steepness index. *Geomorphology*, *209*, 27–38.

939   https://doi.org/10.1016/j.geomorph.2013.12.010

940   D'Arcy, M., & Whittaker, A. C. (2014). Geomorphic constraints on landscape sensitivity to climate in

941   tectonically active areas. *Geomorphology*, *204*, 366–381.

942   https://doi.org/10.1016/j.geomorph.2013.08.019

943   Darling, A., Whipple, K., Bierman, P., Clarke, B., & Heimsath, A. (2020). Resistant rock layers amplify

944   cosmogenically-determined erosion rates. *Earth Surface Processes and Landforms*, *45*(2), 312–330.

945   https://doi.org/10.1002/esp.4730

946   DiBiase, R. A., Whipple, K. X., Heimsath, A. M., & Ouimet, W. B. (2010). Landscape form and

947   millennial erosion rates in the San Gabriel Mountains, CA. *Earth and Planetary Science Letters*,

948   *289*(1–2), 134–144. https://doi.org/10.1016/j.epsl.2009.10.036

949 Duvall, A. (2004). Tectonic and lithologic controls on bedrock channel profiles and processes in coastal

950   California. *Journal of Geophysical Research*, *109*(F3), 1–18. https://doi.org/10.1029/2003jf000086

951 Ferrier, K. L., Huppert, K. L., & Perron, J. T. (2013). Climatic control of bedrock river incision. *Nature*,

952   *496*(7444), 206–209. https://doi.org/10.1038/nature11982

953 Finlayson, D. P., Montgomery, D. R., & Hallet, B. (2002). Spatial coincidence of rapid inferred erosion

954   with young metamorphic massifs in the Himalayas. *Geology*, *30*(3), 219–222.

955   https://doi.org/10.1130/0091-7613(2002)030<0219:SCORIE>2.0.CO;2

956 Forte, A. M., Yanites, B. J., & Whipple, K. X. (2016). Complexities of landscape evolution during

957   incision through layered stratigraphy with contrasts in rock strength. *Earth Surface Processes and*

958   *Landforms*, *41*(12), 1736–1757. https://doi.org/10.1002/esp.3947

959 Fox, M., Goren, L., May, D. A., & Willett, S. D. (2014). Inversion of fluvial channels for paleorock uplift

960   rates in Taiwan. *Journal of Geophysical Research: Earth Surface*, *119*(9), 1853–1875.

961   https://doi.org/10.1002/2014jf003196

962 Gallen, S. F., Wegmann, K. W., & Bohnenstiehl, D. W. R. (2013). Miocene rejuvenation of topographic

963   relief in the southern Appalachians. *GSA Today*, *23*(2), 4–10.

964   https://doi.org/10.1130/GSATG163A.1

965 Gasparini, N. M., & Whipple, K. X. (2014). Diagnosing climatic and tectonic controls on topography:

966   Eastern flank of the northern Bolivian Andes. *Lithosphere*, *6*(4), 230–250.

967   https://doi.org/10.1130/L322.1

968 Gasparini, N. M., Bras, R. L., & Whipple, K. X. (2006). Numerical modeling of non–steady-state river

969   profile evolution using a sediment-flux-dependent incision model. In S. D. Willett, N. Hovius, M. T.

970   Brandon, & D. M. Fisher (Eds.), *Tectonics, Climate, and Landscape Evolution* (Vol. 398, p. 0).

971   Geological Society of America. https://doi.org/10.1130/2006.2398(08)

972 Gasparini, N. M., Whipple, K. X., & Bras, R. L. (2007). Predictions of steady state and transient

973   landscape morphology using sediment-flux-dependent river incision models. *Journal of Geophysical*

974   *Research: Earth Surface*, *112*(3), 1–20. https://doi.org/10.1029/2006JF000567

975 Godard, V., Bourlès, D. L., Spinabella, F., Burbank, D. W., Bookhagen, B., Fisher, G. B., et al. (2014).

976   Dominance of tectonics over climate in himalayan denudation. *Geology*, *42*(3), 243–246.

977   https://doi.org/10.1130/G35342.1

978 Goren, L., Fox, M., & Willett, S. D. (2014). Tectonics from fluvial topography using formal linear

979   inversion: Theory and applications to the Inyo Mountains, California. *Journal of Geophysical*

980   *Research F: Earth Surface*, *119*(8), 1651–1681. https://doi.org/10.1002/2014JF003079

981   Granger, D. E., Kirchner, J. W., & Finkel, R. (1996). Spatially averaged long-term erosion rates measured
982   from in situ-produced cosmogenic nuclides in alluvial sediment. *Journal of Geology*, *104*(3), 249–
983   257. https://doi.org/10.1086/629823

984   Hack, J. T. (1957). *Studies of Longitudinal Stream Profiles in Virginia and Maryland*. Retrieved from
985   https://pubs.usgs.gov/pp/0294b/report.pdf

986   Han, J., Gasparini, N. M., Johnson, J. P. L., & Murphy, B. P. (2014). Modeling the influence of rainfall
987   gradients on discharge, bedrock erodibility, and river profile evolution, with application to the Big
988   Island, Hawai'i. *Journal of Geophysical Research: Earth Surface*, *119*(6), 1418–1440.
989   https://doi.org/10.1002/2013JF002961

990   Han, J., Gasparini, N. M., & Johnson, J. P. L. (2015). Measuring the imprint of orographic rainfall
991   gradients on the morphology of steady-state numerical fluvial landscapes. *Earth Surface Processes*
992   *and Landforms*, *40*(10), 1334–1350. https://doi.org/10.1002/esp.3723

993   Harel, M. A., Mudd, S. M., & Attal, M. (2016). Global analysis of the stream power law parameters based
994   on worldwide 10Be denudation rates. *Geomorphology*, *268*, 184–196.
995   https://doi.org/10.1016/j.geomorph.2016.05.035

996   Henck, A. C., Huntington, K. W., Stone, J. O., Montgomery, D. R., & Hallet, B. (2011). Spatial controls
997   on erosion in the Three Rivers Region, southeastern Tibet and southwestern China. *Earth and*
998   *Planetary Science Letters*, *303*(1–2), 71–83. https://doi.org/10.1016/j.epsl.2010.12.038

999   Howard, A. D. (1994). A detachment-limited model of drainage basin evolution. *Water Resources*
1000   *Research*, *30*(7), 2261–2285. https://doi.org/10.1029/94WR00757

1001   Howard, A. D., & Kerby, G. (1983). Channel changes in badlands. *Geological Society of America*
1002   *Bulletin*, *94*, 739–752.

1003   Insel, N., Ehlers, T. A., Schaller, M., Barnes, J. B., Tawackoli, S., & Poulsen, C. J. (2010). Spatial and
1004   temporal variability in denudation across the Bolivian Andes from multiple geochronometers.
1005   *Geomorphology*, *122*(1–2), 65–77. https://doi.org/10.1016/j.geomorph.2010.05.014

1006   Kirby, E., & Whipple, K. X. (2012). Expression of active tectonics in erosional landscapes. *Journal of*
1007   *Structural Geology*, *44*, 54–75. https://doi.org/10.1016/j.jsg.2012.07.009

1008   Kober, F., Zeilinger, G., Hippe, K., Marc, O., Lendzioch, T., Grischott, R., et al. (2015). Tectonic and
1009   lithological controls on denudation rates in the central Bolivian Andes. *Tectonophysics*, *657*, 230–
1010   244. https://doi.org/10.1016/j.tecto.2015.06.037

1011 Lague, D. (2014). The stream power river incision model: Evidence, theory and beyond. *Earth Surface*
1012   *Processes and Landforms*, *39*(1), 38–61. https://doi.org/10.1002/esp.3462

1013 Miller, S. R., Sak, P. B., Kirby, E., & Bierman, P. R. (2013). Neogene rejuvenation of central
1014   Appalachian topography: Evidence for differential rock uplift from stream profiles and erosion rates.
1015   *Earth and Planetary Science Letters*, *369–370*(May), 1–12.
1016   https://doi.org/10.1016/j.epsl.2013.04.007

1017 Molnar, P. (2001). Climate change, flooding in arid environments, and erosion rates. *Geology*, *29*(12),
1018   1071–1074. https://doi.org/10.1130/0091-7613(2001)029<1071:CCFIAE>2.0.CO

1019 Morell, K. D., Sandiford, M., Rajendran, C. P., Rajendran, K., Alimanovic, A., Fink, D., & Sanwal, J.
1020   (2015). Geomorphology reveals active décollement geometry in the central Himalayan seismic gap.
1021   *Lithosphere*, *7*(3), 247–256. https://doi.org/10.1130/L407.1

1022 Murphy, B. P., Johnson, J. P. L., Gasparini, N. M., & Sklar, L. S. (2016). Chemical weathering as a
1023   mechanism for the climatic control of bedrock river incision. *Nature*, *532*(7598), 223–227.
1024   https://doi.org/10.1038/nature17449

1025 Mutz, S. G., Ehlers, T. A., Werner, M., Lohmann, G., Stepanek, C., & Li, J. (2018). Estimates of late
1026   Cenozoic climate change relevant to Earth surface processes in tectonically active orogens. *Earth*
1027   *Surface Dynamics*, *6*(2), 271–301. https://doi.org/10.5194/esurf-6-271-2018

1028 Neely, A. B., & DiBiase, R. A. (2020). Drainage area, bedrock fracture spacing, and weathering controls
1029   on landscape-scale patterns in surface sediment grain size. *Earth and Space Science Open Archive*,
1030   1–22. https://doi.org/10.1002/essoar.10502617.1

1031 Olen, S. M., Bookhagen, B., & Strecker, M. R. (2016). Role of climate and vegetation density in
1032   modulating denudation rates in the Himalaya. *Earth and Planetary Science Letters*, *445*, 57–67.
1033   https://doi.org/10.1016/j.epsl.2016.03.047

1034 Ouimet, W. B., Whipple, K. X., & Granger, D. E. (2009). Beyond threshold hillslopes: Channel
1035   adjustment to base-level fall in tectonically active mountain ranges. *Geology*, *37*(7), 579–582.
1036   https://doi.org/10.1130/G30013A.1

1037 Perron, J. T. (2017). Climate and the Pace of Erosional Landscape Evolution. *Annual Review of Earth and*
1038   *Planetary Sciences*, *45*(1), 561–591. https://doi.org/10.1146/annurev-earth-060614-105405

1039 Portenga, E. W., Bierman, P. R., Duncan, C., Corbett, L. B., Kehrwald, N. M., & Rood, D. H. (2015).
1040   Erosion rates of the Bhutanese Himalaya determined using in situ-produced 10Be. *Geomorphology*,
1041   *233*, 112–126. https://doi.org/10.1016/j.geomorph.2014.09.027

1042 Poulsen, C. J., Ehlers, T. A., & Insel, N. (2010). Onset of convective rainfall during gradual late miocene
1043   rise of the central andes. *Science*, *328*(5977), 490–493. https://doi.org/10.1126/science.1185078

1044 Reinhardt, L. J., Bishop, P., Hoey, T. B., Dempster, T. J., & Sanderson, D. C. W. (2007). Quantification
1045   of the transient response to base-level fall in a small mountain catchment: Sierra Nevada, southern
1046   Spain. *Journal of Geophysical Research: Earth Surface*, *112*(3).
1047   https://doi.org/10.1029/2006JF000524

1048 Riebe, C. S., Sklar, L. S., Lukens, C. E., & Shuster, D. L. (2015). Climate and topography control the size
1049   and flux of sediment produced on steep mountain slopes. *Proceedings of the National Academy of*
1050   *Sciences of the United States of America*, *112*(51), 15574–15579.
1051   https://doi.org/10.1073/pnas.1503567112

1052 Rigon, R., Rodriguez-Iturbe, I., Maritan, A., Giacometti, A., Tarboton, D. G., & Rinaldo, A. (1996). On
1053   Hack's Law. *Water Resources Research*, *32*(11), 3367–3374. https://doi.org/10.1029/96WR02397

1054 Riihimaki, C. A., Anderson, R. S., & Safran, E. B. (2007). Impact of rock uplift on rates of late Cenozoic
1055   Rocky Mountain river incision. *Journal of Geophysical Research: Earth Surface*, *112*(3), 1–15.
1056   https://doi.org/10.1029/2006JF000557

1057 Rinaldo, A., Dietrich, W. E., Rigon, R., Vogel, G. K., & Rodrlguezlturbe, I. (1995). Geomorphological
1058   signatures of varying climate. *Nature*, *374*(6523), 632–635. https://doi.org/10.1038/374632a0

1059 Roe, G. H. (2005). Orographic Precipitation. *Annual Review of Earth and Planetary Sciences*, *33*(1), 645–
1060   671. https://doi.org/10.1146/annurev.earth.33.092203.122541

1061 Roe, G. H., & Baker, M. B. (2006). Microphysical and geometrical controls on the pattern of orographic
1062   precipitation. *Journal of the Atmospheric Sciences*, *63*(3), 861–880.
1063   https://doi.org/10.1175/JAS3619.1

1064 Roe, G. H., Montgomery, D. R., & Hallet, B. (2002). Effects of orographic precipitation variations on the
1065   concavity of steady-state river profiles. *Geology*, *30*(2), 143–146. https://doi.org/10.1130/0091-
1066   7613(2002)030<0143:EOOPVO>2.0.CO;2

1067 Roe, G. H., Montgomery, D. R., & Hallet, B. (2003). Orographic precipitation and the relief of mountain
1068   ranges. *Journal of Geophysical Research: Solid Earth*, *108*(B6).
1069   https://doi.org/10.1029/2001jb001521

1070 Roe, G. H., Whipple, K. X., & Fletcher, J. K. (2008). Feedbacks among climate, erosion, and tectonics in
1071   a critical wedge orogen. *American Journal of Science*, *308*(7), 815–842.
1072   https://doi.org/10.2475/07.2008.01

1073   Royden, L., & Perron, J. T. (2013). Solutions of the stream power equation and application to the
1074   evolution of river longitudinal profiles. *Journal of Geophysical Research: Earth Surface*, *118*(2),
1075   497–518. https://doi.org/10.1002/jgrf.20031

1076   Safran, E. B., Bierman, P. R., Aalto, R., Dunne, T., Whipple, K. X., & Caffee, M. (2005). Erosion rates
1077   driven by channel network incision in the Bolivian Andes. *Earth Surface Processes and Landforms*,
1078   *30*(8), 1007–1024. https://doi.org/10.1002/esp.1259

1079   Scherler, D., Bookhagen, B., & Strecker, M. R. (2014). Tectonic control on 10Be-derived erosion rates in
1080   the Garhwal Himalaya, India. *Journal of Geophysical Research: Earth Surface*, *119*(2), 83–105.
1081   https://doi.org/10.1002/2013JF002955

1082   Scherler, D., DiBiase, R. A., Fisher, G. B., & Avouac, J. P. (2017). Testing monsoonal controls on
1083   bedrock river incision in the Himalaya and Eastern Tibet with a stochastic-threshold stream power
1084   model. *Journal of Geophysical Research: Earth Surface*, *122*(7), 1389–1429.
1085   https://doi.org/10.1002/2016JF004011

1086   Schoenbohm, L. M., Whipple, K. X., Burchfiel, B. C., & Chen, L. (2004). Geomorphic constraints on
1087   surface uplift, exhumation, and plateau growth in the Red River region, Yunnan Province, China.
1088   *Bulletin of the Geological Society of America*, *116*(7–8), 895–909. https://doi.org/10.1130/B25364.1

1089   Siler, N., & Roe, G. (2014). How will orographic precipitation respond to surface warming? An idealized
1090   thermodynamic perspective. *Geophysical Research Letters*, *41*(7), 2606–2613.
1091   https://doi.org/10.1002/2013GL059095

1092   Sklar, L. S., Riebe, C. S., Marshall, J. A., Genetti, J., Leclere, S., Lukens, C. L., & Merces, V. (2017). The
1093   problem of predicting the size distribution of sediment supplied by hillslopes to rivers.
1094   *Geomorphology*, *277*, 31–49. https://doi.org/10.1016/j.geomorph.2016.05.005

1095   Tucker, G E, & Whipple, K. X. (2002). Topographic outcomes predicted by stream erosion models:
1096   Sensitivity analysis and intermodel comparison. *Journal of Geophysical Research: Solid Earth*,
1097   *107*(B9), ETG 1-1-ETG 1-16. https://doi.org/10.1029/2001jb000162

1098   Tucker, Gregory E., & Slingerland, R. (1997). Drainage basin responses to climate change. *Water
1099   Resources Research*, *33*(8), 2031–2047. https://doi.org/10.1029/97WR00409

1100   Vanacker, V., von Blanckenburg, F., Govers, G., Molina, A., Campforts, B., & Kubik, P. W. (2015).
1101   Transient river response, captured by channel steepness and its concavity. *Geomorphology*, *228*,
1102   234–243. https://doi.org/10.1016/j.geomorph.2014.09.013

1103   Ward, D. J., & Galewsky, J. (2014). Exploring landscape sensitivity to the Pacific Trade Wind Inversion

1104   on the subsiding island of Hawaii. *Journal of Geophysical Research: Earth Surface*, *119*(9), 2048–
1105   2069. https://doi.org/10.1002/2014JF003155

1106   Whipple, K. X. (2001). Fluvial landscape response time: How plausible is steady-state denudation?
1107   *American Journal of Science*, *301*(4–5), 313–325. https://doi.org/10.2475/ajs.301.4-5.313

1108   Whipple, K. X., & Meade, B. J. (2006). Orogen response to changes in climatic and tectonic forcing.
1109   *Earth and Planetary Science Letters*, *243*(1–2), 218–228. https://doi.org/10.1016/j.epsl.2005.12.022

1110   Whipple, K. X., & Tucker, G. E. (1999). Dynamics of the stream-power river incision model:
1111   Implications for height limits of mountain ranges, landscape response timescales, and research
1112   needs. *Journal of Geophysical Research: Solid Earth*, *104*(B8), 17661–17674.
1113   https://doi.org/10.1029/1999jb900120

1114   Whipple, K. X., & Tucker, G. E. (2002). Implications of sediment-flux-dependent river incision models
1115   for landscape evolution. *Journal of Geophysical Research*, *107*(B2), 2039.
1116   https://doi.org/10.1029/2000jb000044

1117   Whittaker, A. C. (2012). How do landscapes record tectonics and climate? *Lithosphere*, *4*(2), 160–164.
1118   https://doi.org/10.1130/RF.L003.1

1119   Whittaker, A. C., Cowie, P. A., Attal, M., Tucker, G. E., & Roberts, G. P. (2007). Bedrock channel
1120   adjustment to tectonic forcing: Implications for predicting river incision rates. *Geology*, *35*(2), 103–
1121   106. https://doi.org/10.1130/G23106A.1

1122   Willenbring, J. K., Gasparini, N. M., Crosby, B. T., & Brocard, G. (2013). What does a mean mean? The
1123   temporal evolution of detrital cosmogenic denudation rates in a transient landscape. *Geology*,
1124   *41*(12), 1215–1218. https://doi.org/10.1130/G34746.1

1125   Wittmann, H., Malusà, M. G., Resentini, A., Garzanti, E., & Niedermann, S. (2016). The cosmogenic
1126   record of mountain erosion transmitted across a foreland basin: Source-to-sink analysis of in situ
1127   10Be, 26Al and 21Ne in sediment of the Po river catchment. *Earth and Planetary Science Letters*,
1128   *452*, 258–271. https://doi.org/10.1016/j.epsl.2016.07.017

1129   Wobus, C., Whipple, K. X., Kirby, E., Snyder, N., Johnson, J., Spyropolou, K., et al. (2006). Tectonics
1130   from topography: Procedures, promise, and pitfalls. *Special Paper of the Geological Society of
1131   America*, *398*(04), 55–74. https://doi.org/10.1130/2006.2398(04)

1132   Yang, R., Willett, S. D., & Goren, L. (2015). In situ low-relief landscape formation as a result of river
1133   network disruption. *Nature*, *520*(7548), 526–529. https://doi.org/10.1038/nature14354

1134   Zachos, J., Pagani, H., Sloan, L., Thomas, E., & Billups, K. (2001). Trends, rhythms, and aberrations in

1135   global climate 65 Ma to present. *Science*, *292*(5517), 686–693.
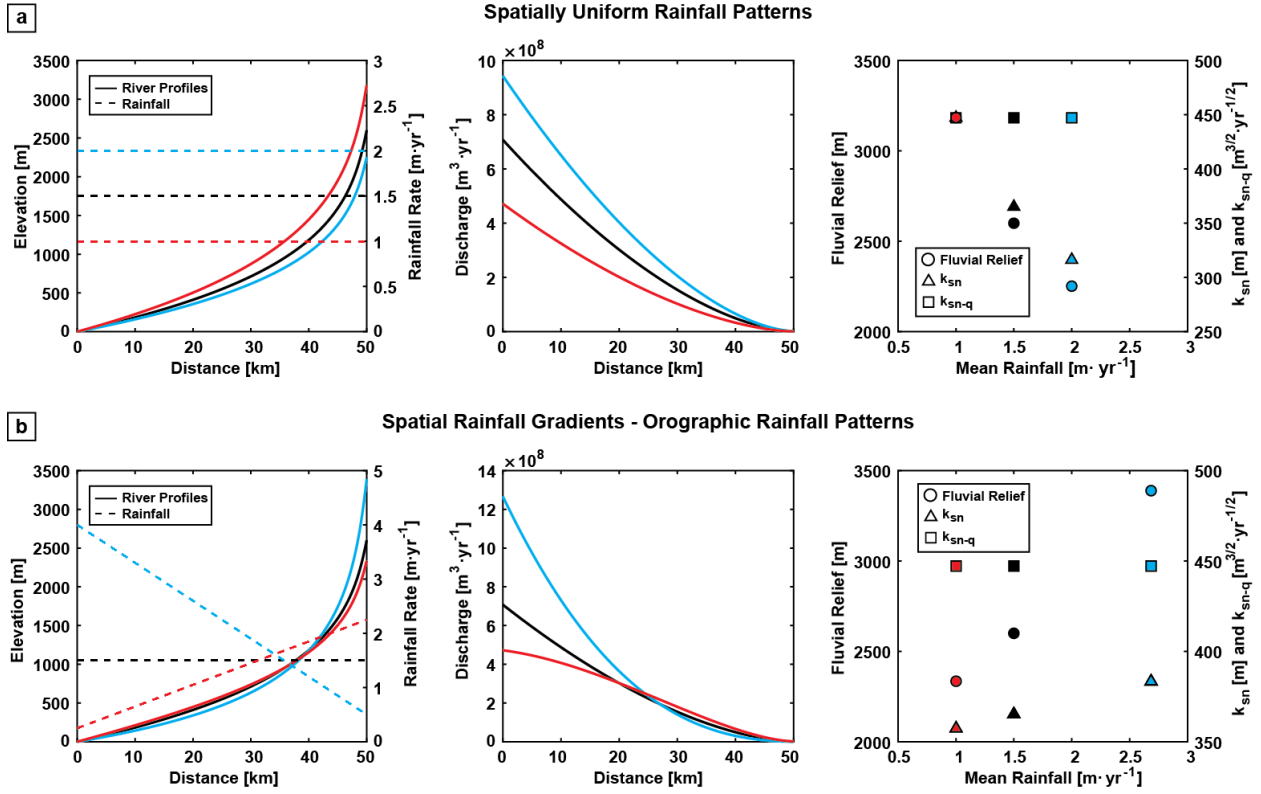
1136   https://doi.org/10.1126/science.1059412

1137

1138   **Figures and Tables**

Table 1. Model Parameters

Parameters	Value	Units
U	5.0×10^{-4}	m·yr^{-1}
K_p	2.5×10^{-9}	m^{-1}·yr^{-1}
m	1	
n	2	
k_a	6.69	
h	1.67	
L		
Trunk	50	km
Tributaries	5	km
A		
Trunk	472	km^2
Tributaries	11	km^2
A_c	1	km^2
Node spacing	25	m
Time step	50	yr
Tributary Spacing	1	km

1139

Figure 1. Influence of rainfall on channel profile form and topographic metrics at steady state. a) Top row – left panel shows river profiles adjusted to different amounts of spatially uniform rainfall. Corresponding discharge accumulation curves are shown in the middle panel. Right panel shows the relationship between mean rainfall (defined as Q/A) calculated at the outlet, with fluvial relief (R), k_{sn}, and k_{sn-q} for a fixed uniform rock uplift rate. Note, at steady state fluvial relief and k_{sn} are inversely related to mean rainfall, while k_{sn-q} is independent of changes in rainfall. b) Bottom row – all panels as in (a) but for a comparable suite of steady-state profiles adjusted to spatially uniform rainfall, a decreasing upstream rainfall (bottom-heavy) pattern, and an increasing upstream (top-heavy) pattern. Note intersections that occur between profiles in the left panel and middle panels, and that fluvial relief and k_{sn} are positively related to mean rainfall in these cases (right panel), inverted from (a). All other model parameters are equal (see Table 1).
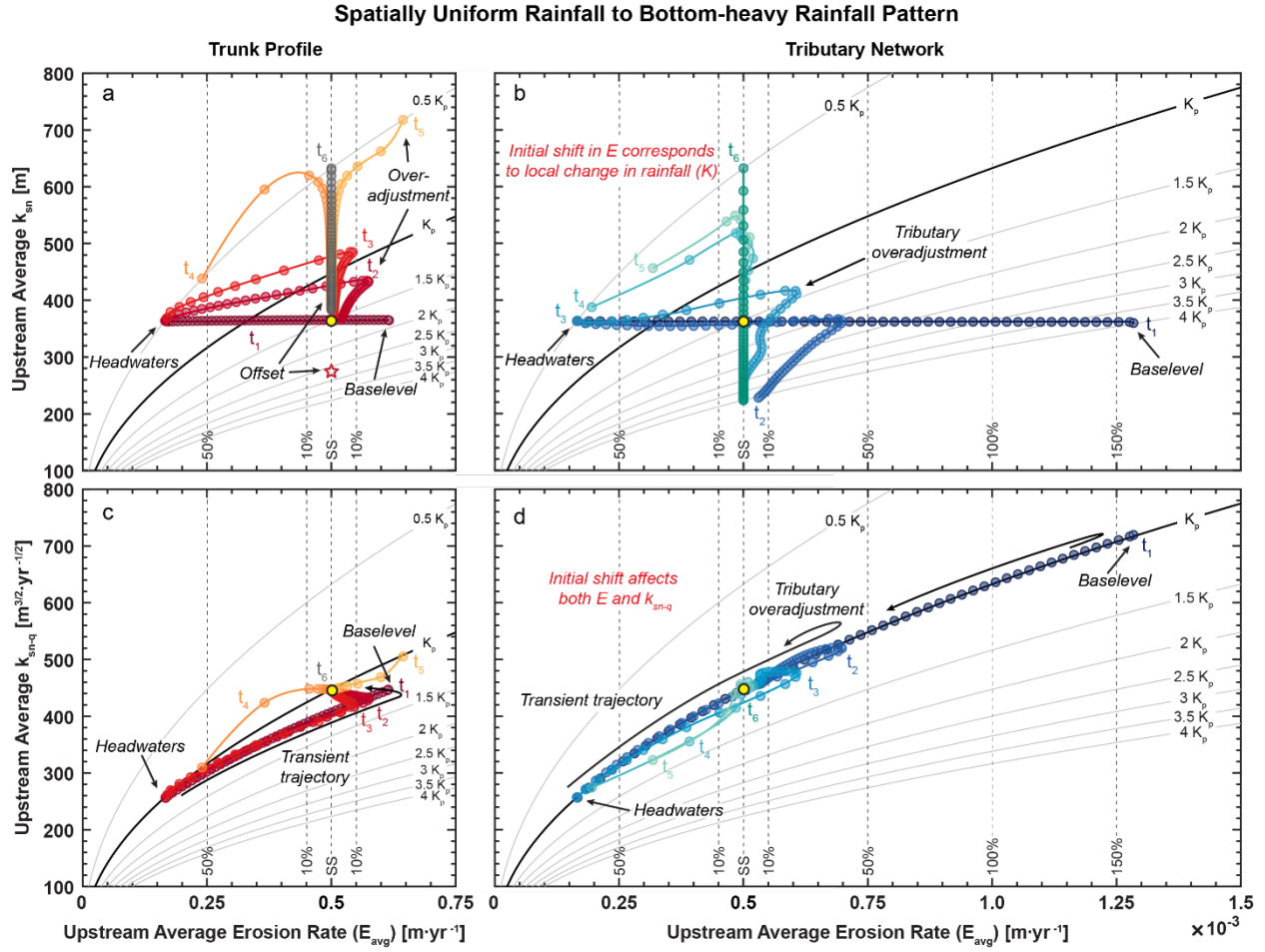
Figure 2. Schematic illustration of key aspects of complex transient responses – defined in section 3.3 – that can result from changes to a relatively bottom-heavy (a) or a top-heavy rainfall gradient (b) – rainfall shown in inset. Horizontal grey bars highlight resulting net change in fluvial relief (ΔR) and maximum elevation change (Δz_{sc}) along the center of the profile. Colored circles mark positions of x_{sc} (yellow) and x_{zc} (red) that also demarcate segments of net divergent and convergent transient adjustments – see text for definitions and discussion. Net modes of transient adjustment are indicated along top axis. Note reversal at position x_{zc} (net incision downstream, net uplift upstream); however, during transience, adjustment upstream of x_{sc} is variable with time. Inset shows both local rainfall rate (P, blue) and upstream averaged rainfall ($\overline{P}$, black). $P = \overline{P}$ for spatially uniform rainfall; only P is depicted for initial rainfall. Positions of x_{sc} and x_{zc} in inset correspond to those along the profiles in the main figure. Note along-stream offset in position where P and $\overline{P}$ exceed the initial rainfall rate, the latter corresponding to x_{sc}. Also, note that the difference between P and $\overline{P}$ increases systematically downstream.
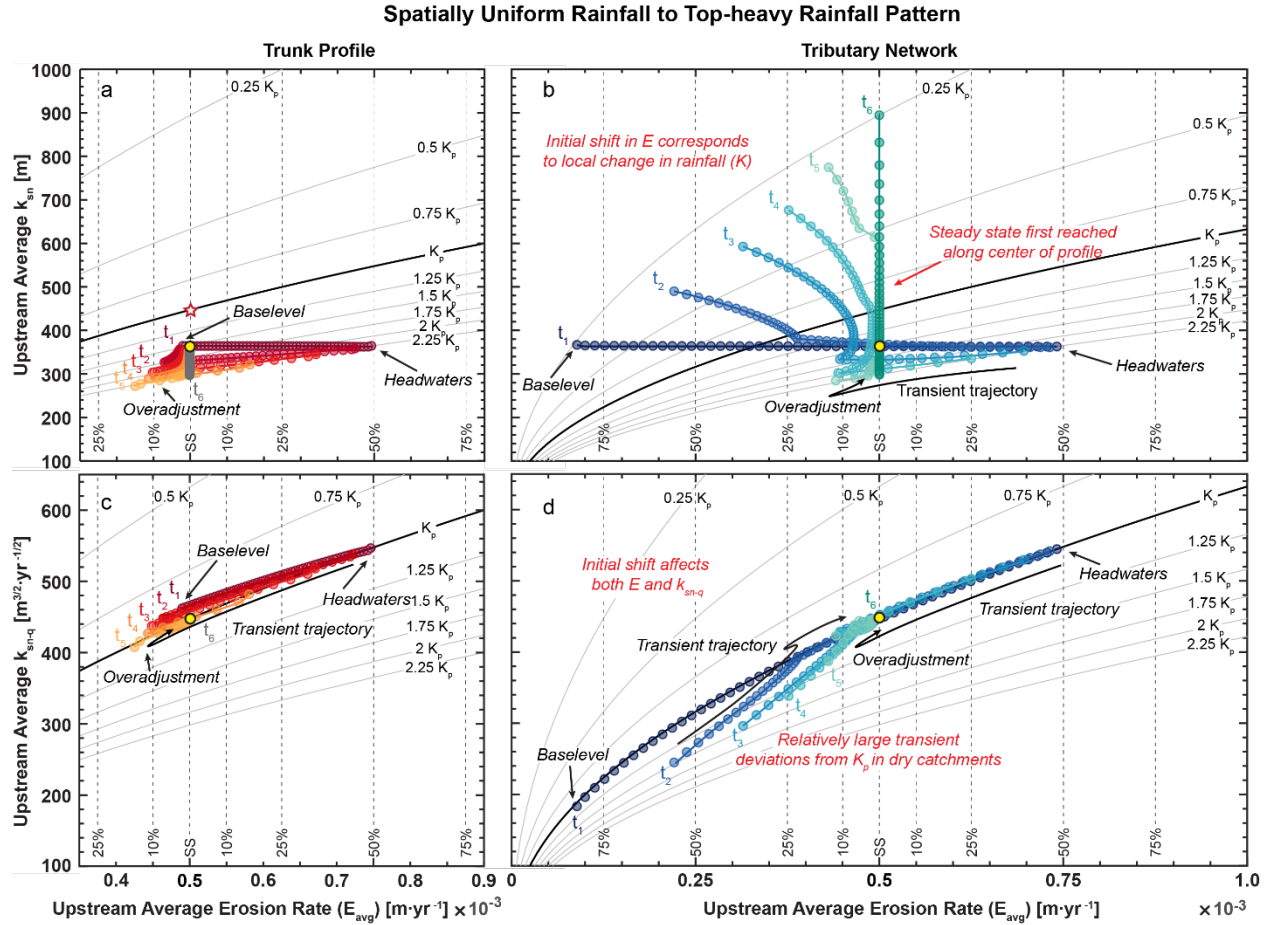
Figure 3. Sensitivity analysis of a river profile to different spatial gradients in rainfall. a) Defines general domains of behavior described in the sensitivity analysis shown in (b) – see text for descriptions of different fields. Black star in (a) marks the initial condition; note, initial conditions in panels (a) and (b) are different. Top-heavy and bottom-heavy domains are separated by the 1:1 line. The primary influence of different h values in Hack's Law is on the slope of Q_f/Q_i, as indicated. b) Same as (a) but where the initial profile is adjusted to spatially uniform $P = 1.5$ m/yr, and grey fields in (a) are colored by magnitude of Δz_{sc} (e.g., Figure 2). White stars show rainfall gradient scenarios explored in section 3 – Cases 3 & 4. Contours of Q_f/Q_i are shown in grey dashed lines, and contours of R_f/R_i in black dotted lines.
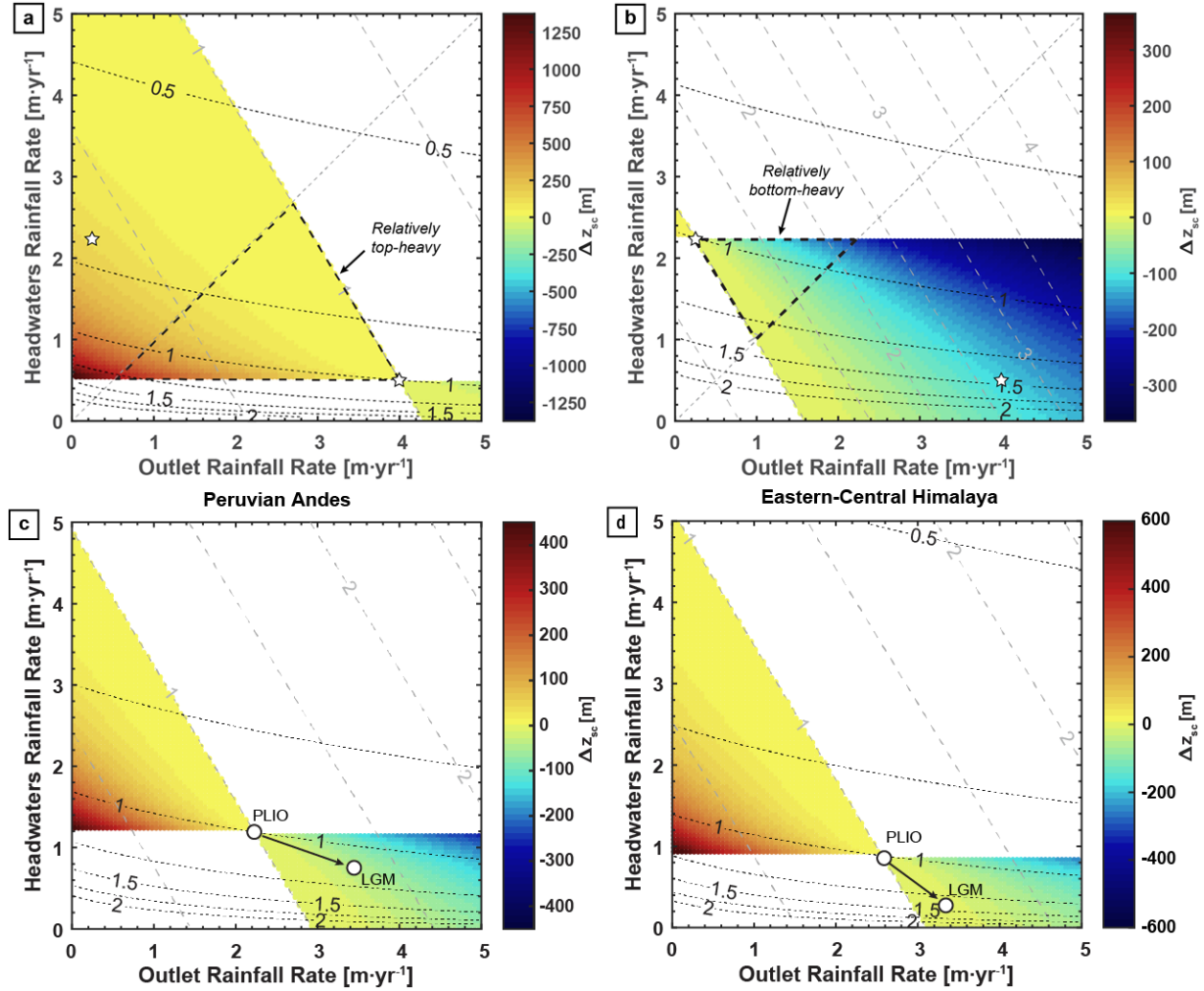
1175

Figure 4. Representative time slice of transient evolution for Case 1 (uniform decrease in rainfall) and Case 2 (uniform increase in rainfall) through (a) k_{sn}-E_{avg} and (b) k_{sn-q}-E_{avg} parameter spaces. Case 1 is shown in red shaded domain (transient decrease in erosion rate, $E < U$), and Case 2 is in blue shaded domain (transient increase in erosion rate, $E > U$). Curves expressing the expected steady state relationship between channel steepness and erosion rate with different uniform erosional efficiencies are shown; $K = K_p$, is shown in black solid line, and grey lines show different values of K as multiples of K_p. Vertical dashed lines show percent deviations from steady state erosion rate. Initial and final conditions shown with yellow circles, as labelled. Model data from different positions along the trunk profile and individual tributaries shown with red and blue data points, respectively. Trunk data shown are only profile nodes at tributary junctions – all trunk profile datapoints have a corresponding tributary datapoint at the same position. Trunk profile data show upstream mean values from their respective position, and tributary data show mean values for the tributary profile measured at the junction with the trunk profile.

1188

Figure 5. Transient evolution of the trunk profile (a & c) and network of tributaries (b & d) in Case 3 (spatially uniform to bottom-heavy) through k_{sn}-E_{avg} (a & b) and k_{sn-q}-E_{avg} (b & d) parameter spaces. Layout of individual panels is like Figure 4. Six representative time slices are shown; t_1 shows time at 10 kyr model time (i.e., first timestep following change in rainfall), t_6 is at final steady state. Time intervals are not equal in duration but t_1-t_6 are the same timestep for all panels. Note range in k_{sn} values and erosional efficiency values spanned at final steady state in panels (a) and (b). Also, note the relatively muted responses by the trunk profile relative to the network of tributaries in both k_{sn} and k_{sn-q}. Star in panel (a) shows expected erosional efficiency calculated from equation (1b) based on the final mean rainfall of 2.68 m/yr ($2.68 \cdot K_p$) at steady state, which corresponds to a predicted mean k_{sn} of ~275. Note offset between this value and range of erosional efficiency and k_{sn} values exhibited at t_6.
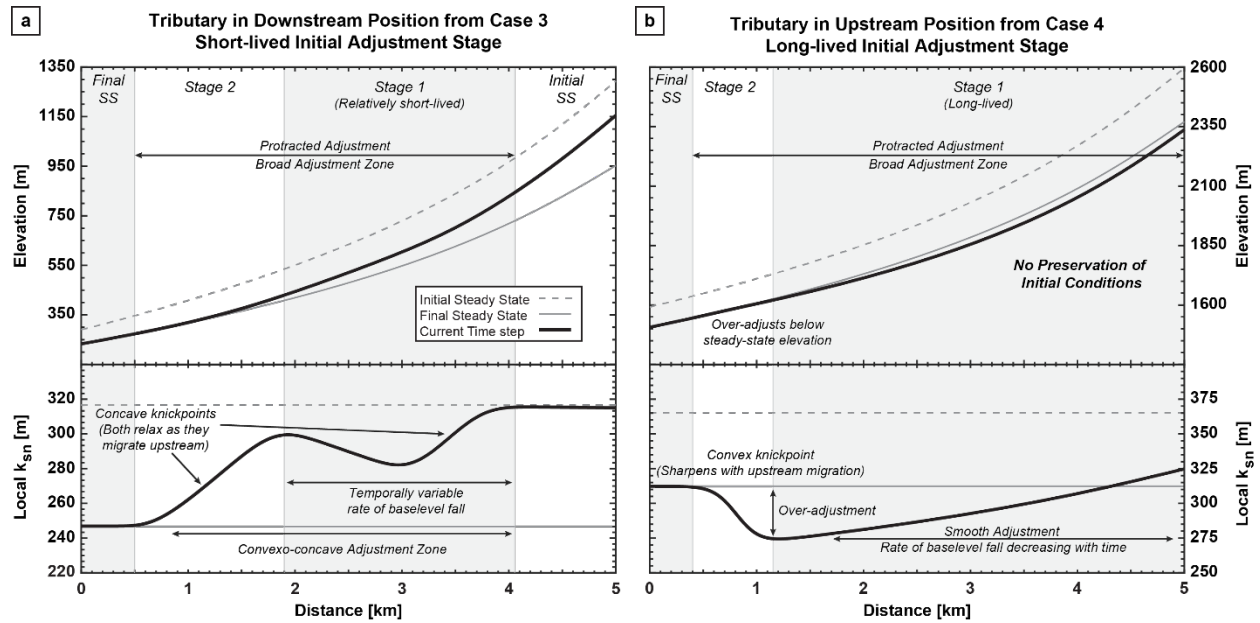
Figure 6. Transient evolution of the trunk profile (a & c) and network of tributaries (b & d) in Case 4 (spatially uniform to top-heavy) through k_{sn}-E_{avg} (a & b) and k_{sn-q}-E_{avg} (c & d) parameter spaces; figure layout is same as Figure 5. Like Case 3, the trunk response is muted relative to the network of tributaries, but the disparity is more extreme in this case. Star in panel (a) shows K calculated from equation (1b) based on the final mean rainfall of 1 m/yr ($K = K_p$) at steady state, which corresponds to a predicted mean k_{sn} of ~450. Again, note offset between this value and range of erosional efficiency and k_{sn} values exhibited at t_6.
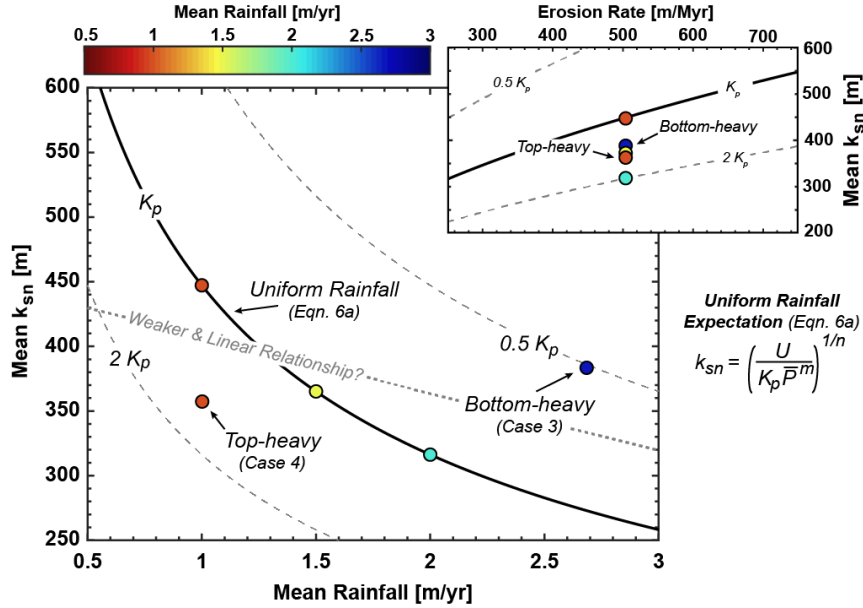
1209

Figure 7. Sensitivity analysis where initial conditions use final rainfall patterns from Case 3 (a) and Case 4 (b), and examples from the eastern flank of the Peruvian Andes (c) and eastern-central Himalaya (d). Panel layouts are the same as in Figure 3b. Triangular fields in demarcated in black dashes in (a) and (b) bound rainfall gradients with the same pattern as the initial condition (i.e., bottom-heavy or top-heavy), but cause complex transient responses similar to those expected for reversals in polarity of the rainfall pattern as the rainfall becomes *relatively* bottom- or top-heavy – see section 5.1 for further discussion. Panels (c & d) show examples of climate change scenarios from model simulations reported in supplementary tables by Mutz et al. (2018), for a hypothetical transverse river with parameters in Table 1. Initial condition is set in the Pliocene (PLIO), and representative evolution of the orographic rainfall pattern through to the Last Glacial Maximum (LGM) is plotted, illustrating that climate changes that are predicted to trigger complex responses are likely not uncommon.
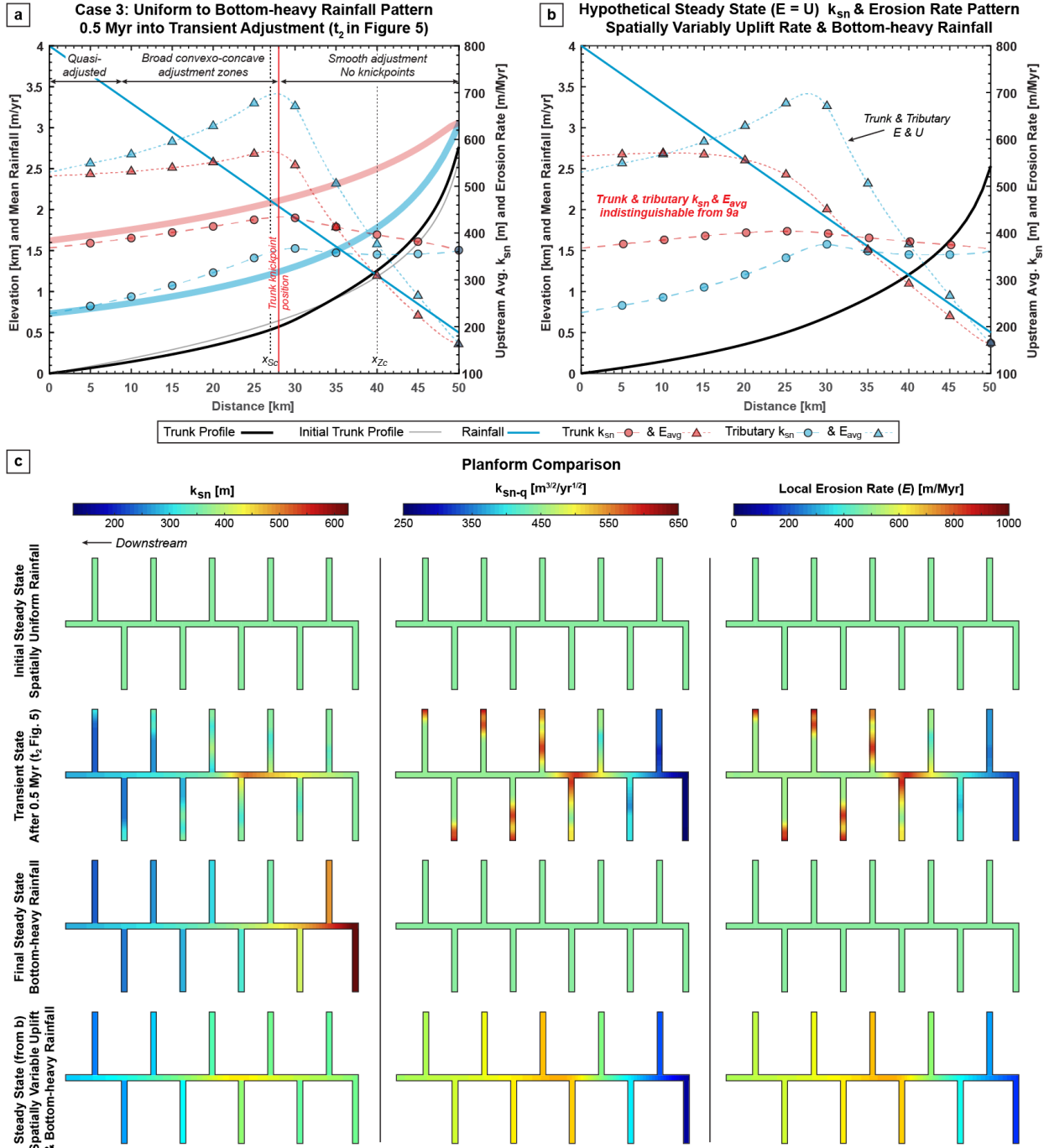
1221

1222

1223

Figure 8. Representative examples of multi-stage tributary response in Cases 3 (a) & 4 (b). Note, upstream positions always experience relatively longer initial adjustment stages than downstream positions, regardless of rainfall gradient. Grey shaded and white regions show where initial and final steady states (SS) and different adjustment stages are represented along the profile lengths, as indicated across top axis. a) Shows a tributary located in a relatively downstream position, 15 km from trunk outlet and downstream from x_{sc} after 300 kyr of transient adjustment in Case 3, where the initial adjustment stage is relatively short-lived. Despite this, protracted adjustment creates a several-kilometer-wide adjustment zone with relatively smooth but notable along-stream variations in k_{sn}. This pattern is subtle on the longitudinal profile. b) Shows a tributary located in an upstream position, 45 km from the trunk outlet and upstream from x_{sc} after 1.725 Myr of transient adjustment in Case 4, where the initial adjustment stage is long-lived. The initial adjustment stage reshapes the entire profile prior to adjustment of the trunk profile, but no transient knickpoints or other obvious topographic indicators of such significant modification are present, with smoothly varying local k_{sn} values within 10% of the mean. Also, note overadjustment means that the increase in channel steepness required to reach steady state contrasts with net reduction in channel steepness during transient adjustment.

Figure 9. Plot illustrating how rainfall gradients systematically influence correlation between mean rainfall and k_{sn} at steady state, and consequences for relationship between channel steepness and erosion rate (inset). A common symbology is used in both the main figure and the inset. Expected SPM relationship based on uniform climate (uniform erosional efficiency, K) is shown in solid back line. Grey long-dashed lines represent changes in $K = K_p \bar{P}^m$. Circles colored by mean rainfall reflect scenarios shown in Figure 1 – uniform rainfall of 1, 1.5, and 2 m/yr, and bottom- and top-heavy gradients (also used in Cases 3 & 4). While K_p is equivalent for all scenarios, rainfall gradients cause dispersion (apparent differences in erosional efficiency) from the expected relationship (solid black line) equivalent to differences in K_p of approximately a factor of two (inset). For instance, the bottom-heavy case where mean rainfall is ~2.7 m/yr exhibits an apparent ~50% reduction in erosional efficiency based on mean k_{sn} (plots on $K \approx 0.5 K_p$ curve in main figure) and thus plots where one would expect a catchment that experiences half as much rainfall to plot in the inset. Dotted line in main figure illustrates, conceptually, how this dispersion could distort inferred relationships between mean rainfall and channel steepness (weaker and quasi-linear in this case), even at steady state and in systems where the SPM is a complete description of the controls on channel profile form. Where uplift rates are unknown, this systematic bias in apparent erosional efficiency due to rainfall gradients is a potential source of dispersion in relationships between k_{sn} and erosion rate (inset).

Figure 10. Illustration of potentially misleading spatial patterns that arise among channel steepness, rainfall, and erosion rates during transient adjustment to a change in rainfall pattern, particularly when erosion rate and morphometrics are averaged at catchment scale – see section 5.1.2 for detailed discussion. a) Shows time slice at 0.5 Myr into transient adjustment of Case 3 (t_2 in Figure 5). For clarity, a subsample of ten data points is shown for each model dataset; connecting dashed line is populated from full model. Thick colored bands (red = trunk, blue = tributaries) show final steady state upstream-averaged k_{sn} pattern toward which the modelled catchment is adjusting. Position of trunk knickpoint, defined as upstream extent

1265   of quasi-equilibrium adjustment, is shown by red solid line, and zones describing morphological

1266   characteristics of tributary catchments are shown across the top axis (compare both with panel c). b)

1267   Modelled steady state k_{sn} and trunk erosion rate pattern of hypothetical catchment experiencing a bottom-

1268   heavy rainfall gradient and a spatial gradient in uplift rate that matches the catchment-averaged erosion rate

1269   pattern recorded by the tributary network in a). c) Shows planform development of local k_{sn}, k_{sn-q}, and

1270   erosion rates at initial and final steady states, a transient time slice from Case 3, and steady state pattern

1271   from (b). Downstream is to the left. Transient time slice and tributaries are the same as in panels (a & b).

1272   Note that trunk and tributary profiles are not illustrated to scale (Table 1).